Exploration of unique physiological features of dentate gyrus granule cells

Ph.D. dissertation

Máté Neubrandt

Semmelweis University
János Szentágothai Doctoral School of Neurosciences

Supervisor:	János Szabadics, Ph.D.
Official Reviewers:	Márk Kozsurek, Ph.D.
	Gábor Molnár, Ph.D.

Members of the Final Examination Board:

Anita Kamondi, DSc.

Gábor Gerber, CSc.

Bence Rácz, Ph.D.

Budapest

2017

Table of contents

Abbreviations

AAC	Axo-axonic cell
ABGC	Adult-born granule cell
AMN082	mGluR7 selective agonist
AMPA	α-amino-3-hydroxy-5-methyl-4-isoxazolepropionic acid
AP	Action potential
ASL	Average slope of the input-output funftions
BC	Basket cell
BINA	Selective positive allosteric modulator of mGluR2
CA1-3	Hippocampal regions, stands for *cornu ammonis*
CA3 GC	Ectopic granule cell located in the CA3 region
Calphostin C	Diacylglycerol binding domains inhibitor
CCK	Cholecystokinin
CNQX	AMPA/kainate receptor antagonists
DAB	3,3'-Diaminobenzidine
DCG IV	Group II mGluRs agonist
DG	Dentate gyrus; *gyrus dentatus*
DIC	Nomarski's differential interference contrast microscopy
diEPSC	Disynaptic inhibitory postsynaptic current
diIPSC	Disynaptic excitatory postsynaptic current
DMSO	Dimethyl sulfoxide
EGTA	Ethylene glycol-bis(2-aminoethylether)-N,N,N′,N′-tetraacetic acid
EPSC	Excitatory postsynaptic current
FFI	Feedforward inhibition
FF-IN	Feedforward interneuron

GABA	Gamma-aminobutyric acid, inhibitory neurotransmitter
Gabazine	(SR 95531); GABA$_A$ antagonist
GC	Granule cell
GFP	Green fluorescent protein
GIRK	G protein gated inwardly-rectifying potassium channel
Go 6976	PKC inhibitor
GF 109203X	(Bisindolylmaleimide I); PKC inhibitor
IN	Interneuron
IPSC	Inhibitory postsynaptic current
IvyC	Ivy cell
KT5720	Protein kinase A inhibitor
LEC	Lateral entorhinal cortex
L-group	ABGCs with linear input-output transformation
LTD	Long-term depression
LTP	Long-term potentiation
MEC	Medial entorhinal cortex
MF	Mossy fiber
MFB	Mossy fiber bouton
mGluR	Metabotropic glutamate receptor
ML297	GIRK1/2 channel selective activator
MSOP	Group III mGluRs selective inhibor
PC	Pyramidal cell
PDBu	Phorbol 12,13-dibutyrate, diacylglycerol analoge
PKA	Protein kinase A
PKC	Protein kinase C

PKC (19-36)	Protein kinase C inhibitory peptide
PLC	Phospholipase C
PP	Perforant pathway
PPR	Paired pulse ratio
PTP	Post-tetanic potentiation
PV	Parvalbumin
RFP	Red fluorescent protein
R_{in}	Input resistance
SLC	Spiny lucidum cell
Str.	*Stratum*
S-group	ABGCs with supra-linear input-output transformation
U 73122	Phospholipase C inhibitor
VAR	Average variance of the slope of input-output functions

1. Introduction

The hippocampus, being a simple cortical structure with many generally applicable properties became one of the most extensively studied brain region. On the other hand, hippocampus also have some unique anatomical and physiological specializations, consistently with its essential role in important cognitive functions. Many of these features, despite the long history of gaining the interest of researchers, remain poorly understood. My Ph.D. studies aimed to address intriguing and unique aspects of the hippocampal physiology on the cellular and circuit level. Accordingly, I am providing a general introduction of the hippocampus first, than I am discussing specifically the dentate gyrus (DG; *gyrus dentatus)* – CA3 interface which was the main focus of the research presented here. Notably, most of the available experimental data originates from the rodent hippocampus, and we used rats as model organism. Therefore, I will primarily discuss the rodent hippocampus, supplemented with some relevant human aspects.

Due to the coexistence of partly different nomenclatures in the literature I clarify what I use in this thesis hereafter. Although "hippocampus" sometimes only used to refer the CA regions (*cornu ammonis* or hippocampus proper) I consider dentate gyrus as part of the "hippocampus" because of its essential and inseparable role in some "hippocampus related" functions and phenomena e.g. pattern separation, sparse coding, will also be discussed. The "hippocampal complex" refers the complex of entorhinal cortex, DG, CA regions, subiculum, presubiculum, parasubiculum.

1.1. General introduction of the hippocampus

1.1.1. Functions of the hippocampus

Mnemonic functions

Association of the hippocampal complex with certain memory functions largely arose from the extensive studies of human amnesiac patients. Among them, the most famous is H.M. who developed severe memory dysfunctions after his brain surgery, when large part of his medial temporal lobe has been removed in order to treat his epileptic seizures (Scoville and Milner, 1957; Squire, 2009). The removed structures included significant portion of the hippocampus and the associated cortical regions bilaterally. After the

operation, H.M. had anterograde and retrograde global amnesia, even though many of his cognitive abilities remained unaffected. For instance, he could actively participate in an ongoing conversation, followed the topic, until it was disrupted. Upon the partner left the room for a short time, H. M. forgot the entire conversation and could not even recognize the person he talked with. He was incapable of storing new memories (anterograde amnesia), and did not remember a certain period preceded the surgery (retrograde amnesia), however he could clearly recall older memories. On the other hand, he was capable of learning motoric tasks that required practice, indicating that his ability to form so called "procedural memory" was remained. H. M. showed day by day improvements in these tasks even though he did not remember the process of the practices. Later, the conclusions of the extensive studies of H.M. were supported by further observations. Learning of random associations of complex multimodal inputs for a single exposure is impaired in patients with lesion of the hippocampal complex. In contrast, simple associative pairings like classical conditioning, and motor learning remain intact. Moreover, the largely intact short-term memory of these patients indicate the involvement of different cortical regions in those specific abilities (Squire, 1992; Andersen et al., 2007). Supporting the uncompromised episodic memory functions, many evidence is accumulated so far that hippocampus also has crucial role in learning the order of sequential events (Eichenbaum, 2013). In summary, the consensus is that hippocampus is essential for processing complex, multi-sensory experiences and establishing new memories. Such memories however transiently deposited in the hippocampus, for long-term storage they might be transferred to other cortical regions.

Spatial navigation

Another major and well described function of the hippocampal complex is its essential role in spatial navigation. The discovery of this feature was recognized by the Nobel Prize in 2014 received by John O'Keefe, May-Britt Moser and Edvard I. Moser "for their discoveries of cells that constitute a positioning system in the brain". While recording hippocampal cells in freely moving rats O'Keefe and Dostrovsky recognized that the activity of certain cells remarkably increase when the animal enters a specific restricted area of the environment, what they denominated as place fields (**Fig. 1**). When an animal explores a new environment it progressively recruits assemblies of place cells, with place fields covering the elapsed route, thereby forming a cognitive map of the entire

environment. Later, when the animal returns to the familiar environment, the firing fields of the previously established place cells remain the same. A hippocampal cell with an existing place field, however, still can contribute to mapping of a distinct novel environment, by forming a new place field (O'Keefe and Dostrovsky, 1971; O'Keefe and Nadel, 1978). It was believed for a long time that a place cell has a single firing field, because in general experimental conditions animals explore only small spaces. However, it was found recently by using much larger environments, that hippocampal neurons have their own individual propensity for forming place fields in random manner during exploration. Therefore, some cells express many firing fields and many form few or none (Rich et al., 2014). Place cells were initially described in the CA1 and these cells are showing the sharpest edges by their place field and the highest firing rate, the existence of place cells was reported in all hippocampal sub-regions. After long standing controversy regarding the spatial behavior of dentate gyrus granule cells, it was recently clarified that even though they are sparsely active during exploration they can form single stable place fields. When the animal traverses through their place fields, granule cells can fire remarkably high frequency bursts of action potentials (Jung and McNaughton, 1993; Leutgeb et al., 2007; Neunuebel and Knierim, 2012; Danielson et al., 2017; GoodSmith et al., 2017; Senzai and Buzsáki, 2017).

The other milestone linking the hippocampal formation with spatial navigation was the discovery of grid cells in the medial entorhinal cortex by the group of May-Britt Moser and Edvard I. Moser. Whereas place cells mostly have single firing fields in a given environment in the case of grid cells the entire space is tiled by multiple firing fields of cells forming a grid (**Fig. 1**). Such a grid constituted of equilateral triangles and therefore showing a characteristic hexagonal pattern with 60° rotation symmetry when illustrated by a spatial autocorrelogram. Grid cells retain their grid-spacing and also the orientation of the grid relative to the borders in any environment, thereby provide a reference metric for the neural representation of the spatial environment (Hafting et al., 2005; Moser et al., 2014).

The way rodents explore the environment by sniffing and whisking during locomotion is markedly different from how humans or primates approach the same task, predominantly by visual observation. Accordingly, the neural equivalents of place and grid cells were also identified in primates when visually exploring a virtual environment.

Similar spatial representations were found during visual observation in human epileptic patients, when recordings were performed during surgery, in order to identify the locus of epileptic activity in the temporal lobe (Killian et al., 2012; Jacobs et al., 2013; Miller et al., 2013).
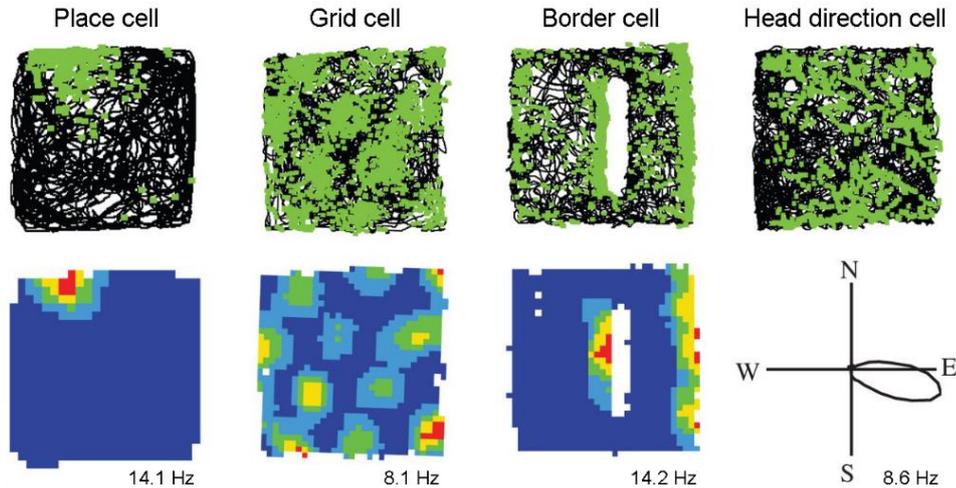
Figure 1. Examples of four fundamental spatial cells in the hippocampal complex. The upper row shows the animals trajectory (black line) in square boxes (1 x 1 m with 50 cm high walls, except in the case of the place cell, where the box was 62 x 62 cm) with indication of the neurons firing activity (green dots). In the case of border cells an additional 50 cm long barrier is inserted. Lower row: heat maps show the locational firing rate or polar plot shows the directional firing rate of the cells. The peak firing rates are shown below the rate maps. The figure is adopted with modifications from (Hartley et al., 2013).

It is generally accepted that the brain needs to maintain two cooperative mechanisms to efficiently accomplish the various challenges related to spatial navigation. First, it is necessary to build an accurate so called "allocentric" map, the static positional representation of the spatial environment (O'Keefe and Nadel, 1978). The other component is a self-referenced navigation system that requires information of the locomotion speed, the elapsed time and the starting point as a reference. This is a complex mechanism, required for example to calculate the shortest way home after an exploratory trip without the necessity of repeating the exact same route in the reverse direction (McNaughton et al., 1996). In addition to behavioral evidences linking both mechanisms to hippocampus, further related specific representations were also described in the hippocampal complex (Buzsáki and Moser, 2013; Moser et al., 2014). Such neural elements are head direction cells in the entorhinal cortex which not only show directional tuning but also found to be modulated by the moving speed (Sargolini, 2006), and border

cells that respond to environmental boundaries in orientation specific manner (**Fig. 1**) (Agster et al., 2014).

Current perspectives of the hippocampal functions

As discussed above, the hippocampal complex has long history of being associated with two main, seemingly distinct brain functions, the episodic memory and the spatial navigation. On the other hand, these two functions supposable must have much in common since they obviously share similar computational and circuit requirements (Buffalo, 2015). How these functions relate to each? The reconciliation of mnemonic and spatial functions was addressed from at least two perspectives so far. First, Buzsáki and Moser proposed that these two functions are in direct evolutional relationship, considering their underlying mechanisms. Their hypothesis is memory formation was evolved from spatial navigation, and the neuronal mechanisms of navigation in both physical and mental space is fundamentally the same. The review highlights the dichotomy in both navigation and memory. The numerous similar aspects and cellular activities related, on one hand, to the *explicit* "allocentric cognitive map" and "semantic memory", and to the *first person experience* of "path integration" and "episodic memory" on the other hand are paralleled in the review (Buzsáki and Moser, 2013).

Eichenbaum proposed a second, relatively simpler perspective that spatial representation together with the representation of time are the organizing basics of the episodic memory. The same hippocampal neuron population that provide place cells can also encode temporal regularities of experience. If the activity of neurons is linked to a specific moment within a temporally structured episode it is called "time cell". During learning, the dimension of the context determines whether the activity of a cell will be associated with either time or space (Eichenbaum, 2013, 2014).

Some recent results further elaborated the functions of hippocampus. In a clever behavioral paradigm, rats had to identify and find a specific sound frequency by adjusting the tone on a continuous scale by a "joystick" to deserve a reward. Remarkably, during this task certain hippocampal and entorhinal cortical cells were activated, so that they mapped the entire sound spectrum by each being rendered to a specific narrow sound frequency range. The progressive mapping of the changing sound showed many similarities to the well described manner of mapping the spatial environment (Aronov et

al., 2017). These results also argue that the hippocampus has a general ability to encode and map various environmental contexts and more abstract dimensions than the space. Thereby the same neural circuit elements might concurrently support spatial and mnemonic functions. Next, I am going to discuss the structural basis of these functions.

1.1.2. Anatomy and connectivity of the hippocampus

Architecture of the hippocampal regions

The hippocampus is an archicortical brain region with evolutionary conserved structure that is similar across all mammalian species. The hippocampus has a relatively simple laminar structure that distinguishes it from the other, more complex cortical regions. The simple architecture was also an important factor that made the hippocampus a popular research subject, beyond the broad interest of its implications in memory functions. Some fundamental principle determine the laminar structure at each hippocampal sub-region. The somata of the principal cells are concentrated into a single dense layer, their apical dendrites distributed parallel, and the major afferent- and efferent fiber tracts densely permeate certain cellular domains. In a trans-section, the hippocampus appears as two opposing "horse shoes" these are the major regions, the dentate gyrus (DG) and the hippocampus proper (**Fig 2**). The latter is divided into further sub-regions CA1, CA2, CA3 denominated according to the abbreviation of its Latin name *cornu ammonis* (Lorente de Nó, 1934; Andersen et al., 2007).

In the DG, granule cells (GC) are the principal cells. The uniformly polarized morphology of GCs designates the three layers of the DG. The GC dendrites are located in the *str. moleculare,* the somata in the *str. granulosum* and the axons in the centrally positioned *hilus*. The *hilus* hosts another glutamatergic cell population, the mossy cells that provide an excitatory feedback loop to GCs in both the ipsi- and the contralateral hemispheres (Amaral, 1978). The principal cells of the *cornu ammonis* are pyramidal cells (PC). The somata of the PCs are organized into a single dense layer called *str. pyramidale.* This pyramidal cell layer forms a successive continuum along the CA3-CA2-CA1 sub-regions. The thin basal dendrites of PCs radiate in the *str. oriens* towards the *alveus.* The majority of the dendritic tree of PCs, deriving from their much thicker apical dendrites, is largely located in the *str. radiatum,* only the distal most branches terminate in the *str. lacunosum moleculare.* Beyond this general scheme, the CA3 region has an

additional sublayer the *str. lucidum.* This layer is formed by the dense mossy fiber (MF) tract, the efferent axons of DG GCs that target the most proximal part of the apical dendrites of PCs (Andersen et al., 2007).

Figure 2. The rodent hippocampal complex. Position and orientation (upper, drawing) of the hippocampus and its related structures in the intact brain and in a traverse section (bottom). Abbreviations: MEC and LEC – medial and lateral entorhinal cortex, PrS and PaS – pre- and parasubiculum. The figure is adopted with modifications from (Moser et al., 2014)
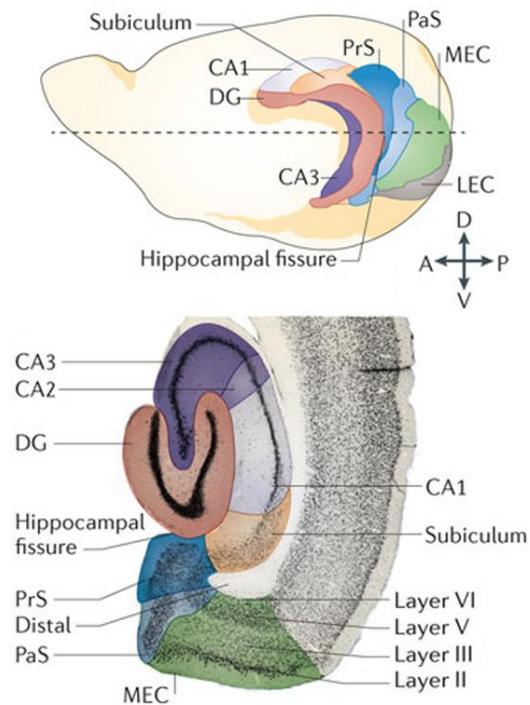
Excitatory connectivity – orthogonal information flow

The hippocampal complex is reciprocally connected with practically all sensory and associative cortices consistently with its central role in many cognitive functions. What is the secret of the hippocampus that distinguish it from other brain areas? One major unique feature of the hippocampal circuitry is the orthogonalized information flow that proposed to be a key element in its functions (**Fig. 3**)(Cajal, 1893). The entorhinal cortex provides the major input to the hippocampus, this afferentation is called the perforant pathway (PP). The entorhinal cortex layer 2 fibers terminate in the DG in the outer 2/3 of the *str. moleculare*, and the CA3 *str. lacunosum moleculare*. The layer 3 fibers project to the CA1 *str. lacunosum moleculare.* The MF pathway originating from the DG GCs provides the intrahippocampal afferentation of the CA3 region. The CA3 PCs are extensively connected with each other and forming a so called associative network that also involves commissural fibers coming from the contralateral CA3. Such an

14

autoassociative network is capable of information storage. It is believed that in the hippocampus, previously acquired information is stored in the associative synapses of the CA3 network (Rolls, 2007). The efferent projection of the CA3 PCs is called Schaffer collaterals that terminate in the *str. radiatum* of the CA1. The CA1 PCs project to the subiculum and the entorhinal cortex thus closing the hippocampal loop. Notably, the above described fundamental circuit did not consider the CA2 region which is much smaller than the two neighboring regions. The CA2 starts where the MF pathway ends and accordingly the stratum lucidum diminishes. The main afferentation of the CA2 comes from the layer 2 of the entorhinal cortex which distinguishes it from the CA1. Recently, the identification of some appropriate marker molecules facilitated the research of this region, which predicts novel understanding of its role in the hippocampal circuitry in the near future (Cui et al., 2013; Kohara et al., 2013).
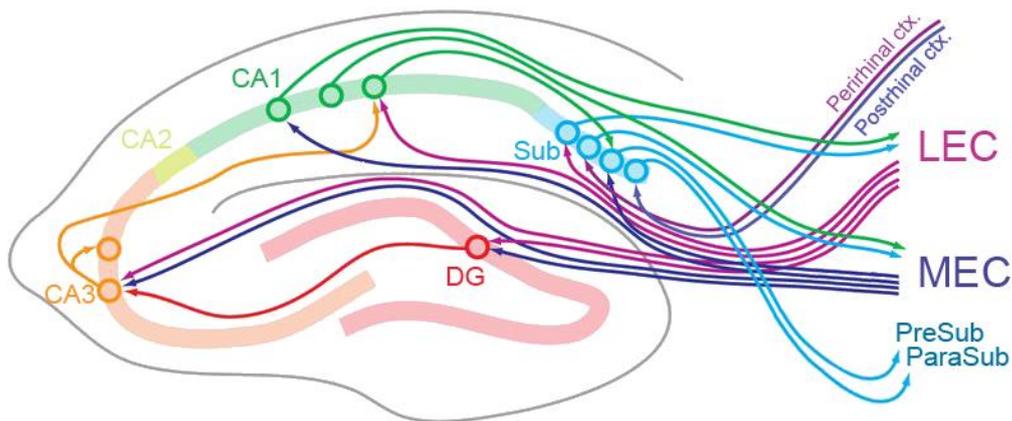
Figure 3. Connectivity of the hippocampus. The main local as well as the afferent and efferent excitatory pathways of the hippocampus. Abbreviations: MEC and LEC - medial and lateral entorhinal cortex, Sub - subiculum. The figure is adopted with modifications from (Hartley et al., 2013).

Inhibitory cells of the hippocampus

Like in other cortical regions, the hippocampal GABAergic cells show substantially larger heterogeneity than that was found in the case of principal cells. Exact classification of GABAergic cells requires consideration of their multiple features, such as the localization of the axonal and dendritic arborization, target cell specificity, neurochemical markers, electrophysiological properties, timing of activity relative to the network oscillations and developmental origin (Freund and Buzsáki, 1998; Buzsáki et al., 2004; Klausberger and Somogyi, 2008; Kepecs and Fishell, 2014). Instead of going into detailed

classification I would like to highlight some key aspects of the diversity that relates to the generalized connectivity schemes and the major network functions.

Key determinant of GABAergic cells function is their target selectivity. Specific IN populations innervate the *perisomatic region* of principal cells (such as axo-axonic and basket cells), they are optimally positioned to effectively control the spiking output of their postsynaptic partners (Somogyi et al., 1982; Papp et al., 2013; Szabó et al., 2014). Others, innervating different dendritic domains of the principal cell, are suited to control local signaling and integrative processes of the distal inputs (Klausberger, 2009; Lovett-Barron et al., 2012). However most of the inhibitory cells are indeed local, and rightly referred to as interneurons, projecting GABAergic cells are also exist in the hippocampus (Jinno et al., 2007; Jinno, 2009). Such projecting hippocampo-septal cells inhibit other inhibitory cells of the medial septum that project back to hippocampal GABAergic cells closing a recurrent inhibitory loop. Besides the cholinergic afferents, the septal inhibitory connections have important role in rhythmic network activities of the hippocampus (Freund and Antal, 1988; Bland et al., 1999). A specific inhibitory cell population selectively target other GABAergic cell types within the circuit, similarly to the local collaterals of the hippocampo-septal cells. This circuit motif, the indirect control of the network excitability by the *interneuron selective inhibitory cells* is referred to as dis-inhibition (Hájos et al., 1996; Tóth et al., 1997; Chamberland and Topolnik, 2012).

Another functionally important property of inhibitory cells is the localization of their soma-dendritic arbor, which determines the main source of their excitatory input. In accordance with this notion, GABAergic cells mostly involved in either one of the two fundamental inhibitory wiring motif, feedforward or feedback inhibition (Glickfeld and Scanziani, 2006; Andersen et al., 2007). Those GABAergic cells whose activity is mostly driven by the afferent projections from extra hippocampal areas or upstream sub-regions contribute the feedforward inhibition. A largely different cell population is recruited by the recurrent collaterals of the local principal cells establishing the feedback inhibition.

The above discussed main categories of inhibitory cells (e.g. target specific and functional types) can be found all over the hippocampus and comprise largely equivalent cell populations across sub-regions.

1.2. The dentate gyrus -CA3 interface

As I discussed earlier, several hippocampal functions require the fast storage and subsequent recall of specific sets of multimodal environmental stimuli. What is so special in hippocampus that enables establishing complex memory traces? Why the neocortex which is responsible for the highest order cognitive functions needs the hippocampus? Neocortex is assumed to be involved in continuously creating and referring to a general internal representation of the observed world. However, it seems that the structure of the neocortex may not be suited for rapid interference free acquisition of new memory traces. By contrast, the hippocampus appears to be evolved exactly for this task, to complement the learning capacity of the neocortex (Acsády and Káli, 2007). What are the key features, specific roles, and computational tasks that assumed to be accomplished by the DG-CA3 circuit?

1.2.1. Computation requirements from the DG and the CA3 circuit

Autoassociative memory networks and pattern completion

At the CA3 region PCs are connected to each other, with local and contralateral collaterals, forming a so-called autoassociative network. Moreover, these associative synapses are plastic that establishes the basis of information storage. Because of these features, the CA3 region has been considered for a long time to have a central role in memory formation. In theoretical models, such an autoassociative memory network is optimal for storing large amount of information and capable of recalling complex memory traces even when only a fraction of the original input is presented to the network. This latter feature is referred to as pattern completion. More specifically, it is believed that when the hippocampus is encoding a complex memory trace, a set of CA3 neurons, so-called ensemble, become active, and the synapses connecting them become potentiated. Thereafter a certain set of neurons will be allocated to a specific memory trace. During memory recall activation of a subset of the neurons belonging to a certain memory trace will recruit the rest of the neurons coding the memory. To be able to perform these tasks independently, CA3 network needs to maintain two distinct, specialized input system. The PP input is suggested to be activated during memory recall, and the MF input is responsible for encoding memory traces (Marr, 1971; Treves and Rolls, 1992, 1994;

Debanne et al., 1998; Kesner, 2007; Guzman et al., 2016; Mishra et al., 2016). Multiple unique features, such as the "detonator" synapse, the sparse physiological activity, and the target specificity of GCs cooperatively support the MF system to perform this operation. I will discuss these features in more details in the following sections.

Pattern separation

To avoid interference between memories, pattern separation is an essential step in information processing. In general, pattern separation occurs in a network when the output patterns are less similar to each other than the input patterns. In the entorhinal cortex two different experiences likely represented with a certain degree of overlap in the populations of active cells. Particularly, when only subtle differences distinguish two items to be encoded, it is essential to separate them in order to produce independent representations. In the hippocampus, the DG is assumed to perform this key step of memory formation. Multiple features of the DG support this function. First, the anatomical arrangement of this region seems to be optimized for this computation by showing a large divergence. The number of cells in the DG is an order of magnitude larger than that is found in its primary input source, the entorhinal cortex. Second, individual GCs are capable of effectively depolarize, and drive the firing their downstream target neurons, the CA3 PCs. Finally, DG operates with the so-called sparse coding scheme. In this type of neural code each event is encoded by the strong activation of a small set of neurons. (Marr, 1971; McNaughton and Morris, 1987; Deng et al., 2010; Knierim and Neunuebel, 2016).

Sparse coding, the hippocampus specific code

Sparse coding is a coding scheme falls between the two extremes of the so-called localist coding, where a single neuron codes a single memory item, and the fully distributed coding, where each memory is coded by the activity of large neuron populations. In the hippocampus, each memory trace or item is represented by the strong activation of a small set of neurons. Consequently, in the hippocampus the background activity in principal neurons is remarkably low, and only minority of the cells are active at a given time, those who are participating in the ongoing coding processes. These features of the neuronal activity, and the sparse coding scheme is largely different from most of the other cortical regions. Those are usually characterized by higher background

activity and relatively weaker modulation by their relevant stimuli, and perform denser coding (Acsády and Káli, 2007; Rolls and Treves, 2011; Wixted et al., 2014).

In the light of the above notions, the DG can be considered as the gate of the hippocampus and its roles are to form pattern separated, sparse representations of the entorhinal cortical activities and effectively transmit it to the CA3 network (Acsády and Káli, 2007). These complex functions require unique solutions, functional specializations from the DG-CA3 circuit, which were the main focus of my Ph.D. studies.

1.2.2. Granule cells

Morphological properties

GCs are the principal cells of the DG and they represent the most numerous neuron type in the hippocampus as their number reaches about one million cells in the rodent brain (Bayer, 1982). The morphology of GCs markedly differs from that of PCs. GCs do not have a pronounced apical dendrite, instead one or a few main dendritic branches originate from their small somata. These dendrites are branching close to the cell body resulting in multiple equivalent thin dendrites which are densely covered by spines (Claiborne et al., 1990; Schneider et al., 2012). Our earlier results revealed a mechanism that is optimal for silencing individual dendrites by an unusual postsynaptic mGluR2 receptor mediated current (Brunner et al., 2013). Another interesting finding of our laboratory is related to GC dendrites: back propagating action potentials retain analog information about the somatic membrane potential which affects local dendritic Ca^{2+} signaling.

Probably the most unique morphological feature of GCs is their axon, called mossy fiber (MF) that is substantially different from any other cortical axons. Usually a single axon fiber runs through the CA3 *str. lucidum* and only a few collaterals branch in the *hilus*. In healthy conditions GCs do not innervate each other, which is ensured by the polarized arrangement of the axons and dendrites (Claiborne et al., 1986; Williams et al., 2007). MF have three different types of axon terminals (**Fig. 4**). The most special is the large MF bouton (MFB) with its exceptional size reaching 4-10 µm in diameter. This huge presynaptic structure contains on average 25 individual active zones (Rollenhagen et al., 2007). Large MFBs emanate up to 3-4 filopodial extensions which terminate regular

sized (0.5-2 µm) axon terminals. The number of these filopodia varies depending on the age or even previous learning experiences (Ruediger et al., 2011; Wilke et al., 2013). Finally, regular sized (0.5-2 µm) *en passant* varicosities along the main axon represent the third terminal type (Claiborne et al., 1986; Acsády et al., 1998). The heterogeneity of the terminal types parallels with target specificity, as the large MFBs innervate mossy cells in the hilus and PCs in CA3, while the regular sized terminals specifically target GABAergic cells in both sub-regions (**Fig. 5**). This target selectivity enables the simple estimation of the ratio of excitatory and inhibitory cells among the postsynaptic partners of GCs, that aspect of the circuit also predicts unusual operation and specific functions. First, each GC project to as few as 10-18 CA3 PCs that results in an oddly specific information pathway with minimalized divergence. Second, GCs innervate more GABAergic cells in the CA3 (40-50) than PCs, rendering the DG - CA3 interface as a prototypical feedforward inhibitory circuit (Acsády et al., 1998). In comparison, PCs in other cortical circuits usually form thousands of synapses and only 15-20% of them target inhibitory cells, that emphasize the unique organization of the MF pathway (Gulyás et al., 1993; Sik et al., 1993).

Figure 4. Comparison of the different MF terminal types on electron microscopic level. A-
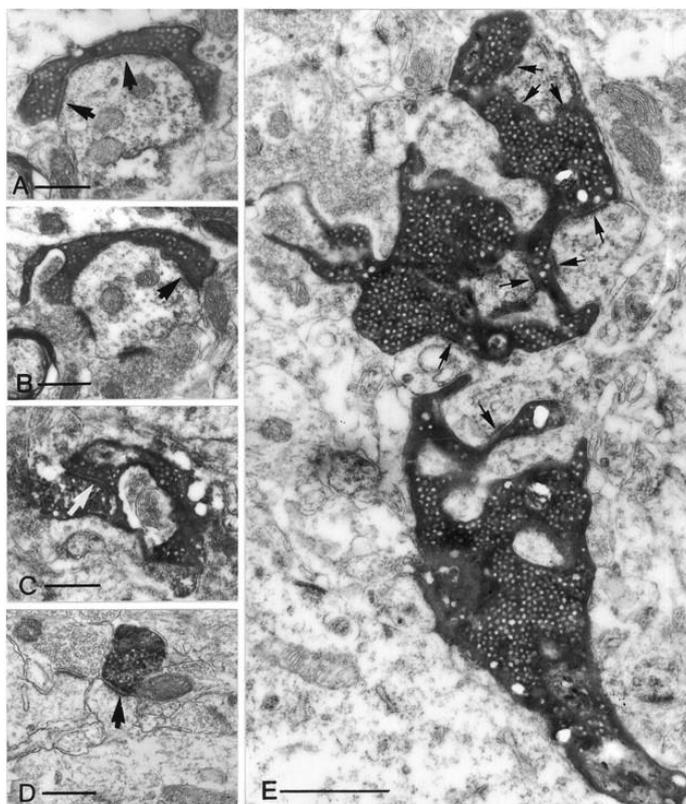
B. Small *en passant* terminals establishes a single asymmetrical synapse on a dendritic shaft with long perforated postsynaptic density (arrows). **C.** A filopodial extension of a mossy terminal forms a synapse (arrow) with a substance-P receptor labeled interneuron. **D.** A CA3 PC terminal on a CA1 PC dendritic spine is presented for comparison. **E.** A large, mossy terminal forms multiple contacts (arrows) with thorny excrescences of a CA3 pyramidal cell. The individual release sites are short. Note that, all micrographs have the same magnification to enable the direct comparison of the sizes of the structures. Scale bars: A-D: 0.5 µm, E:1µm. This figure is adopted from (Acsády et al., 1998).

Figure 5. Filopodial extensions of MF terminals innervate GABAergic cells. Schematic illustration of two MF boutons (MFB), each with four filopodial extensions (large arrowheads). All filopodial terminals contacted the dendrites or spines of six GABAergic neurons. Five out of six postsynaptic interneurons have spiny dendrites. All synapses were identified at the electron microscopic level (data not shown). Arrows indicate the main axons. This figure is adopted from (Acsády et al., 1998).
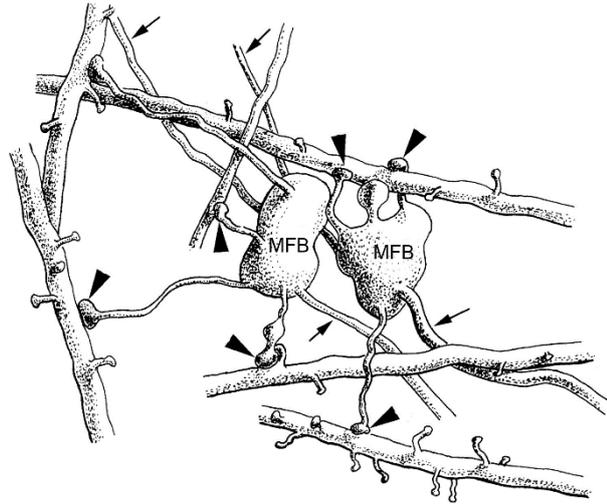
Activity of granule cells

The GCs receive strong feedforward and feedback inhibition from local GABAergic cells, which is reflected by some unusual features of the organization of the inhibitory circuit in the DG (Acsády and Káli, 2007). Basket cells, as well as other interneurons of the DG refrain from innervating the peri-somatic regions of each other, thus, minimalizing the dis-inhibitory influence (Acsády et al., 2000). Moreover, strong excitation from large number of GCs and mossy cells converge onto GABAergic cells of the DG and the *hilus*. These GABAergic cells in turn extensively innervate the peri-somatic region and the outer layer of the *str. moleculare* where the PP input terminates. (Buckmaster and Schwartzkroin, 1995; Sik, 1997; Acsády et al., 2000).

Beyond the strong synaptic inhibition, the intrinsic physiological properties of GCs also appear to be specifically tuned to support extremely low firing activity. GCs were found to have remarkably hyperpolarized membrane potential (about -80 mV) and no spontaneous firing activity in *in vitro* slice experiments (Staley et al., 1992; Schmidt-Hieber et al., 2007; Krueppel et al., 2011). Consistently, GCs were found to be one of the most quiescent neurons with their extremely low overall firing activity (below 1 Hz) during *in vivo* recordings (Munoz et al., 1990; Jung and McNaughton, 1993; Penttonen et al., 1997; Kowalski et al., 2016). When GCs are active, they either fire single action potentials (AP), or short high frequency spike bursts (3-7 APs with 100-200Hz) however their activity is often interrupted with several seconds long inactive periods, which explains the low overall firing rate. The high-frequency bursts are usually generated by non-linear dendritic processes in response to coincident inputs. In hippocampal CA1 PCs,

it was shown that dendritic plateau potentials can be evoked by coincident stimulation of the two major excitatory path of the CA1, the Schaffer collaterals and the PP. These plateau potentials reliably converted in the axon to high frequency burst output (Bittner et al., 2015; Apostolides et al., 2016). Much less is known about the mechanism related to the burst firing of GCs (Krueppel et al., 2011). Because of the lack of knowledge on this common physiological activity form of GCs, and also because high frequency bursts are considered to be distinct neuronal signals (Lisman, 1997), this interesting activity feature of GCs was one specific focus of my Ph.D. studies.

CA3 granule cells

It was reported that a small population of GCs is also present in the CA3 region of the rat hippocampus. CA3 GCs are spread mostly in the *str. radiatum* and *str. lucidum* and their abundance is comparable with certain GABAergic cell types. CA3 GCs express GC specific immunohistochemical markers, such as calbindin and Prox1, and share major morphological and physiological properties of the "normal" GCs (**Fig 6**). They are polarized, their dendrites grow into the *str. lacunosum moleculare* and receive PP innervation. The axons of the CA3 GCs reside in the *str. lucidum* and contribute to the MF pathway forming authentic MF terminal types. Most importantly, the synaptic properties are also remarkably similar to those of the DG GCs and this feature qualifies them as an appropriate model for studying MF synaptic functions (Szabadics and Soltesz, 2009; Szabadics et al., 2010).
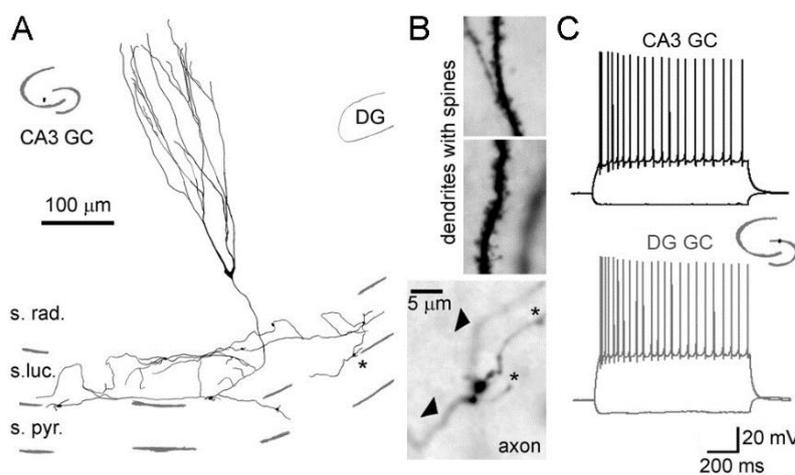
Figure 6. Morphological and firing characteristics of CA3 GCs. A. Dendritic and axonal arborization of a CA3 GC. The cell was biocytin filled during somatic recording and reconstructed by camera lucida. The inset shows the location of the soma in the hippocampus. **B.** Light micrographs of the spiny dendrites (*top*) and the axon with MF terminals (*bottom*). Arrow heads show the main axon, and asterisks indicate the filopodial extensions. **C.** The firing pattern of the CA3 GC in A and B compared to a DG GC. Inset indicates the position of the DG GC. The figure is adopted with modifications from (Szabadics et al., 2010).

1.2.3. Adult born granule cells

In mammals, neurogenesis almost exclusively restricted to the embryonal development of the brain and discontinues during the postnatal age. However, there are two specific areas in the brain where neurogenesis persists throughout the life. The DG hosts one of these regions at the hilar border of the *str. granulosum*, named the subgranular zone. The other dedicated region where adult neurogenesis occurs is the subventricular zone of the lateral ventricle (Altman and Das, 1965; Kriegstein and Alvarez-Buylla, 2009; Deng et al., 2010).

In the subgranular zone of the DG, after division of the neural progenitor cells, some of the progeny become glial cells but the majority chooses neuronal lineage and differentiate to DG GCs (Cameron et al., 1993), hereafter referred to as adult born granule cells (ABGCs). After their birth, ABGCs undergo a continuous maturation process, lasting for 8-10 weeks in rodents (**Fig. 7**). ABGCs became functionally integrated into the hippocampal circuit when they reach 3-4 weeks of age. At this time, ABGCs acquire neuronal properties including synaptic inputs and outputs, and capability of firing action potentials. However, compared to the older GCs they are highly excitable, show enhanced synaptic plasticity and are differently modulated by inhibition compared to ABGCs at the end of their maturation period (Wang et al., 2000; Schmidt-Hieber et al., 2004; Laplagne et al., 2006; Toni et al., 2008; Mongiat et al., 2009; Gu et al., 2012; Marin-Burgin et al., 2012)

Adult neurogenesis provides unique form of plasticity to the neural circuit of the dentate gyrus, which undergoes continuous reconstruction during the postnatal life. Consequently, the adult DG constitutes of GCs that are largely heterogeneous in age, as well as in intrinsic cellular properties. It is currently believed that ABGCs during their maturation process (between 3-10 weeks of age) are engaged in distinct physiological functions compared to mature GCs. Accumulating evidences support that young ABGCs are necessary for the pattern separation function of the hippocampus (Clelland et al., 2009; Deng et al., 2010; Sahay et al., 2011; Nakashiba et al., 2012). Whereas fully matured cells are potentially involved in rapid pattern completion (Nakashiba et al., 2012), in very sparse and specific encoding (Sahay et al., 2011), in the behavioral state-dependent, precise location representation (Neunuebel and Knierim, 2012), in the

preservation of the temporal episodes during later recalls (Aimone et al., 2010a), or that they simply become non-functional, "retired" cells (Aimone et al., 2010b; Alme et al., 2010). However, the transition between young and adult functional states is not completely understood.
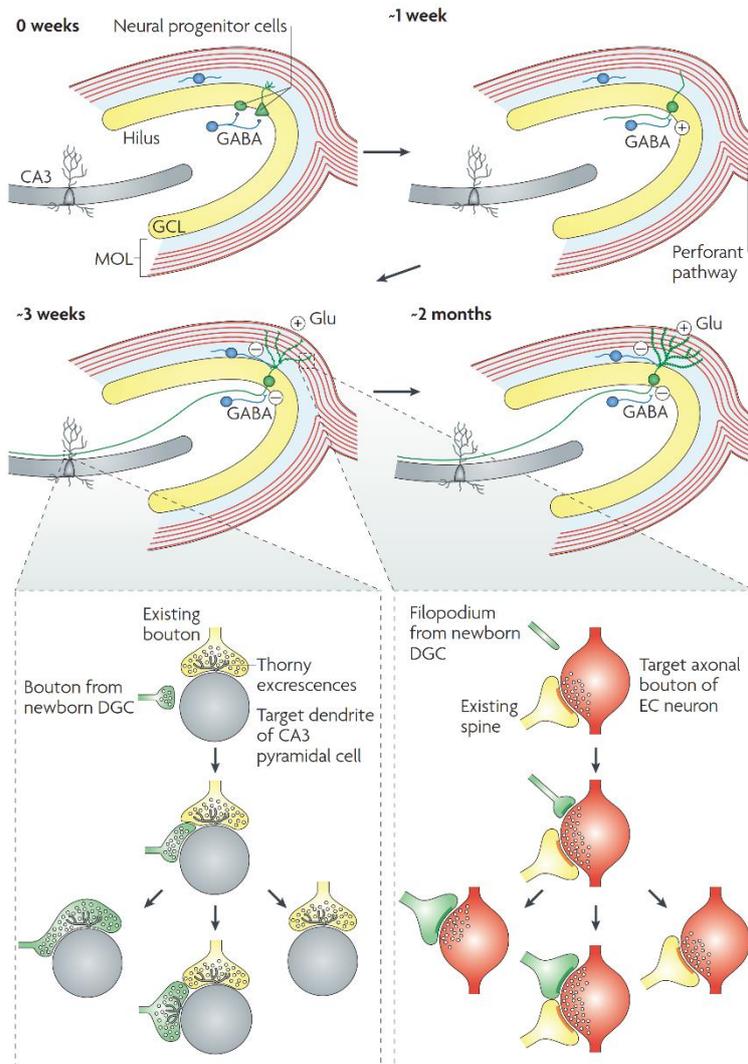
Figure 7. Illustration of the adult hippocampal neurogenesis. The neurogenesis starts with the proliferation of the neural progenitor cells (two different morphologies). They either give rise to adult-born granule cells (ABGCs; green cell) or glial cells (not shown). ABGCs undergo two months of development, with gradual changes in morphological and physiological characteristics. *1st week of the maturation:* the dendrites of ABGCs extend into the *str. granulosum* and *str. moleculare* while their axon grows into the *hilus,* ABGCs receive excitatory (!) GABAergic input from local interneurons (blue cells). *3rd week of the maturation:* at this stage ABGCs integrate into the circuit, they receive PP input and start to form synapses with the CA3 cells; the effect of GABA switches from excitatory to inhibitory. *2 months of age:* the maturation is complete, the structural and physiological properties of ABGCs are indistinguishable from those of the elder DG GCs. The **bottom inset panels** illustrate the competitive nature of synapse formation. **Left:** a small bouton of the ABGC (green) contacts the dendritic shaft of a CA3 PC (gray) at a site near to an existing MF synapse (yellow). The subsequent development might have three different outcomes, the MFB either conquer the thorny excrescence of the existing synapse, or retracts, or by the growth of new dendritic structures both remains. **Right:** the filopodium (green) of an ABGC dendrite extends to a PP bouton (red) that is associated with another spine (yellow), that eventually results in a monosynaptic bouton on the new dendritic spine of the ABGC, or a multisynaptic bouton, or leads to retraction of the filopodium. The figure is adopted without any modifications from (Deng et al., 2010).

Which physiological parameters support pattern separation function of young ABGCs?

The diverse ion channel content of different types of neurons leads to their different sensitivity and different output in response to similar input patterns (Armstrong and Hille, 1998; Nusser, 2009). The intrinsic excitability determines how neurons integrate their synaptic inputs and convert them to spiking output. The capability of ABGCs to respond with different spiking output to subtle differences in their input strength and frequency is optimal for pattern separation. In my first Ph.D. project, we studied the maturation of multiple membrane parameters of ABGCs to gain insight into the maturation of intrinsic excitability, which potentially underlies changes of the cellular function.

1.2.4. The feedforward inhibitory circuit in the CA3 region

Feedforward inhibition (FFI) is a fundamental network motif in which the afferent input activates a population of the local inhibitory cells, the feedforward interneurons (FF-INs) (Buzsáki, 1984). FFI has been implicated in various circuit functions by controlling the excitability of the principal cells. FF-INs can determine the temporal window in which the excitatory inputs might integrate. Depending on the properties of the local FFI this window can even vary among different subcellular domains (Pouille and Scanziani, 2001). By normalizing input strengths, FFI was shown to expand the dynamic range that a neuronal circuit can represent (Pouille et al., 2009).

As it was discussed earlier, the anatomical features of the MF synapses establish a prototypical FFI circuit in the CA3 region. GCs innervate at least four distinct types of GABAergic interneurons in the CA3: fast-spiking, parvalbumin (PV) expressing basket cells, regular-spiking, cholecystokinin (CCK) expressing basket cells, ivy cells, and septum-projecting spiny lucidum cells (Szabadics and Soltesz, 2009). The axonal arbor of these IN types covers both the perisomatic region of the PCs and a substantial part of their dendritic tree that locates in the *str. radiatum* and *str. oriens*. Furthermore, the extensive axon arbor of the INs provide substantial divergence to the their PC targets (Spruston et al., 1997; Vida and Frotscher, 2000). This FFI circuit has been proposed to play key role in the DG – CA3 communication (Lawrence and McBain, 2003; Acsády and Káli, 2007). The strong inhibitory control of the PCs contributes to implementing and maintaining the sparse pattern separated DG input code in the CA3 circuit. The

mechanistic understanding of the operation of the DG-CA3 FFI circuit however is not complete. In a FFI network, depending on the wiring specificity of the afferent input and the FF-INs, fundamentally different functional contributions are possible e.g. in the case of lateral inhibition or ensemble-specific FFI. Consideration of the wiring arrangement on single cellular level is particularly important in the case of the DG GCs because their extremely sparse activity decreases the importance of the population level effects.

1.2.5. Synaptic transmission and plasticity mechanisms

Synapses are intercellular junctions of neurons. In the chemical synapses, which are the most fundamental sites for information transfer between neurons, the electrical activity (AP) of the presynaptic cell is converted to chemical signal by releasing neurotransmitters. Binding of neurotransmitter molecules to their receptors results in ion channel openings, and converted back to electrical activity in the postsynaptic neuron. The release of synaptic vesicles is a remarkably complex process, with multiple successive steps (Südhof, 2013). The AP-evoked membrane depolarization invades the presynaptic terminal and opens voltage gated Ca^{2+} channels. The inflowing Ca^{2+}, by binding to synaptotagmins, is the key signal mediating the release of neurotransmitters. To become ready to release, synaptic vesicles must undergo docking and priming steps. Molecules in the synaptic active zone, such as RIM, Munc13, RIM-BP, α-liprin, and ELKS proteins are identified as key mediators of docking and priming, however these presynaptic processes involve a variety of further molecular components and regulatory mechanisms which are still not completely understood (Südhof, 2012). The presynaptic Ca^{2+} transient itself also triggers further signaling pathways (Schneggenburger and Rosenmund, 2015; Körber and Kuner, 2016).

According to the quantal hypothesis of del Castillo and Katz, the magnitude of the postsynaptic response is determined by three factors: (1) the number of synaptic contacts, namely the 'functional release sites' between the cells, (2) the probability of vesicle release at each release sites, and (3) the quantal size, which is the elementary postsynaptic response for the release of a single neurotransmitter vesicle (Del Castillo and Katz, 1954). Release probability is controlled by presynaptic regulatory mechanisms, while postsynaptic processes affect the quantal size.

Weight of synapses undergoes continuous changes during physiological activity of cells which is necessary for the storage and processing of information. These plasticity phenomena vary on remarkably broad timescale from a few milliseconds to several hours, or even days and weeks (Zucker and Regehr, 2002; Holtmaat and Svoboda, 2009). The scale starts with two fundamental form of short-term plasticity: facilitation and depression. These mechanisms rely on the relationship of the presynaptic Ca^{2+} transients and its sensors (e.g. the accumulation of residual Ca^{2+}) and the depletion rate of the release-ready vesicles (Fioravante and Regehr, 2011; Jackman and Regehr, 2017). Prolonged high frequency activity, so-called "tetanus", in certain synapses can evoke post tetanic potentiation (PTP) or augmentation, forms of plasticity that last for tens of seconds to minutes and usually require the involvement of protein kinase activity, e.g. PKC, PKA beyond the presynaptic Ca^{2+} transients (Zucker and Regehr, 2002; Fioravante et al., 2014). Notably, the nomenclature and the categorization of these plasticity phenomena is not completely consistent in the literature, thus, certain plasticity forms in different synapses involving substantially different molecular mechanisms might referred similarly if sharing similar temporal profile. Finally, the long-term plasticity, potentiation and depression (LTP and LTD), are permanent changes of the synaptic strength and can be accompanied by structural changes (Yuste and Bonhoeffer, 2001; Holtmaat and Caroni, 2016).

What plasticity mechanisms function in MF synapses? How do they operate during their physiological activity?

The GCs target PCs and inhibitory cells with anatomically different types of presynaptic terminals that suggests functional differences. Indeed, the synaptic transmission from MF to the two major postsynaptic targets operates with substantially different short-term plasticity. At MF-PC synapses the initial release probability is low but in the case of high frequency spiking activity the synapse shows strong short-term facilitation. In contrast, in the case of postsynaptic GABAergic cells the synaptic transmission is relatively stable (e.g. mostly varies between slightly facilitating or slightly depressing) during repetitive activity (Salin et al., 1996; Toth et al., 2000). This functional difference establishes a frequency dependent switch from inhibition to excitation as result of the MF activity in the CA3 circuit. Therefore, the MF terminal often referred to as "conditional detonator". Conditional in the sense that high frequency activity, that is a

MF burst, is required to overcome the strong FFI network and successfully drive PCs (Henze et al., 2002; Lawrence and McBain, 2003; Mori et al., 2004).

Similarly to the short-term plasticity, dichotomy was found in the long-term synaptic plasticity phenomena when the two major postsynaptic targets of MF synapses, PCs and interneurons were compared. Maccaferri and colleagues applied tetanic stimulation protocol that induced LTP in PCs, however, the same protocol either had no effect or induced depression in postsynaptic interneurons. Similarly, pharmacological activation of the PKA pathway only potentiated synapses on PCs (Maccaferri, 1998).

Another study specifically addressed plasticity of MF synapses on GABAergic cells of the DG and described the presence of LTP and PTP phenomena. In the study of Alle and colleagues the applied stimulus protocol (25 AP at 30Hz repeated 12 times in every third seconds) was either evoked in a presynaptic somatically recorded GC or the MF tract was extracellularly stimulated. The associative form of the protocol, when firing of the postsynaptic fast spiking basket cells followed the presynaptic stimuli, LTP was developed. Whereas, non-associative protocols, when the postsynaptic cell was held in voltage clamp to prevent firing of the cell resulted in PTP. These two plasticity forms involve different molecular pathways as the PTP was found to be sensitive for the blockade of both PKC and PKA while only blocking of PKC reduced the LTP (Alle et al., 2001).

Prolonged stimulation (100AP, 40Hz) of single presynaptic GCs in hippocampal slice culture has been shown to potentiate MF responses for more than 10 minutes in GABAergic neurons as well as in PCs of the CA3. Based on the sustained increase of feed-forward inhibition the authors propose three different state of the MF-CA3 connection: a resting state with low release probability and high failure rate onto PCs; a bursting mode, in which excitation of PCs predominates; and a post-bursting mode, in which the feed-forward inhibition is greatly enhanced (Mori et al., 2007).

In contrast to generally used artificial stimulation paradigms Gundlfinger and colleagues applied natural spike trains to test synaptic dynamics of mossy fibers. They obtained natural spiking activity of GCs by tetrode recording when the animals traversed their place fields thus such natural spike train contained high frequency epochs.

Stimulation of multiple GCs with these spike trains resulted in short-term facilitation and LTP in CA3 pyramidal cells (Gundlfinger et al., 2010).

In order to understand the communication between two cells, it is essential to consider all types of the synaptic mechanisms operating on various timescales during the physiological activity of the cells (Abbott and Regehr, 2004). This is particularly important in the case of GCs with such an irregular firing activity that consists of single action potentials, short high frequency bursts and long silent periods. Despite the broad spectrum of studies with various protocols and experimental configurations addressing the MF synapses many unresolved questions remain to be answered. It is not clear whether short, truly physiological high frequency GC bursts activate any specific synaptic mechanisms beyond the short-term plasticity. How does the downstream CA3 network interpret the differences of single action potential and single burst firing in the subsequent period?

2. Objectives

My Ph.D. studies addressed the operation of the DG-CA3 circuit and each question aimed to elucidate some yet poorly understood aspects of it. I focused on two main topics with the following specific questions:

My first project, aimed to understand how young and matured adult born granule cells can perform distinct neuronal functions.

- How do the various biophysical properties of ABGCs mature?
- Which specific intrinsic physiological properties enable the emergence of distinct functional populations?
- When and how do ABGCs switch their "young" functionality to "matured" operation state during their postmitotic development?

In the second project, I addressed the synaptic mechanisms responsible for the interpretation of distinct physiological activities of GCs within the CA3 circuit.

- Do short, truly physiological GC bursts accompanied by distinct synaptic plasticity mechanism than single AP firing?
- How physiologically relevant activity patterns, containing single APs, short high frequency bursts and long quiescent periods are translated by the CA3 neurons?

3. Materials and methods

3.1. Virus mediated birth-dating of granule cells

To follow up the development of ABGCs we labeled dividing cells in the DG of 31 to 33 days old rats by Moloney murine leukemia virus vector (Zhao et al., 2006; Jessberger et al., 2007). The surgeries and the virus labeling were done by János Szabadics. Male Wistar rats (95-135 g body weight) were injected with 0.8–1 μl CAG-GFP or CAG-RFP using stereotaxically targeted (5.7-5.8 mm posterior, ±4.4-4.5 mm lateral and 5.6-6 mm ventral from bregma), conventional Hamilton syringe under ketamine/xylazine/pipolphen anesthesia (83/17/7 mg/body kg). By this approach, adult born granule cells were labeled along a broad longitudinal range (2-3 mm) of the hippocampi. Note that in animals 3-10 weeks after virus injection, we never found cells younger than 3-weeks-old based on their cellular properties, indicating the reliability and precision of the birth-dating method. After the surgical procedure two or three siblings were housed together in large cages (75 cm x 35 cm) equipped with a running wheel, toys and shelters until the electrophysiological experiments were performed, because running is known to increase the number of surviving adult-born neurons (Kempermann et al., 1997; van Praag et al., 1999; Tashiro et al., 2003).

3.2. Slice preparation

All the electrophysiological data during my Ph.D. projects were obtained by *in vitro* recordings from acute hippocampal slices prepared from Wistar rats. For recording ABGCs adult, postnatal day 51-105 (corresponding to recording of 20-72 days old virus labeled ABGCs) or postnatal day 68-101 (adult non-labeled) male rats were used. GCs born during the development of the brain were recorded in young, 17-18 days old animals. In the project examining the effect of single GC burst in the CA3 circuit , the acute brain slices were made by using adolescent rats (postnatal day 21–45, both sexes). The animals were deeply anesthetized with isoflurane (in accordance with the ethical guidelines of the Institute of Experimental Medicine Protection of Research Subjects Committee) and 350 μm slices were cut in ice-cold ACSF containing (in mM): 85 NaCl, 75 sucrose, 2.5 KCl,

25 glucose, 1.25 NaH_2PO_4, 4 $MgCl_2$, 0.5 $CaCl_2$, and 24 $NaHCO_3$. The orientation of cutting was close to horizontal, the brains were positioned to obtain multiple slices perpendicular to the axis of the hippocampus at its medial part. This sectioning plane is parallel with the mossy fibers and preserves their connections to target cells in CA3 area (Bischofberger et al., 2006). Slices were incubated at 32°C for 60 minutes after cutting then were kept at room temperature until used for recordings in a solution composed of (in mM): 105,5 NaCl, 37.5 sucrose, 2.5 KCl, 17.5 glucose, 1.25 NaH_2PO_4, 3 $MgCl_2$, 1.25 $CaCl_2$, and 25 $NaHCO_3$. Under these conditions slices were viable and were used for up to 8-12 hours.

3.3. Electrophysiological recordings

Cells were visualized with an upright microscope (Eclipse FN-1; Nikon) with infrared (900 nm) Nomarksi differential interference contrast optics. The standard recording artificial cerebrospinal solution (ACSF) was composed of (in mM): 126 NaCl, 2.5 KCl, 26 $NaHCO_3$, 2 $CaCl_2$ (unless stated otherwise), 2 $MgCl_2$, 1.25 NaH_2PO_4, and 10 glucose. The ACSF was saturated by the mixture of 95% O_2 and 5% CO_2 during the recordings. The temperature was held at 35 - 36°C (unless decreased to 28-29°C see Fig. 14) during the experiments. Electrophysiological recordings were acquired with Multiclamp 700B amplifiers (Molecular Devices) and pClamp10 software.

Presynaptic CA3 GCs and MFBs in "whole cell" configuration were recorded in current clamp configuration (digitized at 50 kHz and low-pass filtered at 10-20 kHz) and were held at ~ -75 mV. The pipette capacitance was greatly reduced and optimized by capacitance neutralization in the bridge balance compensated presynaptic current clamp recordings. Action potentials were evoked by current pulses (usually1.5 ms long, 1.8 nA in the case of somatic, and 1 ms long, 300pA in MFB recordings). MFBs however, were preferentially targeted in cell attached configuration. In these recordings MFBs were stimulated in voltage clamp mode, usually 0.5-1 ms long 140-200 mV pulses were required to reach the AP threshold. Action currents were monitored at leak subtracted traces. Postsynaptic cells were recorded in voltage clamp mode (digitized at 50 kHz and low-pass filtered at 4-6 kHz) the membrane potentials were clamped to -70 mV in standard conditions. The series resistance (5-30 MΩ) was monitored by the capacitive

artefact in response to a 5 mV step in each trace and controlled during the recordings. R_s compensation (70-75%) was only applied in some experiments among the disynaptic IPSC (diIPSC) recordings where pyramidal cells were held at -50mV.

Recording pipettes were pulled from either thin or thick wall (1.12-0.86 ID) borosilicate glass capillaries, the pipette resistance was ranging 3–4.5 MΩ for somatic recordings and 10-12 MΩ for MFB recordings. Three different intracellular solutions were used. First, in standard recording conditions ABGCs and monosynaptic pairs (presynaptic CA3 GCs or MFBs to postsynaptic INs), were recorded in an intracellular solution containing (in mM) 90 K-gluconate, 43.5 KCl, 1.8 NaCl, 1.7 MgCl$_2$, 0.05 EGTA, 10 HEPES, 2 Mg-ATP, 0.4 Na$_2$-GTP, 10 phosphocreatine-disodium, and 8 biocytin (pH 7.25). Second, in certain experiments (Fig. 24) presynaptic recordings were done with a modified version of the first intracellular solution where 40mM KCl was substituted for CsCl. Third, for attempting disynaptic connections, postsynaptic pyramidal cells were patched by gluconate based intracellular solution that allows distinguishing between inhibitory and excitatory postsynaptic currents (IPSCs and EPSCs respectively). This solution was composed of (in mM) 133.5 K-gluconate, 1.8 NaCl, 1.7 MgCl$_2$, 0.05 EGTA, 10 HEPES, 2 Mg-ATP, 0.4 Na$_2$-GTP, 10 phosphocreatine-disodium, and 8 biocytin (pH 7.25).

The chemicals for the intracellular and extracellular solutions were purchased from Sigma-Aldrich and pharmacological compounds were purchased from Tocris Bioscience. DCG IV (1 μM), MSOP (150 μM), SR 95531 (gabazine, 5 μM) were dissolved in ACSF. Phorbol 12,13-dibutyrate (PDBu, 1 μM), Go 6976 (250 nM), GF 109203X (1 μM), Calphostin C (1 μM), U 73122 (2.5 μM), BINA (5 μM), AMN 082 (1 μM) were dissolved first in DMSO and diluted at least 2000 times in ACSF. EGTA (0.5 - 2.5mM) and PKC (19-36) (100 μM) were added to the intracellular solution.

3.4. Calculation of the integrative and biophysical parameters of ABGCs

We characterized the integrative properties of individual ABGCs by two reliable parameters, which measure the gain of the input-output functions: the average slope (ASL) and the variance (VAR) of the slope of input-output curves. The calculated parameters (average slope, variance and offset) were weighted by the different

frequencies using empirically determined correlations to obtain a pooled, frequency-independent data point from each recorded cell. *Average slope (ASL)* was calculated as the arithmetic mean of the first derivative of the input-output function and weighted by the square root of the frequency. Frequency-weighted *variance of the gain of the firing (VAR)* was calculated as the variance of the first derivative of the input-output function divided by the frequency. Thus, these two measures are sensitive to different aspects of the input-output function of a given cell and characterize individual cells with a single and reliable value. High ASL value suggests that the given cell is capable of large output changes in response to unitary input changes; whereas the large VAR highlights that the cell is more sensitive to a particular input intensity range. Importantly, the ASL and VAR values remained stable for individual cells provided stable membrane potential, input resistance and capacitance values and well-compensated bridge balance. These parameters were strictly monitored in every recorded trace using a 50 ms long -50 pA steps and manually corrected when it was necessary. Recordings were excluded if the resting membrane potential changed more than 4 mV compared to the initially measured values. *The offset of the input-output function* was defined as the peak amplitude of the current waveform necessary to reach larger firing frequency than the half of the input frequency. For normalization, we weighted the values with the fourth root of the input frequencies. Correlations are characterized with adjusted R-Square (R^2).

Input resistance (R_{in}) was measured as the average steady-state voltage response to -10 pA current steps (30-100 traces excluding traces with large spontaneous events). *Membrane time constant (τ_M)* was fitted with single exponential on these traces between 2-100 ms both at the onset and the end of the current step. The *maximum rate of rise (peak dV/dt)* was measured on the first spike that was elicited using square pulse currents without *post hoc* filtering. Action potentials were defined as larger deflection in the first derivative of the recorded voltage trace than 20 mV/ms following post hoc low-pass filtering at 4 kHz. The *maximum firing capability* of the cells were challenged by 1 second long square current injections with increasing amplitude (Δ20pA) until depolarization block was reached. *Action potential threshold* was measured as the voltage at 20mV/ms of the dV/dt. The *whole cell capacitance* was measured in voltage clamp recordings using a -5 mV voltage step at -70 mV holding by measuring the integral area of the current

response (measured from the steady-state current level) and divided by the voltage step amplitude.

3.5. Monosynaptic connections from mossy fibers

Altogether, 171 monosynaptic pairs were included in the project exploring the MF burst induced plasticity in different CA3 cells (including IvyCs, AACs, PV+BCs, CCK+BC, SLCs, PCs and unidentified cells). In 164 cases, the presynaptic partner was a CA3 GC which allowed stable recordings for long time; in 7 cases, the presynaptic partner was a MFB. Additionally, 42 monosynaptic connections were recorded to map the connectivity of the CA3 FFI circuit, in 32 cases the presynaptic partner was a MFB.

MFBs were preferentially attempted in cell attached configuration to minimalize the disturbance of the presynaptic milieu (Vyleta and Jonas, 2014). The pipettes were filled with intracellular solution because during long recordings the membrane patch usually broke in, and the recordings continued in whole cell configuration. MFB recordings were prudently monitored and evaluated, especially connections to PCs. Only those recorded epochs where the release was stable were included in the analyses. Traces or whole experiments were excluded if the release properties apparently changed during the experiment, or the synaptic properties in control condition were presumably disrupted, or when single presynaptic action potentials were not clearly recognizable. CA3 GCs were the other presynaptic mossy fiber source, they provide a reliable, easily accessible and stable model for studying single MF inputs by standard whole cell paired recordings (Szabadics et al., 2010). During recordings CA3 GCs were identified based on the location of their soma, their GC identity was verified by their unmistakable firing pattern and morphological features.

During analysis of the data, EPSC amplitude changes were measured on average traces. Minimum 3, but usually 5-10 traces were averaged in all data points. To increase the robustness of the control responses all traces recorded during a single epoch were averaged, thus one single control is related to 3-4 different data points (different post-burst timings or burst lengths). Paired pulse ratios were calculated from the average traces by dividing the average of the 2nd and the 3rd EPSC amplitudes with the 1st EPSC

amplitude at the 20 Hz control and test pulses. Synaptic delays were measured on single traces from the peak of the presynaptic action potential to the onset of the events.

3.6. Disynaptic connections from mossy fibers

To test the effect of single MF bursts on the recruitment of CA3 cells 17 disynaptic inhibitory connections were recorded in PCs, (with n = 1 presynaptic MFB, and n = 16 CA3 GC), and 6 disynaptic excitatory connections were recorded in CA3 INs, (all with presynaptic CA3 GC). To map the connectivity of the MF driven FFI circuit 34 disynaptic connections (with n = 10 MFB, and n = 24 CA3 GC) were identified in 321 tested MF connections to CA3 PCs (with n = 112 MFB, and n = 209 CA3 GC). In addition, 5 disynaptic inhibitory connections (with n = 3 MFB, and n = 2 CA3 GC) were identified in 42 monosynaptic MF to CA3 PC pairs.

Disynaptic inhibitory connections were attempted in paired recordings of CA3 GC and pyramidal cells with the gluconate based intracellular solution and the membrane potential was held below the reversal potential of Cl^- usually at -50 mV, thus IPSCs were clearly distinguishable from EPSCs. Disynaptic excitatory connections were incidentally found during recording MF connections to INs. The onset delays of the disynaptic EPSCs (diEPSCs) were clearly distinguishable from the monosynaptic EPSCs. The excitatory nature of the events was confirmed by depolarizing the postsynaptic cells close to the reversal potential of chloride or gabazine application. The disynaptic connections indirectly reported the strength of the MF connections onto their postsynaptic partners. The stronger the MF connections, the larger the probability of driving AP firing in their postsynaptic partner (not recorded, intermediate cell) resulting in larger incidence of disynaptic events. The analysis of both diIPSCs and diEPSCs were done in a predefined 5 ms long time window (between 1.5 - 6.5 ms or 2-7 ms measured from the peak of the presynaptic action potential). All potential diIPSCs or diEPSCs were counted, and their kinetic properties (10-90% rise time, decay time constant) were measured if it was possible. Since reliable distinction between spontaneous and evoked disynaptic events were impossible, some spontaneous synaptic events were likely included. Note however that, the absolute values are slightly overestimating the frequency of the spontaneous

EPSCs, the relative impact of the burst is therefore still underestimated and thus did not affect the drawn conclusions.

To explore the organization of the feed forward inhibition the presence or absence of disynaptic inhibitory connections were analyzed in the candidate pairs. To provide unbiased recording criteria, presynaptic MF boutons and postsynaptic PCs were recorded at 30-50 μm from the surface of the slice. Presynaptic CA3 GCs were 30-100 μm deep to avoid cut axons. The somatic distance of CA3 GCs and PCs were maximum 200 μm. In all candidate pair, at least 5 traces were tested and all experiments were analyzed by at least two investigators. Pair were included in the analysis only if the data was sufficient to decide on the presence or absence of diIPSCs in them.

3.7. Anatomical analysis

The *post hoc* anatomical processing and the immunohistochemical staining were done by the technicians of our laboratory, Dóra Hegedűs, Andrea Juszel and Dóra Kókay. After electrophysiological recordings, slices were fixed for one day in 0.1 M phosphate buffer containing 2% paraformaldehyde and 0.1% picric acid at 4°C. After fixation, slices were resectioned at 60 μm. For immunocytochemistry, sections were incubated with one or two of the following primary antibodies raised against parvalbumin (PV25, 1:1000, polyclonal rabbit, Swant), SATB1 (sc-5989, 1:400, polyclonal goat, Santa Cruz) cholecystokinin (CCK) (C2581, 1:1000, polyclonal rabbit, Sigma), somatostatin (MAB354, 1:500, monoclonal rat, Chemicon), or neuronal nitric oxide synthase (nNOS; N2280, 1:500 mouse, Sigma) overnight in 0.5% Triton X-100 and 2% normal goat serum or horse serum containing TBS buffer at 4°C. Immunoreactions were visualized with appropriate Alexa 488- or Alexa 594-conjugated secondary goat or donkey antibodies (1:500; Invitrogen, Carlsbad, CA) against rabbit, goat, mouse, and rat IgGs, and biocytin staining was revealed using Alexa-350 or Alexa 488-conjugated streptavidin (1:500; Invitrogen, Carlsbad, CA). After washing and mounting in Vectashield (Vector Laboratories, Burlingame, CA), cells were analyzed by using epifluorescence microscope (DM2500; Leica, Germany). For the visualization of axonal and dendritic arbor multiple stack images were taken from a 60 μm thick slice. The maximum intensity projected black and white fluorescent images were inverted for better visibility.

In rare cases, after determining the immunoreactivity of the recorded cells, some sections were further processed to reveal the fine details of the morphology of the cells using the diaminobenzidine (DAB) staining method. Briefly, endogenous peroxidase activity was blocked with 1% H_2O_2. Sections were incubated with ABC reagent (Vectastain ABC Elite kit, 1:500; Vector Laboratories) in 0.1% Triton X100 containing buffer for 1 hour at room temperature. Sections were preincubated with DAB and $NiCl_2$, and the reactions were developed with 0.2% H_2O_2 for 3–10 minutes. Sections were dehydrated on slides, and mounted using DPX mounting medium (Electron Microscopy Sciences). Cells were visualized with epifluorescence or conventional transmitted light microscopy (DM2500; Leica, Germany).

3.8. Classification of the postsynaptic cells

Identification of the postsynaptic partners of mossy fiber connections was crucial to evaluate the data. The recorded cells were classified based on multiple criteria. Altogether (n=67) Ivy cells were identified by their characteristic firing pattern (late firing, large and slow after hyperpolarization), dense axon arborization and short dendrites. 9/14 tested cells were nNOS, 0/20 were CCK and 0/20 were somatostatin positive. PV+ basket cells PVBCs (n=5) were identified based on their fast spiking activity and axons specifically targeting the *stratum pyramidale* and/or co-immunopositivity for parvalbumin (4/4 tested cells) and SATB1 (2/2 tested cells) (Viney 2013). Axo-axonic cells (AACs, n=10) were identified based on their fast spiking activity and characteristic axons outlining axon initial segments on the border of *strata pyramidale* and *oriens* and also the presence of parvalbumin (8/9 tested cells) and lacking SATB1 immunopositivity (0/6 tested cells). Regular spiking cells (n= 8) were classified as CCK immunopositive interneuron. Spiny lucidum cells (n=25) were identified based on their densely spiny dendrites and somatostatin immunopositivity (15/19 tested cells), additionally 0/13 tested cells were CCK immunopositive. Pyramidal cells were targeted in the *stratum pyramidale* and were identified based on the unmistakable firing pattern and morphology (pyramidal shaped soma, thick densely spiny dendrites, complex spines in the stratum lucidum).

3.9. Statistical analyses

Data were analyzed by pClamp (Molecular Devices), Origin (OriginLab), and Excel (Microsoft) softwares. Data are presented as mean ± standard error. The statistical tests were done by János Szabadics. One-sample or two-sample unpaired Student's *t* test (indicated as *t* test), paired Student's *t* test (indicated as paired *t* test) and One-way ANOVA were used as indicated in the text. Normality of distributions was tested with Shapiro-Wilks test. Different populations within the intrinsic cellular properties were identified by K-means cluster analysis and multiple Gaussian fitting of their distributions. Hierarchical cluster analysis was performed by Ward method on normalized values. The connectivity ratios with markedly different sample size were compared by Fisher's exact test.

4. Results

4.1. Functional maturation of adult born granule cells

It is currently believed that young adult born granule cells (ABGCs) are necessary for pattern separation in the hippocampus (Clelland et al., 2009; Sahay et al., 2011; Nakashiba et al., 2012), and thus they serve distinct function than that of the matured GCs. There is a consensus that the different functional characteristics of young (4 weeks old) and fully matured (8-10 weeks old) ABGCs emerge predominantly from their distinct cellular properties, which originate from the continuous biophysical development of ABGCs, such as an increase in the membrane surface (Wang et al., 2000; Schmidt-Hieber et al., 2004; Mongiat et al., 2009). However, it is not clear what happens between the 4th and the 8th weeks and which intrinsic functional aspects of individual ABGCs allow the emergence of only two functional populations (instead of widely distributed functionalities) besides the continuous maturation process.
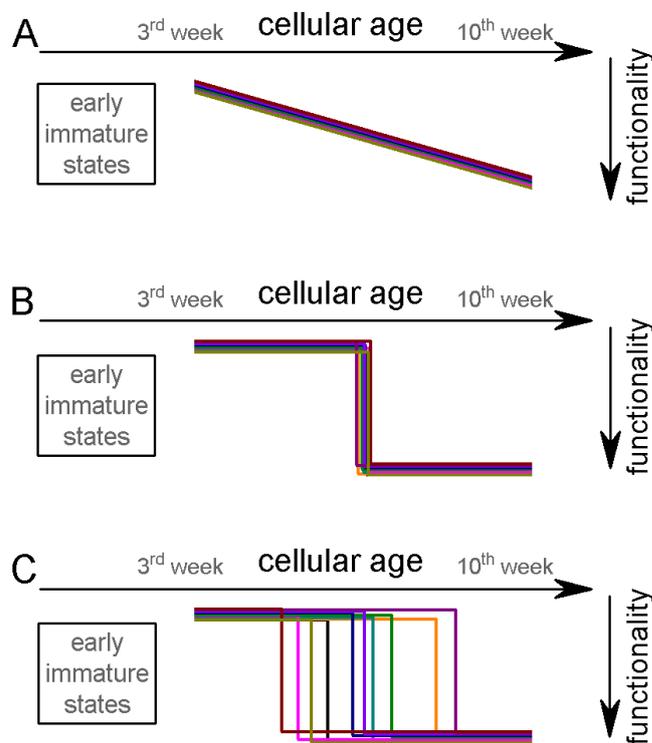
Figure 8. Potential theoretical modes for the postmitotic maturation of functional properties of ABGCs. Each color corresponds to a single ABGC, the predicted distribution of the functionally distinctive properties are shown on the right. **A.** Gradual maturation of the properties results in widely distributed functional continuum. **B.** Temporally predefined functional switch. **C.** The functional switch occurs in an extended temporal window.

We considered three testable possibilities how ABGCs behave between the two stages. First, their functionally distinctive properties may develop continuously (**Fig. 8A**).

However, if this is the case, it may contradict the general notion, the existence of two distinct ABGC populations, instead, ABGCs would provide a functional continuum. The second possibility is that ABGCs during their maturation switch their functionality according to a predetermined program (**Fig. 8B**). In this situation, there are two clearly distinct populations and they would switch within a short temporal window at a predefined stage of their postmitotic life. The third option predicts that ABGCs are susceptible for the functional switch for an extended period waiting for external signals (**Fig.8 C**). Thus, two functionally distinct populations are maintained, but at the level of individual cells the switch can occur within an extended temporal window. Since all three potential maturation processes have important consequences on the physiological potential of the adult neurogenesis, we addressed these hypotheses on a variety of intrinsic biophysical properties in birth-dated individual ABGCs.

4.1.1. Maturation of the biophysical and integrative properties of ABGCs

To analyze the cellular maturation of ABGCs we collected data about a variety of biophysical and integrative properties of individual 3-10 weeks old ABGCs from young adult rats (**Fig. 9**) using a retrovirus mediated labeling method that allows for precise birth-dating of adult born cells (Zhao et al., 2006). Thus, we compared each of the tested parameters in several ABGCs (n = 73 cells) from 8 different age-groups (8-9 cells per age group). ABGCs in the early phase of their maturation (younger than 3 weeks) were not analyzed because they are not yet fully integrated into the hippocampal network due to the lack of reliable spiking. Note that we did not find cells in animals 3-10 weeks after virus injection, with properties of less than 3-week-old cells, indicating the reliability and precision of the birth-dating method.

Majority of the tested membrane properties (including input resistance, membrane time constant, whole-cell capacitance, resting membrane potential, action potential threshold, peak dV/dt of the spikes, and maximal firing rate) of individual 3-10 weeks old ABGCs changed continuously with age, and consequently, the distribution of the data points from individual cells was wide, without the emergence of distinguishable populations (**Fig. 10A-B**) reflecting the continuous maturation of these properties in accordance with previous observations (Mongiat et al., 2009; Marin-Burgin et al., 2012).
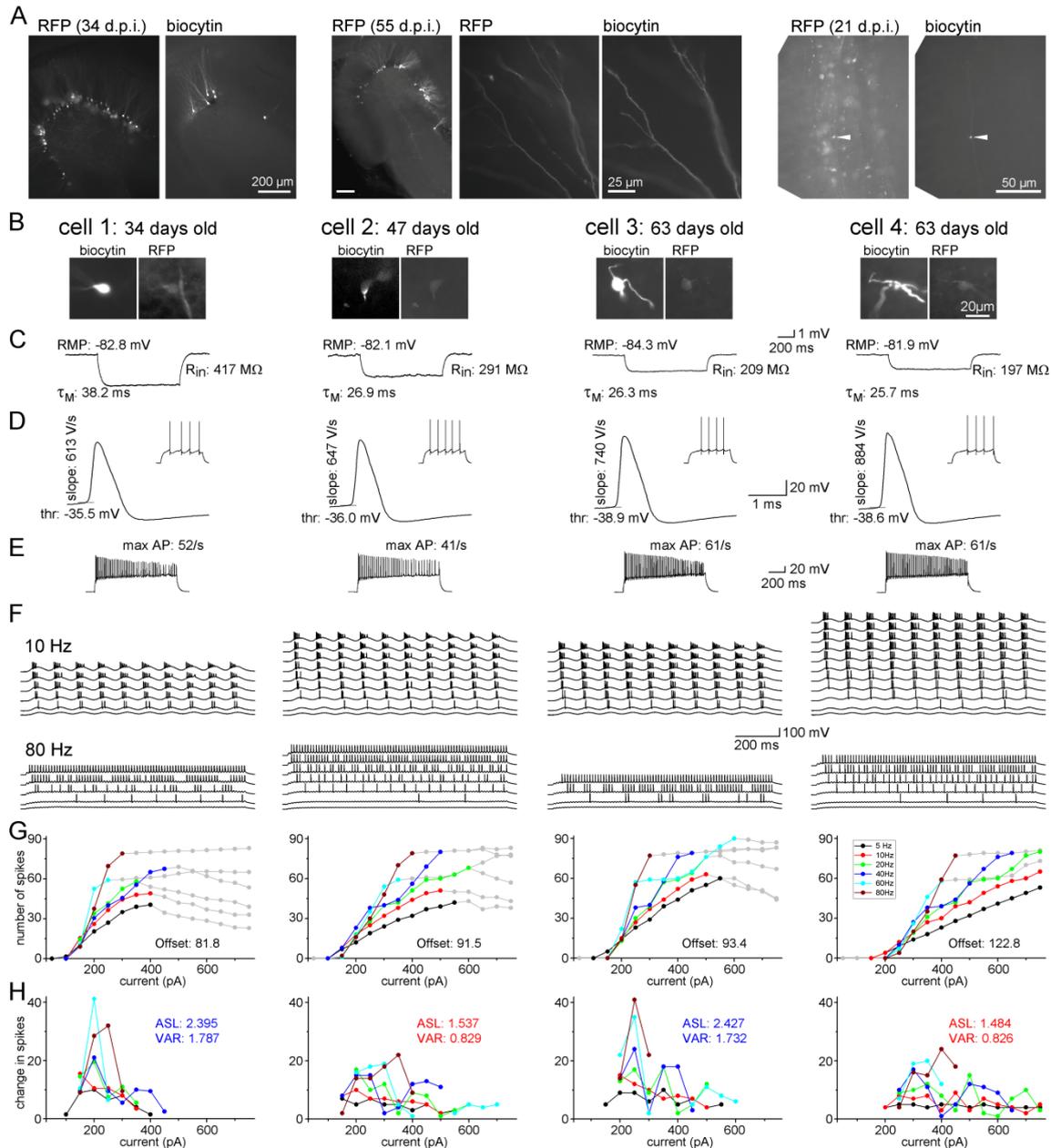
Figure 9. Maturation of the biophysical and integrative properties of ABGCs. A. The RFP and biocytin labeled cells in the dentate gyrus (*left panels*, d.p.i.: day after virus injection), spiny dendrites (*middle panels*), and typical mossy fiber terminals in the stratum lucidum of the CA3 region (*right*) confirm granule cell identity. **B.** Four representative RFP-expressing granule cells 34, 47 and 63 days after CAG-RFP virus labeling. The 63 days old AGBCs were recorded from the same slice. **C.** Average subthreshold voltage responses of the example cells to a small (-10pA) current step. Input resistance (R_{in}), membrane time constant (τ_M) and resting membrane potential (RMP) of the cells are indicated. **D.** Spike parameters of the example cells at lower current intensities (dV/dt: maximal rate of rise, thr: action potential threshold). **E.** Maximal firing rate of the four cells in response to square pulse current injection. **F.** Responses of the cells to sinusoidal current injections with increasing amplitude (Δ50 pA) at 10 and 80 Hz. The traces are shown until the firing reached saturation. **G.** Number of spikes generated in the example cells as a function of the peak amplitude of the injected sinusoid currents at the all tested frequencies. Gray symbols indicate values, which were omitted from the analysis due to lack or saturation of spiking. Offset

values describe the minimum input intensities to reach 50% spiking output. **H.** Increments of the firing (i.e. the first derivative of the curves in panel G) of the cells. These values were used for the calculation of the average slope (as mean, ASL) and the variance of firing (as variance, VAR). Note that cells 1 and 3 have exceptionally large values at certain input intensity ranges indicating that these cells were more sensitive to certain input intensities. This characteristic is quantified by the large VAR value.

In addition to these conventional biophysical parameters we also tested supra-threshold integrative properties of ABGCs. We measured their input-output functions in response to sinusoidal current injections at various frequencies to mimic temporally organized input patterns in physiologically relevant frequency ranges (5, 10, 20, 40, 60 and 80 Hz, **Fig. 9E-H**, (Pernia-Andrade and Jonas, 2014)). It was important to obtain single reliable measures representative of the integrative properties of individual ABGCs that enables their independent analysis. Thus, we derived two measures for each cell, ASL and VAR (standing for average slope and variance of the slope, respectively), from the input-output curves by including all the various tested input frequencies (for further details, see the materials and methods section). In contrast to the conventional membrane properties, the analysis of the gain of the input-output functions of the same cells revealed two significantly distinct populations (**Fig. 10 C-D**, double Gaussian fits, ASL: *F=0.0014,* $R^2=0.849$*,*VAR: *F=0.0001,* $R^2=0.912$ and K-means cluster analysis, *F<10^{-9}*). The input-output function of the first group was characterized by a steep average slope (ASL) and highly variable (VAR) spike responses, suggesting that this cell population is highly suited for disambiguating input-output functions by being exceptionally *sensitive* to certain input strength therefore referred to as S-group (Fig. 9G). Remarkably, within the *S-group* the integrative parameters were independent of the actual age of the individual cells (linear fits on **Fig. 10 C-D**) demonstrating that similar cellular functionality is maintained throughout an extended period (between 3-9 weeks) unless the individual cell switched to the second integrative functions. This second group of ABGCs responded with constantly increasing spike output indicating *linear* input-output characteristics (thereafter referred to as L-group) enabling them to perform distinct computations compared to S-group neurons.
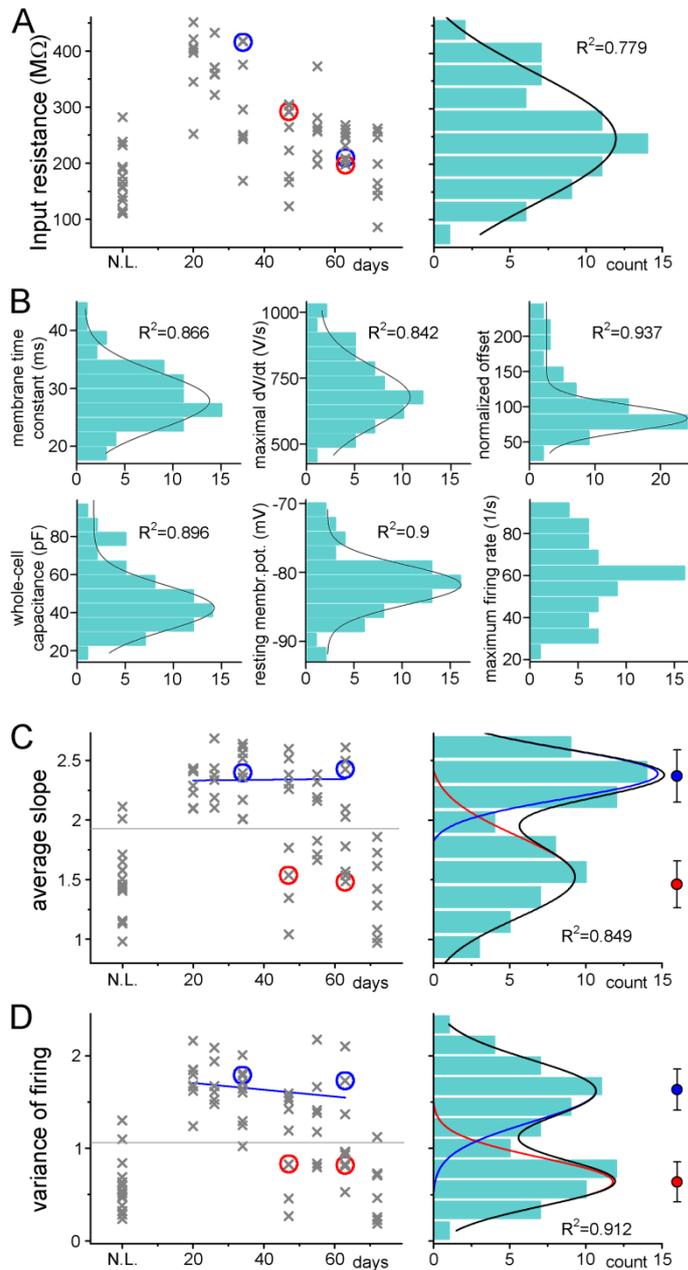
Figure 10. Adult born granule cells can be divided into two distinct populations between 3-10 weeks of age based on cell-to-cell differences in input-output transformation. A. *Left,* Input resistance of individual ABGCs with various ages (gray crosses). Blue and red circles (S- and L-group members, respectively) highlight the values for the example cells shown in Fig. 9. N.L.: not labeled control cells. *Right,* Probability distribution of the data set shows single peak (single Gaussian fit: *F=0.0001*). **B.** Monotonous probability distribution of membrane time constant, whole cell capacitance, resting membrane potential, maximal rate of rise of spikes, relative offset of the input-output curves and action potential threshold data from the same set of cells as above. **C-D.** *Left,* Average slope and variance of the slope of the same individual ABGCs as above with various ages (gray crosses). Blue lines indicate the lack of correlation between the gain of the input-output functions and the age of individual cells within the S-group (linear fit, ASL: $R^2=-0.029$, $p=0.89$, VAR: $R^2=0.01$, $p=0.257$). *Right,* Two populations emerge from the distribution of the average slope values of individual cells (two peaks Gaussian, ASL: *F=0.0014,* VAR: *F=0.0001*). The centers of the two clusters and average distance values from the centers (error bars) are shown on the right (K-means analysis, $F<10^{-9}$, horizontal gray lines on the left panels indicate the separation by the K-means analysis).

4.1.2. Independence of the output properties of individual ABGCs of age and input resistance

Altogether, the above results show that ABGCs form two functionally distinct populations during a long period of their maturation based on their different sensitivity to temporally organized inputs. Intriguingly, members of the two distinct groups (S and L) showed a wide and overlapping range of birthdates (**Fig. 10 C-D** left panels) indicating that age does not directly determine the integrative properties of 3-10 weeks old ABGCs.

Even though their age alone apparently does not directly determine the functionality of individual ABGCs, the probability of whether an individual cell behaved as a member of S- or L-groups shows age-dependence (**Fig. 11A**). All recorded younger cells (3-5 weeks old) were in the S-group and all of the oldest cells (10 weeks old) had L-group properties; however, both functional groups were present with changing probabilities during the intermediate ages between 5-9 weeks of age. This observation was further supported by the parabolic distributions of the mean-variance plots of ASL and VAR (**Fig. 11B**). Thus, the continuously changing probability masked the two functionally distinct groups of ABGCs when global population properties were analyzed as averages.

Our data indicate that in 3-9 weeks old ABGCs, the gain of the input-output properties is not exclusively determined by the input resistance that is generally considered as an indicator of the maturation stage. ABGCs within the S-group achieved similar input-output computations despite largely different input resistances. Strikingly, this becomes clear by the lack of correlations of the gain of individual S-group cells to their input resistance (blue symbols in **Fig. 11C**, ASL: *F<0.045*, R^2=0.087, VAR: *F<0.12*, R^2=0.042). However, the input-output function of ABGCs from the L-group showed the expected dependence on the input resistance of individual cells (red symbols in **Fig. 11C**, ASL: *F<3·10^{-7}*, R^2=0.576, VAR: *F<3·10^{-6}*, R^2=0.47).

Importantly, ABGCs cannot be divided into two populations based on the offset of their input-output functions. In contrast to the gain, it showed a clear dependence on the input resistance of individual ABGCs across both cell populations (**Fig. 11D**, *F<10^{-9}*, R^2=0.697). This indicates that not all functional properties are independent of the fundamental biophysical properties, and also validates the data obtained on the gain parameters.
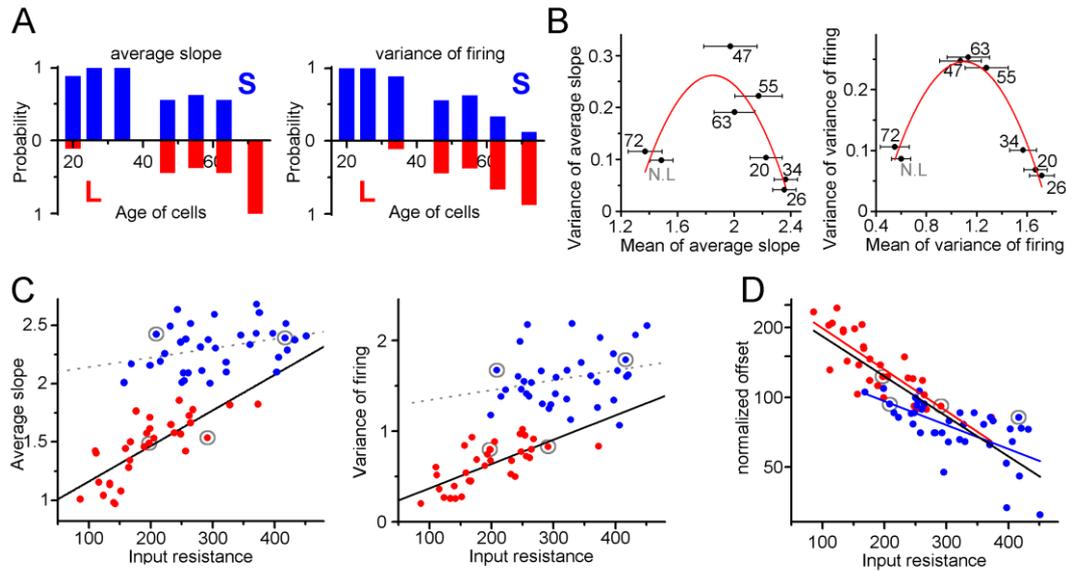
Figure 11. Independence of the output properties of individual ABGCs from age and input resistance. A. Probability of the members of the clusters defined by the K-means analysis continuously shifts from S-group (blue) toward L-group (red) during maturation indicating the higher prevalence of ABGCs with shallow and invariable input-output function. **B.** The occurrence of functional switch on population level is also suggested by the higher variance of the input-output parameters during the transition age period and low variance in the youngest and most matured populations (parabolic fit, ASL: $R^2 = 0.611$, F(ANOVA) = 0.0035; VAR: $R^2 = 0.853$, F = 0.00017). Numbers indicate the age of the data sets. NL stands for non-labeled presumably old cells that were recorded as a control in the same experiments. **C.** Correlation of the integrative parameters with the input resistance within the two functionally different groups (red and blue symbols) defined by K-means cluster analysis. Gray circles indicate the four example cells from Figure 9 (linear fits, ASL: $R^2=0.087$, $p=0.045$ for S-group, $R^2=0.576$, $p=2.9x10^{-7}$ for L-group; VAR: $R^2=0.02$, $p=0.19$ for S-group $R^2=0.467$, $p=2.6x10^{-6}$ for L-group). **D.** Correlation between the offset (normalized current that is needed to reach the half of the input frequency as output) and input resistance of individual ABGCs belonging to the two functionally different groups ($R^2=0.39$, $p=0.0001$ for S-group; $R^2=0.607$, $p=2x10^{-8}$ for L-group; $R^2=0.682$, $p<10^{-8}$ for both groups).

4.1.3. Two functionally distinct populations among non-labeled GCs in adult rats

We tested the supposed coexistence of S- and L-functionalities in "wild type" animals as well, which were not subject to virus injection. Adult rats (P68-101) were kept with running wheels in their home cage to promote neurogenesis (Kempermann et al., 1997; van Praag et al., 1999; Holmes et al., 2004). In order to sample enough ABGCs with various ages, GCs were recorded predominantly in the lower half of the *stratum granulosum* close to the subgranular zone. Importantly, the analysis of the integrative properties (ASL and VAR) confirmed the coexistence of the two populations. The peaks of the double Gaussian distributions in the birth-dated sample (**Fig. 10C**) and in the non-labeled sample (**Fig. 12A**) were remarkably similar (ASL: 1.522±0.056 and 2.389±0.028

46

vs. 1.611±0.008 and 2.377±0.013; VAR: 0.638±0.046 and 1.621±0.052 vs. 0.616±0.02 and 1.477±0.09) and the K-means analyses also predicted similar centers and average distance from centers (ASL: 1.461±0.197 and 2.37±0.219 vs. 1.627±0.182 and 2.409±0.168; VAR: 0.637±0.217 and 1.643±0.223 vs. 0.659±0.163 and 1.536±0.251). The group-specific dependence (or lack of that) of the slope on the input resistance was similar to the birth-dated ABGCs (**Fig. 12B**, compare to Fig. 11C).
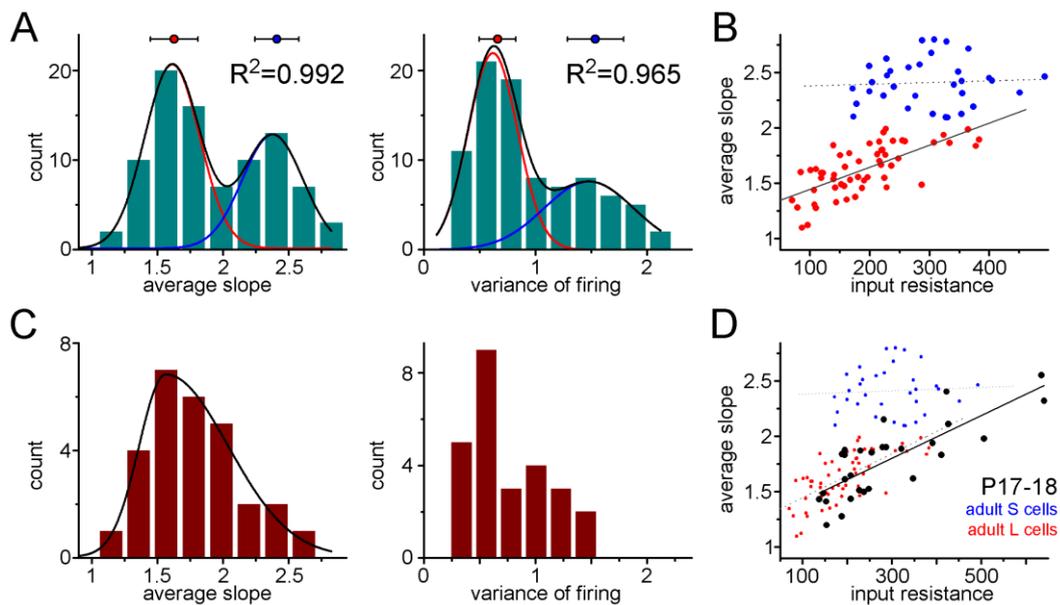
Figure 12. Integrative properties of individual GCs in adult and young (P17-18) non-labeled animals. A. Coexistence of S- and L-functionalities among non-labeled granule cells (unknown cellular age) in adult (P68-101) rats. The peaks of the double Gaussian distributions: ASL: 1.611±0.008 and 2.377±0.013; VAR: 0.616±0.02 and 1.477±0.09. Centers and average distance from centers determined by K-means analyses: ASL: 1.627±0.182 and 2.409±0.168; VAR: 0.659±0.163 and 1.536±0.251. **B.** The observed group-specific dependence (or lack of that) of the slope on the input resistance was similar in birth-dated ABGCs. **C.** Lack of two functional population in young (P17-18) rats. **D.** The ASL of all individual cells shows similar correlation with adult L-group cells (1.93±0.29/GΩ in P17-18 vs. 1.99±0.29/GΩ L-cells in adults) the P16-17 data is plotted over the adult data (panel B) for direct comparison.

Next, we addressed whether S and L-functionalities are also present in developmentally generated GCs. In these experiments, we measured the integrative properties of granule cells in P17-18 rats and used the same analysis criteria as in recordings from adult animals. At this postnatal age, all spiking granule cells are from the first generation of developmentally generated population (Bayer, 1980a, 1980b). Surprisingly, the tested cells were not separable based on the slope of the input-output

function and we found that large majority of the tested cells showed L-functionality (**Fig. 12C-D**) similar to the oldest ABGCs (10 weeks old). Importantly, when all cells from these young animals are considered, their slope of input-output function showed a very similar correlation to their input resistance as in the case of L-group cells from adult animals (1.93±0.29/GΩ in P17-18 vs. 1.99±0.29/GΩ L-cells in adults). This correlation holds in spite of the larger average and wider range of input resistance (288±23MΩ vs. 191±10MΩ) of the cells in young animals compared to L-cells in adults. This shows that in young animals practically all granule cells follow the generally accepted dependence of the slope of input-output curve on the general parameters of cellular excitability such as input resistance. This important observation may suggest that the slope of input-output function mature differently in developmentally born cells compared to adult-born ones.

4.1.4. Complex mechanisms maintain the two stable states of the input–output transformation of individual cells

To reveal the underlying mechanisms responsible for sustaining two distinct integrative states, first, we tested the possibility whether all measured biophysical parameters of individual ABGCs can cooperatively predict the functional separation. We performed hierarchical cluster analysis of the recorded cells based on the seven intrinsic parameters (resting membrane potential, membrane time constant, whole cell capacitance, input resistance, AP threshold, maximum dV/dt of the APs, maximal firing rate) in order to define two groups (**Fig. 13**). These two groups were correlated with the S- and L-group identity of the same cells as defined by the K-means analysis above. The two intrinsic parameter groups determined by cluster analysis did not match with the S- and L-group identity of the individual cells. This result shows that consideration of multiple parameters by their arithmetical values, similarly to input resistance alone, is not sufficient to predict the functional separation of S- and L-groups.

Having established the clear separation of the two integrative functionalities in non-labeled GCs in the adult DG (**Fig. 12A-B**), we took advantage of the large number of easily accessible GCs for further analysis. First, biophysical and integrative properties were recorded in control conditions, than we determined the same parameters after one of the four following general interventions in each cell.

1.) Lowering the recording temperature from 35-36°C to 28-29ºC resulted in the elimination of the separation of S- and L- groups (**Fig. 14A**). With this intervention, practically the same mechanisms (such as activation of voltage-gated channels) were available during the two recording conditions, but the cellular excitability was altered in a complex manner. For example, changes in the classical excitability parameters (e.g. input resistance, AP threshold) suggested increased excitability, whereas the capability to elicit high frequency firing is decreased.

2.) Increasing the extracellular calcium concentration from 2 mM to 4 mM challenged the excitability of the cells by enhancing calcium dependent mechanisms (**Fig. 14B**). The effect on the ASL did not depend on the initial values (i.e. there was no group specific effect); even though the calcium elevation have similar effects on the general excitability parameters of the cells as the decreased temperature.

3.) Activation of GIRK channels by ML297 (2.5 µM) application increased the ASL only in a subset of the recorded cells, which had low ASL during control conditions like the L-group cells (**Fig. 14C**). In spite of the similar group specific effects on ASL, GIRK activation and lower temperature had largely opposite effects on the biophysical properties.

Figure 13. Hierarchical cluster analysis considering multiple biophysical parameters of the individual cells. Cluster analysis was performed with Ward method on the normalized values of resting membrane potential, membrane time constant, whole cell capacitance, input resistance, threshold, peak dV/dt, maximal firing rate. Data from individual cells are aligned vertically, thus the order of the points along the X-axes is determined by the results of the cluster analysis. Blue and red symbols are corresponding to S- and L-functionalities.

4.) Blockade of synaptic receptors by GABA$_A$ antagonist gabazine (5µM) and AMPA/kainate receptor antagonists CNQX (10µM) slightly increased the ASL value (**Fig. 14D**). However, the effect was not depended on the initial state of the tested cells

excluding the possibility that S- and L-group properties emerge from distinct synaptic drives (Dieni et al., 2013).
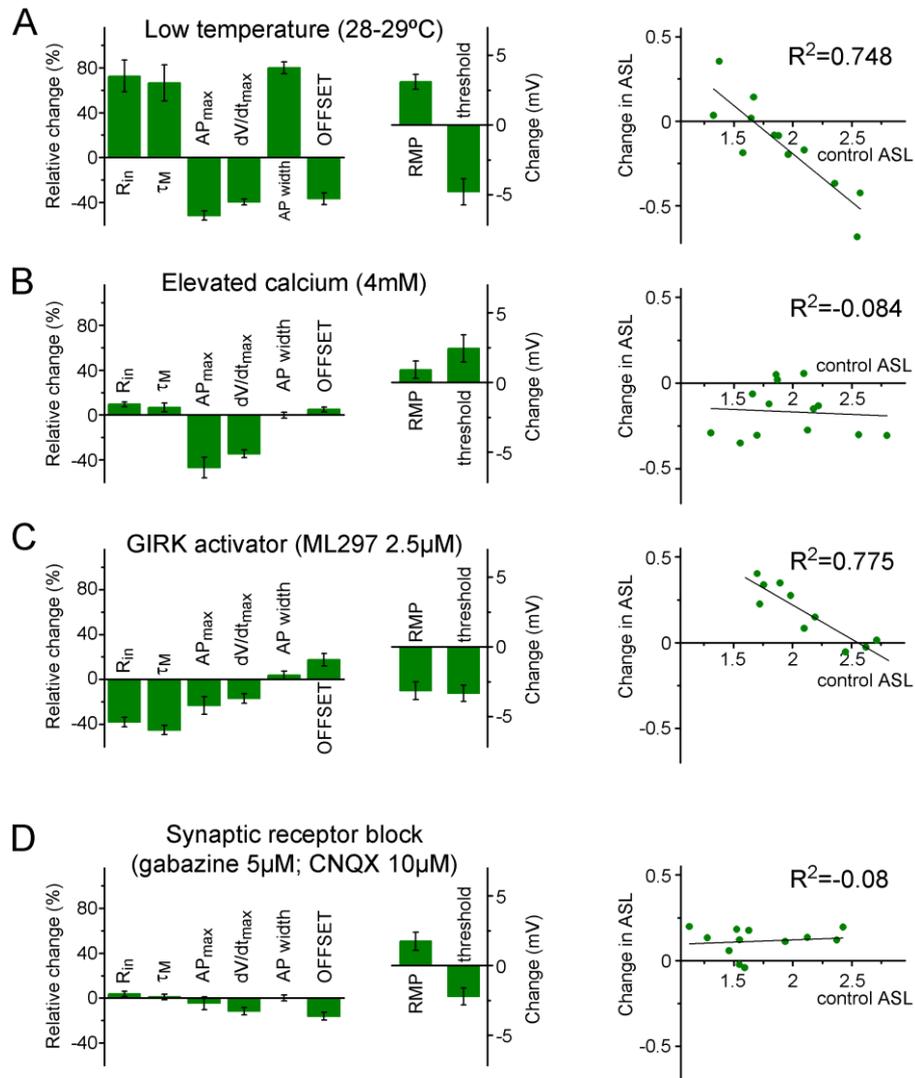
Figure 14. Alteration of multiple biophysical properties by robust general interventions. Left column graphs show the relative changes and absolute values of voltage shifts in the biophysical properties of the recorded non-labeled cells. The right graphs show the change in the ASL during interventions plotted against the initial ASL value of individual cells (R^2 values corresponding the linear fits are indicated above the graphs). **A.** The recording temperature was decreased from 35-36°C to 28-29°C. **B.** The extracellular calcium concentration was increased from 2 mM to 4 mM. **C.** GIRK channels were activated by ML297 (2.5 µM) **D.** Synaptic receptors were bloched by $GABA_A$ antagonist gabazine (5 µM) and AMPA/kainate receptor antagonists CNQX (10 µM).

4.2. Effect of single physiological granule cell bursts on the recruitment of postsynaptic CA3 neurons

In the next study, we addressed the synaptic plasticity mechanisms responsible for the interpretation of distinct physiological activities of GCs within the CA3 circuit. We tested the consequences of single MF bursts on the monosynaptic connections in various types of CA3 neurons. In the first set of experiments, we recorded 78 connected pairs with identified postsynaptic feedforward interneurons (FF-INs), further 39 reliable connections with non-identified postsynaptic GABAergic cells, 12 pairs with postsynaptic PCs and 25 pairs with septum-projecting spiny lucidum cells (SLCs). The FF-INs included Ivy cells (IvyCs, n = 55 pairs), axo-axonic cells (AACs, n = 10 pairs), parvalbumin-expressing, fast-spiking basket cells (PV+BCs, n = 5 pairs), and cholecystokinin (CCK) expressing interneurons (CCK+INs, n = 8 pairs). Note, that the differences in the number of paired recordings from each postsynaptic target reflect neither the occurrence of the cell types nor the probability of connectivity from GCs (Szabadics and Soltesz, 2009). We applied two different approaches to obtain precise control of the synaptic outputs of single MFs. First, direct intracellular or cell-attached recordings from MF terminals (n = 7 pairs) allowed us to assess the properties of unitary EPSCs from individual DG GCs to CA3 neurons (Szabadics and Soltesz, 2009). Second, we took advantage of ectopic GCs located in the CA3 (CA3 GCs), whose morphological and synaptic properties are indistinguishable from those of DG GCs (Szabadics et al., 2010), allowing us to perform longer and more stable somatic recordings. The results from the two types of presynaptic MF recordings were comparable and therefore grouped together for analysis. In the first set of experiments, which aimed to reveal the effects of physiological activity patterns of single GCs, the bursts were modelled as a single train of 15 APs at 150 Hz. Before and with various time delays after each burst, the unitary connections were tested with 3 APs at 20 Hz (**Fig. 15**). Notably, the 3 APs were not intended to model physiological activities but to enable monitoring synaptic changes (see later). Thus, the first APs of the low frequency spike triplets were considered to examine the postsynaptic responses for single APs before and after burst while the purpose of the 2nd and the 3rd APs were to test the short-term plasticity.
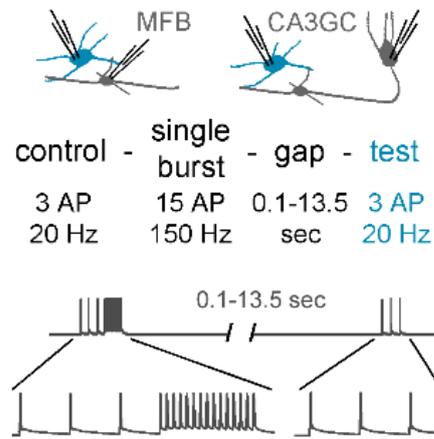
Figure 15. Experimental approach. Schematic representation of the two alternative strategies for recording unitary MF responses in CA3 neurons. Large MF terminals or CA3 GCs were first stimulated with 3 APs at 20 Hz, followed by a single, usually 15-AP burst (150 Hz). After various time delays (0.1-13.5 s) the 3AP stimulation at 20 Hz was repeated. The effects of a single presynaptic burst on each identified postsynaptic cell was tested using similar protocols with different time delays between burst and test AP-triplets. The elapsed time between each test protocol was 1 or 1.5 minute. This protocol was designed to model all the unique temporal features of the GC activity such as low frequency firing, short high frequency bursts and different lengths of quiescent periods. To examine the postsynaptic responses for single APs the first APs of the low frequency spike triplets were considered while the 2nd and the 3rd APs were evoked to gain insight of the short-term plasticity.

4.2.1. Effect of single presynaptic MF bursts in FF-INs

In our experimental conditions the basal properties of MF-EPSCs onto FF-INs and their short-term plasticity, ranging between slight facilitation and slight depression, were consistent with previous results (Tóth and McBain, 1998; Toth et al., 2000; Szabadics and Soltesz, 2009; Torborg et al., 2010).

Strikingly, during our protocol modeling the physiologically relevant activity patterns of GCs, single MF bursts had an unexpectedly large effect on the subsequent monosynaptic EPSCs in FF-INs, demonstrated in a representative IvyC on (**Fig. 16**). The amplitudes of single-AP-evoked unitary responses tripled between 1.5 and 6.7 s following single presynaptic bursts compared with the responses before the burst (3.09 ± 0.13-fold amplification, from average -43.8 ± 4.6 pA to -109 ± 8.6 pA; n = 78 pairs, n = 154 individual data points, see the summary graph of all identified FF-INs on **Fig. 16H**). Importantly, the amplification of MF-EPSCs in FF-INs was not instantaneous and instead developed during the first second after single presynaptic bursts. After this initial increase, the amplification was maintained at a similar level between 0.7-8 s ($p = 0.54$, One-Way ANOVA) before returning to similar amplitudes as their baseline ($p = 0.081$, n = 6 data points, *t* test, 9.5-13.5 s after burst). The unique temporal profile of the phenomenon differentiates it from classical post-tetanic potentiation (Alle et al., 2001; Mori et al., 2007), that is the largest immediately after high-frequency stimulation and continuously decays back to baseline.

Importantly, single MF bursts had remarkably similar effects on all the tested postsynaptic FF-IN groups, including IvyCs, AACs, CCK+INs and PV+BCs, despite their specialized roles and mechanisms within hippocampal circuits (Somogyi et al., 2013). See the summary plots comparing the effect of MF bursts to the pooled FF-IN data on **Figs. 17-20** showing representative examples of the identified FF-IN types.

Figure 16. Single MF bursts robustly enhance monosynaptic EPSCs in CA3 FF-INs. A-G. The effect of a single burst is demonstrated on a CA3GC to IvyC connection. **A.** Typical firing patterns of the pre- and postsynaptic cells. **B.** Inverted fluorescent image of the biocytin-labelled CA3 GC and IvyC marked by gray and blue asterisks, respectively. **C.** Characteristic dendritic morphology (left) with spines (right, top) and large MF terminals (right, bottom) of the CA3 GC. **D.** Axons of postsynaptic IvyC in the *stratum radiatum* of the CA3. **E.** The presynaptic stimulus protocol is shown to highlight the unusual timescale. Control: 3 APs at 20 Hz, burst: 15 APs at 150 Hz, gap: 1, 3.5, 6, 8.5 seconds. One trace was recorded in every minute to let the connection rest and recover to the original state. **F.** Average response for the burst. **G.** Average responses of the four different data points after the single 15 AP burst (blue traces) compared with the control responses (black traces). The duration of the silent period (gap) after the burst is indicated for each trace pair. **H.** Summary graph shows the time-course of the amplification of the single-AP-evoked monosynaptic EPSCs after single 15-AP presynaptic bursts in all postsynaptic cells identified as FF-INs. Data is presented relative to the control (1, dashed line). The average data includes n = 280 individual data points in n = 78 pairs where the postsynaptic cell was a FF-IN (IvyCs: n = 55 pairs; AACs: n = 10; PV+BC: n = 5; CCK+IN, n = 8).
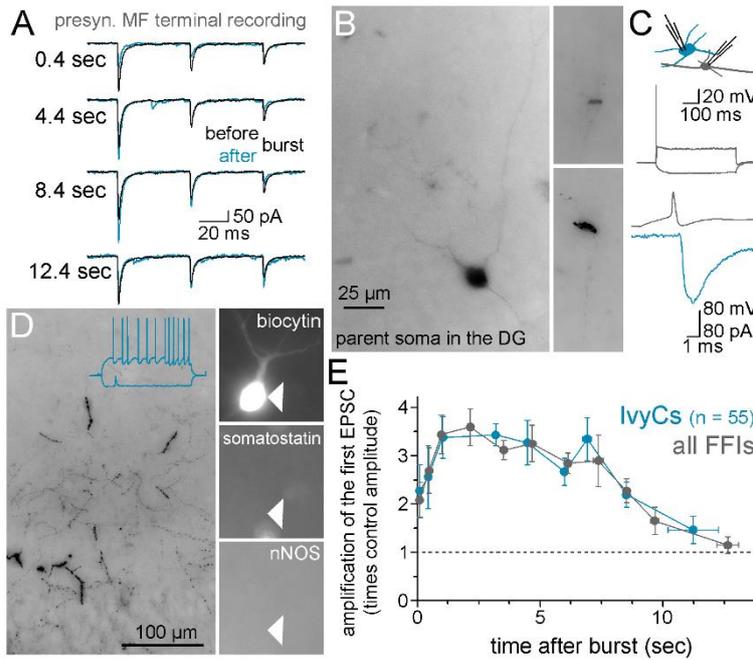
Figure 17. Effect of single MF bursts in postsynaptic IvyCs. A. Effects of single bursts on unitary EPSCs in a representative MF terminal to an IvyC pair at four different time points after the bursts. **B.** *Left*: the back-labeled parent soma in the DG of the presynaptic MF terminal recorded in the CA3; *right*: MF terminals along the recorded axon. **C.** *Upper*: typical firing pattern of the presynaptic MF terminal; *lower*: a single trace pair showing a simultaneous AP in the presynaptic MFB and a single EPSC in the IvyC, which were collected at the beginning of the intracellular recording. **D.** *Left*: axons of the postsynaptic IvyC in the *stratum radiatum* of the CA3; *right*: immunolabeling of the soma for somatostatin and nNOS (negative for both). The inset shows the firing pattern of the IvyC. **E.** Comparison of the amplification of the MF responses from all IvyC pairs (n = 55) with the pooled FF-IN data.
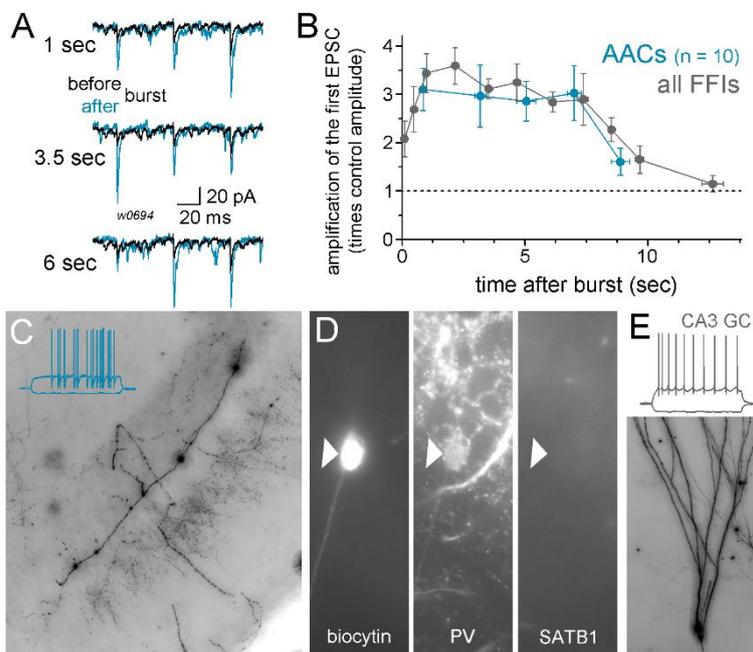
Figure 18. Effect of single MF bursts in postsynaptic AACs. A. Effects of single bursts on EPSCs in a representative CA3 GC to an AAC pair at three different time points after the bursts. **B.** Comparison of the amplification of the MF responses from AAC pairs (n = 10) with the pooled FF-IN data. **C.** Axons of the postsynaptic AAC spread along the borderline of the *strata pyramidale* and *oriens*. The MF that originated from the presynaptic CA3 GC is visible at the border of *strata lucidum* and *pyramidale*. The inset shows the fast-spiking properties of the postsynaptic AAC. **D.** Immunolabeling for parvalbumin (PV) and SATB1 (negative) of the postsynaptic AAC (Viney et al., 2013). **E.** Firing pattern and dendrites of the presynaptic CA3 GC in the *stratum radiatum*.
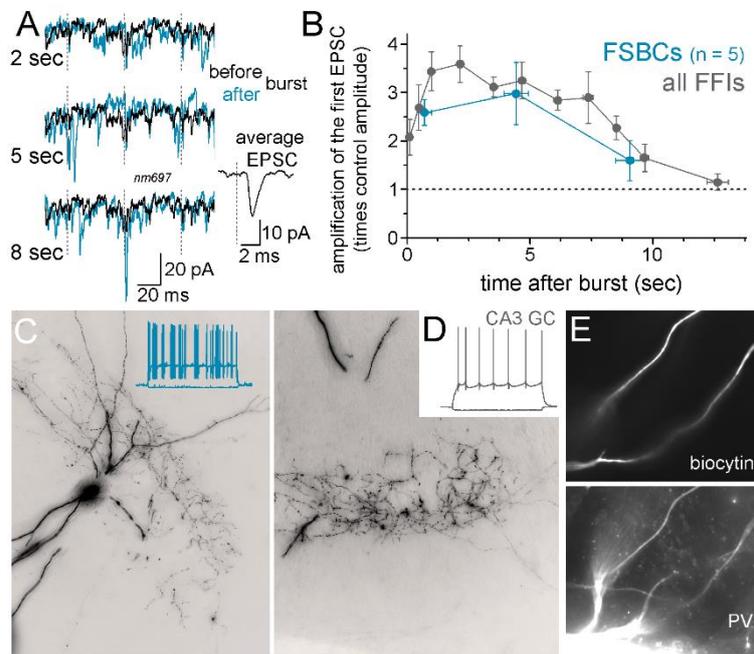
Figure 19. Effect of single MF bursts in postsynaptic PV+BCs. A. Effects of single bursts on EPSCs in a representative CA3 GC to a PV+BC pair at three different time points after the bursts. The dotted vertical lines represent the presynaptic APs. Note the abundant spontaneous synaptic events, which is characteristic for PV+BCs. An average EPSC response is shown on larger magnification. **B.** Comparison of the amplification of the MF responses from PV+BC pairs (FSBCs, n = 5) with the pooled FF-IN data. **C.** Basket axons, dendrites and firing pattern of the postsynaptic PV+BC. **D.** Firing pattern of the presynaptic CA3 GC. **E.** Immunolabeling of the postsynaptic dendrites for parvalbumin (PV).
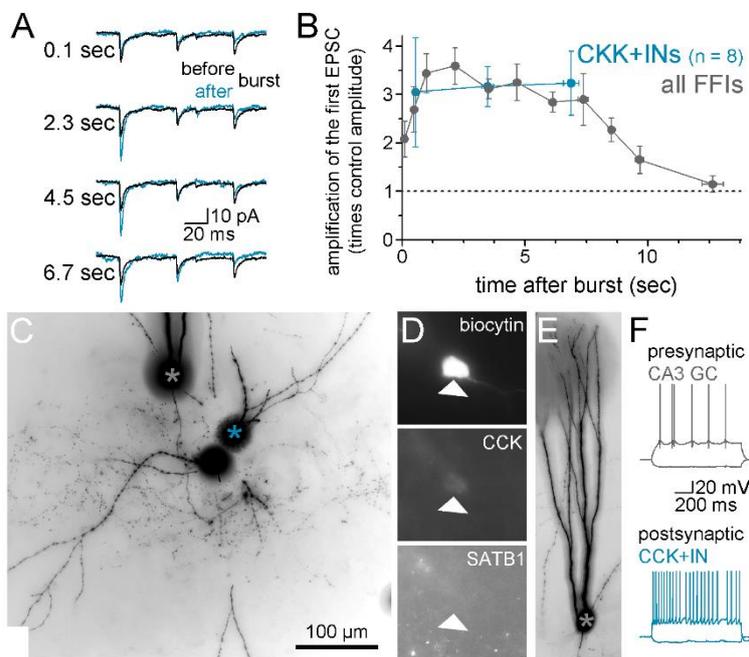
Figure 20. Effect of single MF bursts in postsynaptic CCK+INs. A. Effects of single bursts on EPSCs in a representative CA3 GC to a CCK+ basket cell pair at four different time points after the bursts. **B.** Comparison of the amplification of the MF responses from CCK+IN pairs (n = 8 pairs) with the pooled FF-IN data. **C.** The presynaptic CA3 GC and the postsynaptic CCK+ cell is labeled by gray and blue asterisks, respectively. **D.** Immunolabeling of the postsynaptic cell for CCK and SATB1 (negative). **E.** Soma and dendrites of the presynaptic CA3 GC. **F.** Firing patterns of the pre- and postsynaptic cells.

4.2.2. Postsynaptic cell type-specificity of the single burst-effects

Next, we tested whether MF synapses on other postsynaptic cell types are similarly sensitive to the preceding bursting. In CA3 pyramidal cells, the MF responses after the burst were larger than the initial single-AP-evoked EPSCs ($204 \pm 31\%$, $n = 24$ data points between 1.5-6.7 seconds after 6- or 15-AP bursts, $n = 12$ pairs), which is consistent with the described low-frequency-activated short-term facilitation (Salin et al., 1996; Toth et al., 2000). However, in contrast to postsynaptic FF-INs, the responses in pyramidal cells remained negligible compared with the burst-evoked compound responses, even if the bursts consisted of only 6 APs ($34.9 \pm 4.5\%$ of the burst-EPSC in PCs, and $158 \pm 7\%$, in FF-INs **Fig. 21.** An example for an experiment with a MF-PC pair is shown in **Fig. 22**).

Figure 21. Summary graph showing the effects of single MF bursts on the three different groups of postsynaptic cells. Because of the negligible initial response amplitudes in the MF-SLC pairs (Szabadics and Soltesz, 2009), we compared the post-burst EPSCs with the compound maximal amplitudes during the bursts (dashed line). The relative amplitudes of the first responses before the bursts are shown separately. The MF-FF-IN EPSCs were re-analyzed similarly. *Red*, pyramidal cells: $n = 46$ data points from $n = 12$ pairs*; dark blue*, SLCs: $n = 61$ data points from $n = 20$ pairs; *blue*, FF-INs: $n = 280$ data points from $n = 78$ pairs.
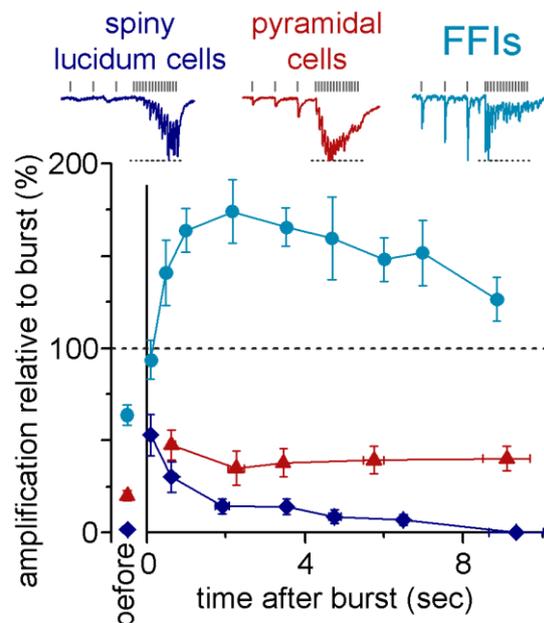
The effect of single MF bursts was also different in projecting GABAergic cells. We investigated the spiny lucidum cells (SLC), which provide negligible local axonal arbor (i.e., do not contribute to feedforward inhibition) and are part of the hippocampo-septal GABAergic projection. SLCs receive excitatory inputs only from MFs (Wittner et al., 2006; Takács et al., 2008) and these connections have extremely low initial release probability, which increases only after sustained high-frequency presynaptic activity (Szabadics and Soltesz, 2009). Synaptic release onto SLCs was increased shortly after the 15-AP MF bursts (**Fig. 21**). However, in contrast to postsynaptic FF-INs, the EPSCs after the bursts remained small compared with the compound amplitudes evoked during the

bursts. Moreover, the amplitudes of the single-AP responses quickly returned to the minimal initial release state. Thus, the bursts were not able to induce the sustained amplification of MF-EPSCs in SLCs (**Fig. 23**). Importantly, similar burst effects were observed when the presynaptic release from MF-SLC connections was artificially increased by elevating extracellular Ca^{2+} levels (3.5-5 mM) and intracellularly adding cesium ions (**Fig. 24**), suggesting that the postsynaptic cell-type specificity of the amplification is not simply a consequence of the different initial release probabilities of the MF input to the SLCs and FF-INs.
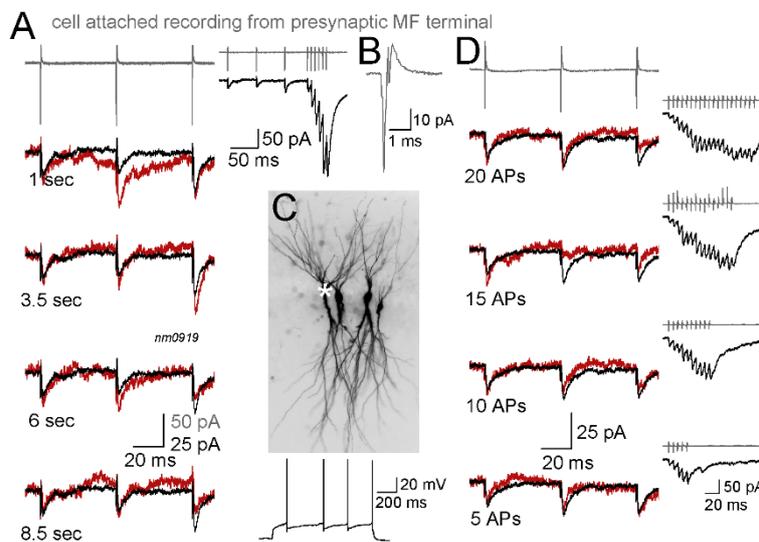
Figure 22. Effect of single MF bursts in postsynaptic PCs. A. Changes in MF-EPSCs various times after single 6-AP bursts. The facilitating burst response is shown on the right. **B.** The presynaptic MF terminal was recorded in cell-attached configuration, and this panel shows an evoked presynaptic spike. **C.** Four attempted pyramidal cells, of which the left-most cell was the postsynaptic cell, whose firing pattern is shown below. **D.** The same pair as in panel A was tested in these recordings 3 s after the 5-20-AP bursts. Note that short and longer bursts have similar effects on the MF-pyramidal cell EPSCs.
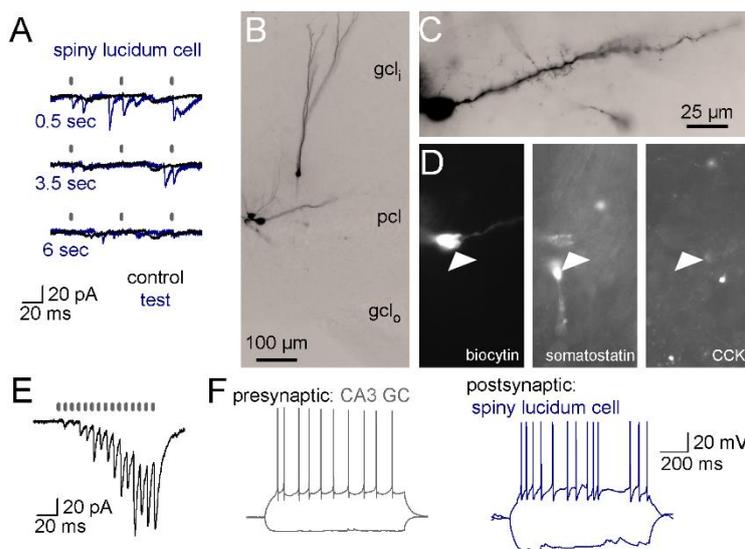
Figure 23. Effect of single MF bursts in postsynaptic SLCs. A. Control and post-burst test MF-EPSCs from a CA3 GC-SLC pair at three different time points after single presynaptic bursts. The APs are indicated as gray bars to highlight the weak responses among the frequent spontaneous events. **B.** Dendritic morphology of the presynaptic CA3 GC and the postsynaptic SLC at low magnification. **C.** Dendritic spines of the postsynaptic SLC within the stratum lucidum. **D.** Immunolabeling of the postsynaptic SLC for somatostatin and CCK (negative). **E.** The MF responses of the same SLC during the burst. **F.** Firing patterns of the cells.
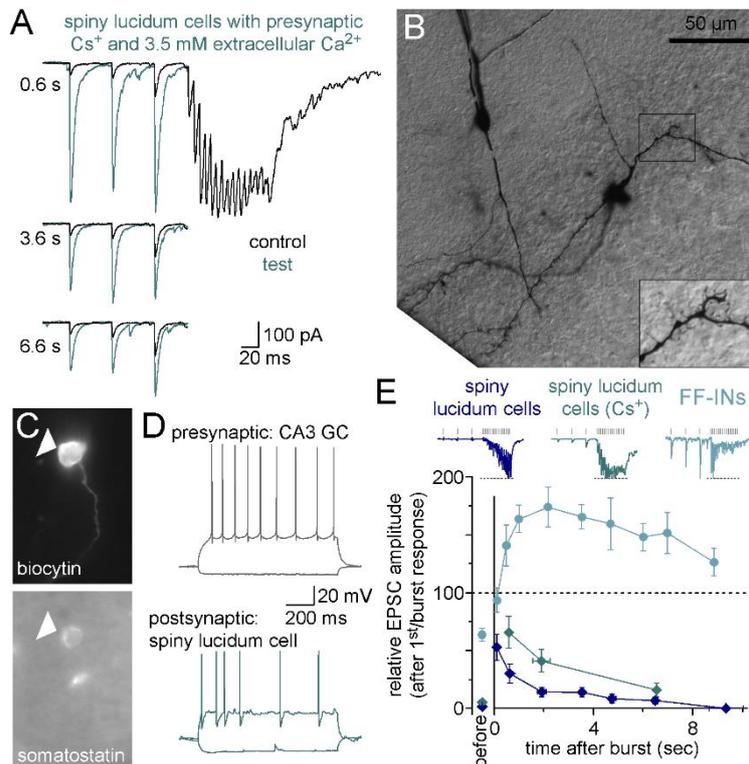
Figure 24. Experimentally increased transmission probability did not unmask single burst induced amplification of MF connections onto SLCs. A. A representative experiment in which reliable synaptic transmission was obtained in the CA3 GC-to-SLC connection by increasing the extracellular Ca^{2+} level to 3.5 mM and replacing 40 mM KCl in the intracellular solution with CsCl to inhibit presynaptic potassium channels. **B.** Nomarski DIC image of the DAB-stained presynaptic CA3 GC and postsynaptic SLC. The inset shows the spiny dendrites of the SLC. **C.** Immunolabeling for somatostatin in the postsynaptic SLC. **D.** Firing patterns of the presynaptic CA3 GC and the postsynaptic SLC. **E.** Summary graphs showing the effects of single-MF bursts on postsynaptic SLCs with an artificially increased transmission probability (gray, n = 15 data points from n = 5 pairs) compared with SLCs under standard recording conditions and FF-INs. The relative amplitudes of the first responses before the bursts are shown separately.

4.2.3. Burst length dependence of the burst induced potentiation

The previous presynaptic protocol included 15 APs in the bursts, which is more than what was found (2-7 APs) in the typical GC bursts *in vivo* (Buzsáki et al., 1983; Henze et al., 2002; Pernia-Andrade and Jonas, 2014). We also tested the effectiveness of shorter, truly physiological single bursts in recruiting the amplification by single MFs and the optimal presynaptic activity ranges. In these recordings, the time delay between the burst and the test stimulation was fixed (3 s) and only the numbers of APs within bursts were systematically changed (n = 91 protocols from 24 pairs, including postsynaptic IvyC, n = 16, AAC, n = 1, PV+BC, n = 1 and unidentified cells with reliable transmission, n = 6; **Fig. 25**). The exponential fit of the measured amplification against the AP-number of the preceding bursts predicted that the amplification would reach 50% of its maximal capacity with a theoretical 2.79-AP burst (±5% confidence range: 2.38 – 3.33 APs; fit R^2

= 0.967). A single burst with 5 APs activated 69.8 ± 6.4% of the maximal capacity, whereas 10 AP bursts almost completely exploited it (90.3 ± 6.3%). These results indicate that physiological GC bursts are within the dynamic induction ranges of this type of amplification. Importantly, the 3-, 5- and 7-AP bursts had remarkable effects on the EPSC amplitudes (2.4 ± 0.15, 2.87 ± 0.17 and 3.16 ± 0.16-fold predicted amplifications, respectively) indicating that the amplification in FF-INs is extremely robust after single physiological GC bursts.
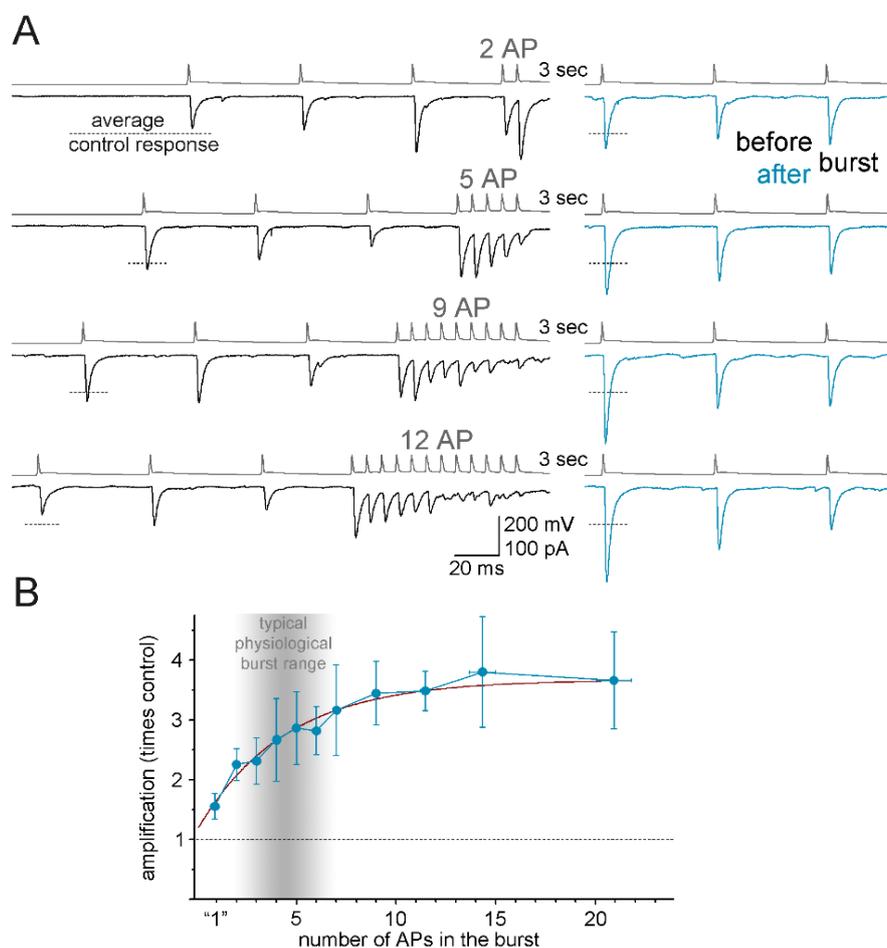
Figure 25. The burst length dependence of the single burst induced. A. A representative pair showing the amplification after bursts with various numbers of APs after the same three-second gap. **B.** Summary of the burst-length-dependence of the amplification from n = 91 protocols, n = 24 pairs including postsynaptic IvyCs (n = 16), AAC (n = 1), PV+BC (n = 1) and unidentified cells with reliable transmission (n = 6). The brown curve shows the exponential fit of the data (R^2 = 0.967). The gray area on the x-axis indicates the usual range of the *in vivo* GC burst length.

4.2.4. Presynaptic origin of the burst-induced amplification in FF-INs

Next, we addressed the underlying synaptic mechanisms of the single-burst-induced amplification. First, we tested whether the amplification of the MF-responses in FF-INs was due to pre- or postsynaptic changes. The failure rate of the responses consistently decreased after single bursts (from $53.6 \pm 3\%$ to $25.0 \pm 3\%$; $p = 3.5 \times 10^{-20}$, n = 68 FF-IN pairs, paired t test), indicating presynaptic changes (**Fig. 26A**). Interestingly, no failure was detected in 23 pairs after the burst (only one of them was failure-less before burst).
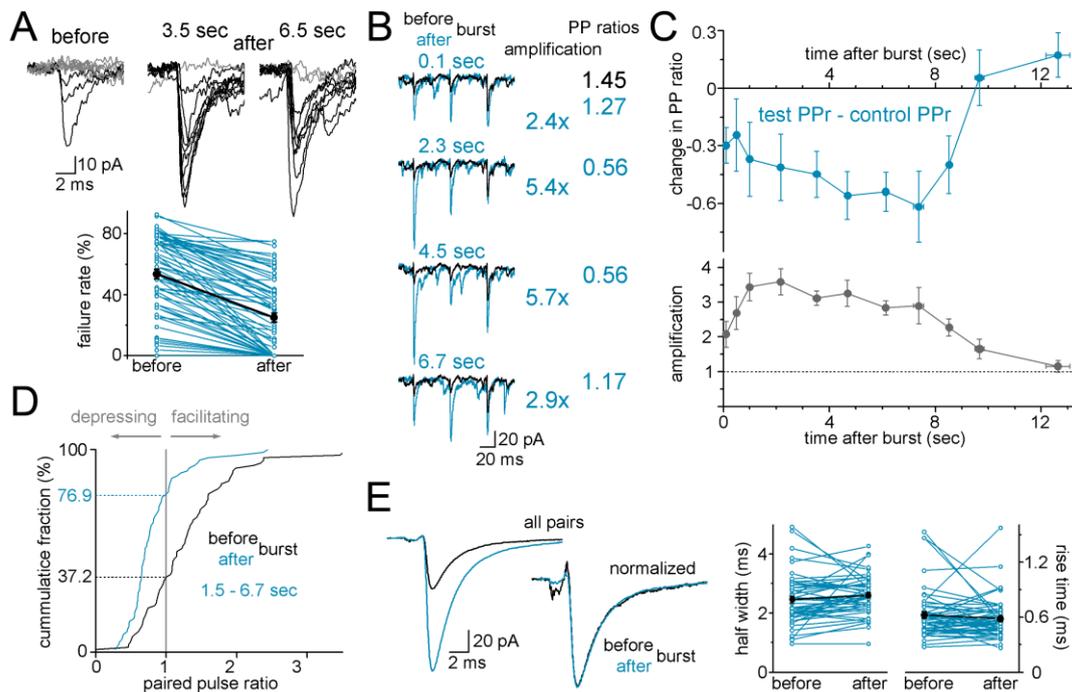
Figure 26. Presynaptic origin of the single-burst-induced amplification. A. The failure rates of single AP-responses decrease after MF bursts. Representative traces of a CA3 GC-CCK+ basket cell pair before and after the burst. Successes are shown in black, and failures are shown in grey. The graph below shows the summary data of the effect of single bursts on the failure rates in individual FF-IN pairs (n = 67 pairs; 1.5-6.7 s). Blue lines: individual pairs, black line: average. **B.** Short-term plasticity of EPSCs in an IvyC at 20 Hz before and various times after bursts. The extent of the amplification and the paired pulse ratio (PPR) is indicated next to the traces. **C.** Changes in the short-term plasticity of MF responses in identified FF-INs. Values were calculated as control PPR subtracted from the PPR after bursts, therefore negative values indicate less facilitation or more pronounced depression, positive values refer changes toward more facilitation or less depression. The same dataset shown in **Fig. 16H** was analyzed here, and the original graph showing the amplification (gray) is copied below for comparison of the time course, n = 201 data points from n = 78 pairs. **D.** The PPR values in control and after bursts (1.5 – 6.7 second range) are compared directly by cumulative probability plot. The same dataset as shown on C. **E.** Total and normalized average EPSCs evoked in FF-INs (n = 51 pairs) by single MF APs before and 1.5-6.7 s after single presynaptic bursts. The events were aligned to the presynaptic AP peak. The graphs show the half-width and rise times of the MF responses in individual FF-INs (blue) and their average (black), which were similar before and after the bursts ($p = 0.13$, $p = 0.26$, paired t test).

We next compared the short-term plasticity of the responses before and after single bursts by calculating the paired-pulse ratio (PPR; were calculated as the ratio of the average of the 2nd and 3rd amplitudes to the 1st amplitude) from the low-frequency spike triplets in anatomically identified FF-INs (same pairs as in **Fig. 16H**). Changes of the PPR is an indicator of altered release probability of synaptic vesicles, and only expected in case of presynaptic mechanisms. In our experiments, after bursts the PPR decreased and remained small concomitantly with the enhanced and maintained periods of amplification (**Fig. 26B-C**). The proportion of the depressing connections is increased from 37.2 % to 76.9 % in the 1.5-6.7s period after the burst (**Fig. 26D**). These observations, the alteration of failure rate and short-term plasticity clearly indicate changes in presynaptic release machinery and increased release probability after the bursts. In contrast, the rise times and half-widths of the EPSCs remained unchanged after the burst (Carta et al., 2014), precluding the involvement of changes at the postsynaptic receptors (625 ± 38 µs vs. 583 ± 31 µs, p = 0.26; 2.46 ± 0.12 ms vs. 2.61 ± 0.09 ms, p = 0.13, paired t test; **Fig. 26E**).

4.2.5. The amplification does not require large Ca^{2+} influx

The presynaptic origin of the amplification and its dependence on the numbers of APs within the bursts propose the large burst-evoked Ca^{2+} influx as a candidate mechanism for triggering the amplification. If the large presynaptic Ca^{2+} influx during the bursts is indeed required for the amplification, then diminished amplification is expected during decreased Ca^{2+} influx, for example, when the extracellular Ca^{2+} concentration is lowered. Therefore, we compared the same MF-EPSCs in FF-INs and their amplifications first in standard extracellular solution (2 mM Ca^{2+}) and then with lower (1.3 mM) Ca^{2+} levels. As expected, the response amplitudes decreased due to the reduced Ca^{2+}-influx (**Fig. 27A**). However, single bursts remained effective in inducing the amplification. In fact, the amplification of the same MF-EPSCs became apparently larger with less Ca^{2+}-influx in decreased extracellular Ca^{2+} (control: 1.76 ± 0.16-fold amplification vs. in 1.3 mM Ca^{2+}: 3.39 ± 0.5, p = 0.005, paired t test, n = 12 data points), which was the consequence of the larger reduction of the EPSCs before the bursts than after the bursts (reduction of EPSCs before burst: $-76.5 \pm 2\%$ vs. after burst: $-54.8 \pm 6.3\%$, p = 0.004). Thus, the persistence of amplification in low Ca^{2+} levels argues against the involvement of the

burst-evoked large Ca^{2+} influx in triggering the amplification. This was also consistent with additional experiments, in which presynaptic loading of the Ca^{2+} chelator EGTA did not prevent the single-burst-induced amplification (**Fig. 28**).

The bursts ability to evoke the amplification persisted in 5 mM Ca^{2+} concentration (control: 3.4 ± 0.31-fold amplification vs. in 5 mM Ca^{2+}: 2.39 ± 0.12, p = 0.004, n = 15 data points), albeit the magnitude of the amplification was apparently smaller also due to the larger changes of the EPSCs before the bursts than after the bursts (**Fig. 27B**). These observations indicate that regardless of the amount of the Ca^{2+} influx single bursts evoke the amplification.
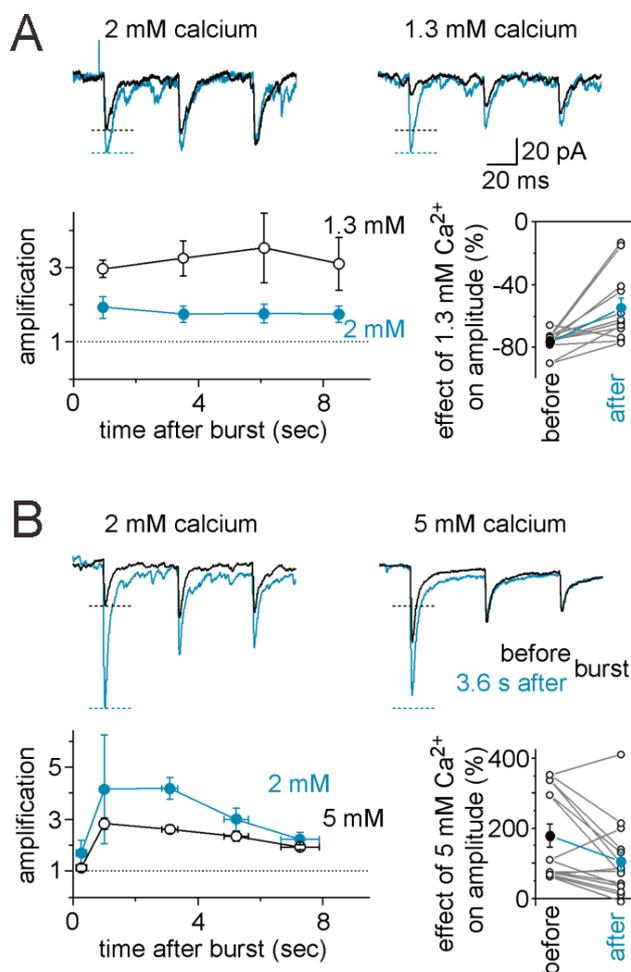
Figure 27. The plasticity induced by single MF bursts is not sensitive to alterations of the extracellular Ca^{2+} concentration. A. An example MF-IvyC pair in which the effects of single presynaptic bursts were first tested in the presence of standard 2 mM Ca^{2+} concentrations and then in 1.3 mM Ca^{2+}. The dashed lines indicate the amplitudes of the corresponding responses in 2 mM Ca^{2+}. The left graph below shows the time-course of the amplification after single GC bursts with two Ca^{2+} concentrations (n = 7 pairs including 6 IvyCs, and one anatomically not-identified postsynaptic cell). Note the apparently larger post-burst amplification in 1.3 mM Ca^{2+} than the amplification of the same pairs in standard Ca^{2+} (2 mM) levels. The right graph shows that the first amplitudes of the responses after single bursts (15 APs, 1.5-6.7 s after the burst, n = 12 data point) were less affected by the lower extracellular Ca^{2+} concentration than the responses of the same pairs before the bursts. Connected open symbols indicate the relative effect of Ca^{2+} (i.e., 0 corresponds to no change in the amplitude) from individual pairs and timing protocols, and the filled circles are their averages. **B.** An example MF-CCK+IN pair in which the effects of single presynaptic bursts were first tested in the presence of normal Ca^{2+} concentrations and then in 5 mM Ca^{2+}. Below the left graph shows the time course of the apparently smaller amplification after single MF bursts (n = 7 pairs including 2 IvyC, 2 AAC, 2 CCK+IN, and 1 non-identified postsynaptic cell, n = 15 data points) and the smaller increase of the post-burst amplitudes than the control amplitudes in high (5 mM) extracellular Ca^{2+}.

The above results led to two conclusions. First, the large presynaptic Ca^{2+} influx during the burst is not responsible for triggering the amplification. Second, the decreased sensitivity of the release machinery to the changes of the extracellular Ca^{2+} concentration after the bursts, and the persistence of the amplification in the presence of intracellular EGTA suggests that residual Ca^{2+} or sensitized Ca^{2+} sensors do not underlie the amplification. Therefore, we reasoned that the synaptic mechanisms activated by the burst are upstream of the Ca^{2+} influx.
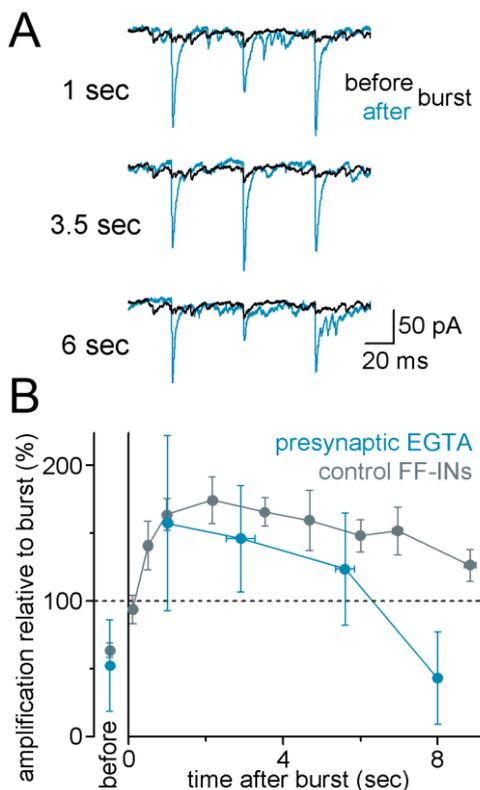
Figure 28. Presynaptic loading of the intracellular Ca^{2+}-chelator EGTA did not prevent the effect of the burst on the postsynaptic responses. A. An example experiment showing the EPSCs in an AAC evoked by three APs at 20 Hz before and at three different data points after single presynaptic CA3 GC bursts. The presynaptic CA3 GC was recorded with an intracellular solution containing 1 mM EGTA. **B.** Summary graph showing the effect of single bursts on FF-IN pairs, in which the presynaptic CA3 GCs were recorded with intracellular EGTA (0.5-2.5 mM; blue; n = 15 datapoints from 5 pairs, including 3 identified IvyC, 1 AACs and 1 non-identified cell with fast-spiking firing pattern). Here the amplification was measured by normalizing the post burst amplitudes to the maximal compound amplitudes during the bursts similarly as it was done in the case of postsynaptic SLCs and PCs, because the EGTA efficiently inhibited the initial release and comparison of the first amplitudes was not possible. Similar analysis of all FF-IN pairs is shown for comparison. The amplification did not differ between pairs with control or EGTA-loaded presynaptic cells (1.5-6.7 s, p = 0.32, *t* test).

4.2.6. Complete utilization of release capacity after single bursts

Intriguingly, in several cases during the above experiments the responses after the burst were minimally affected by the alterations of the extracellular Ca^{2+} concentration which suggests the saturation of the release capacity after bursts (see **Fig. 27**). Moreover, under baseline conditions (before burst) the release probabilities and consequently the PPR of the MF responses varied over a relatively wide range across FF-IN pairs (**Fig. 29A**). The extent of amplification evoked by the bursts linearly correlated with the

baseline PPR of the cells ($R^2 = 0.438$, slope: 1.54 ± 0.13, **Fig. 29B**). This observation indicates that for connections whose release probability was initially low, single bursts led to larger amplification, whereas the relative amplification of the more reliable connections was rather small. In contrast, the PPRs of the amplified responses did not correlate with the initial PPRs of the same connection ($R^2 = 0.035$, slope: 0.139 ± 0.048). The PPRs were invariably low after the bursts (i.e., highly reliable, depressing responses), indicating that single bursts turn on a uniform high-release state in every MF-FF-IN synapse regardless of their initial release probability.
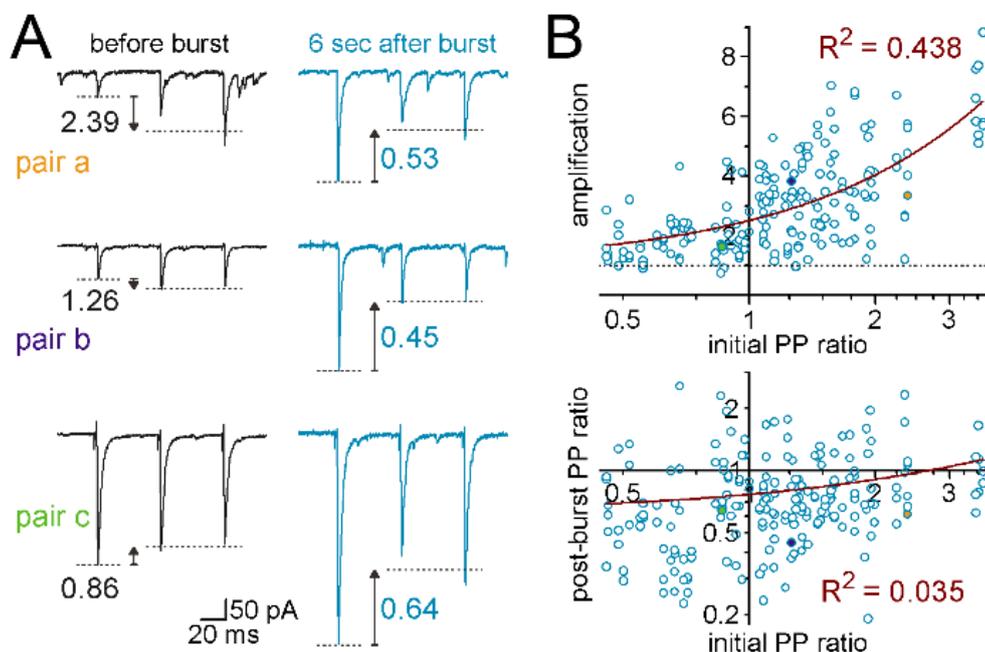
Figure 29. Complete utilization of release capacity after single bursts. A. Three MF-IvyC pairs with different initial PPRs showed remarkably similar short-term depression 6 s after single presynaptic bursts of 15 APs. **B.** Linear correlations between the PPR of the pairs before the bursts and the magnitude of amplification (top) or the PPRs at 1.5-6.7 s after the bursts (bottom). Each circle represents a post-burst data points in the identified pairs (n = 201 data points from 78 pairs). Note the logarithmic scaling of the PPR axes.

4.2.7. Occlusion of the amplification by phorbol esters suggests that bursts promote vesicle priming

Within the synaptic release process, the first upstream step to Ca^{2+} influx is vesicle priming. Previous studies on MF synapses reported diverse roles for the protein kinase C (PKC) pathways (Alle et al., 2001; Pelkey et al., 2005; Hainmuller et al., 2014), which enable plasticity by interacting with the release machinery (Korogod et al., 2007;

Fioravante et al., 2011; Chu et al., 2014). In addition, the members of the presynaptic Munc13 protein family share several domains with PKCs and are crucial and dynamic components of the release machinery (Betz et al., 1998; Augustin et al., 1999; Rosenmund et al., 2002; Basu et al., 2007). Importantly, the activation of either pathways facilitates vesicle priming. Therefore, to interfere with this step, we tested the effects of the phorbol ester PDBu, which promotes vesicle priming and saturates the capacity of the release machinery by interacting with the diacylglycerol (DAG) binding domain of PKCs and/or Munc13s (Rhee et al., 2002; Lou et al., 2008; Fioravante et al., 2014; Taschenberger et al., 2016). As expected, PDBu (1 µM) strengthened the initial release before the bursts (the first amplitude increased by $344 \pm 92\%$, from -30.8 ± 15.2 pA to -132.5 ± 86 pA, p $= 0.028$; whereas the PPR decreased from 1.28 ± 0.27 to 0.64 ± 0.07, p $= 0.036$, t test, n $= 5$ pairs) indicating that at least one of the PKCs or Munc13s participates in the release machinery at MF-FF-IN synapses. Importantly, PDBu almost completely prevented the single-burst-induced amplification of MF-EPSCs in FF-INs (1.32 ± 0.2 and 3.65 ± 0.5-fold amplification in the same pairs after and before PDBu, respectively, p $= 0.0001$, paired t test, n $= 10$ data points from 5 pairs, 1.5-6.7 s after bursts, **Fig. 30**). Nevertheless, prevention of amplification by PDBu does not necessary imply that the effect of the bursts is mediated via promoted vesicle priming, simply because PDBu seems to already maximize the release, excluding the possibility of further amplification. Therefore, we next investigated the effects of PDBu in the presence of reduced extracellular Ca^{2+} (1-1.6 mM) to compensate for its amplitude-enhancing effects, thereby enabling us to unequivocally test whether saturated vesicle priming alone is capable of occluding amplification. Thus, the apparent PDBu-induced increase of release probability was compensated by the low Ca^{2+} (first amplitudes were $124 \pm 41\%$ of their controls, p $= 0.29$, t test, n $= 7$ pairs), whereas vesicle priming remained maximized by the PDBu. The burst-induced amplification remained small under these conditions (1.69 ± 0.2 and 3.34 ± 0.36-fold amplification in the same pairs after and before PDBu in low Ca^{2+}, p $= 0.0005$, paired t test, n $= 14$ data points). Note that the reduced Ca^{2+} concentration alone would have been expected to increase amplification (see **Fig. 27**).
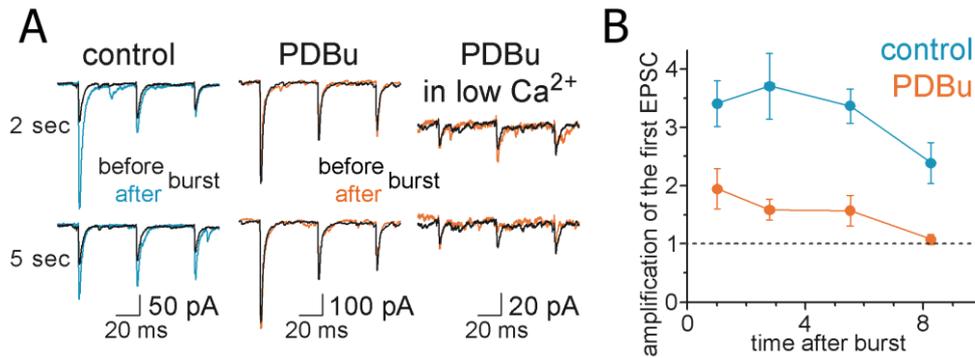
Figure 30. Occlusion of amplification by phorbol ester PDBu. **A.** A representative pair shows that PDBu increased MF-EPSC amplitude before bursts (note the different scale bars) and prevented single-burst-induced amplification. Subsequent reduction of the release probability by decreased extracellular Ca^{2+} concentration (1 mM) in the PDBu solution significantly reduced the average amplitudes, but burst-induced amplification remained negligible in the same pair. **B.** The right graph summarizes the single-burst-induced amplification in 11 MF pairs under control conditions and in the presence of PDBu (includes data from pairs that were recorded either under normal or reduced, 1-1.6 mM, Ca^{2+} level).

4.2.8. The amplification is accompanied by accelerated release

The above experiments suggested that promoted priming occurs and potentially underlie the single burst induced amplification. These burst-induced modifications in the synaptic machinery are expected to be reflected by the onset delay changes of the synaptic responses. Therefore, we compared the delays of individual monosynaptic events that were evoked by single APs either before or after the single bursts. The mean of the delays was reduced after single bursts in practically all FF-IN pairs (from 0.949 ± 0.023 ms to 0.868 ± 0.023 ms, n = 57, p = 9×10^{-12}, paired t test, **Fig. 31A-B**). Furthermore, the variance of the delays was also significantly decreased (from 0.0294 ± 0.0023 ms^2 to 0.018 ± 0.0018 ms^2, p = 3×10^{-5}).

Interestingly, neither the paired-pulse depression nor facilitation was associated with changes in the synaptic delay in the same pairs before the bursts indicating that the mechanisms of the amplification at these synapses are likely different from these fundamental short-term plasticity phenomena (Boudkkazi et al., 2007) (**Fig. 31C**). Importantly, PDBu prevented the bursts from accelerating the delay of the responses, confirming the mechanistic convergence of the burst and PDBu effects (in PDBu: 0.96 ± 0.07 ms and 0.967 ± 0.084 ms, before and after the burst, respectively, p = 0.87, paired t test; under control conditions: 1.005 ± 0.069 ms and 0.944 ± 0.082 ms, p = 0.017; ANOVA One-way repeated measure, multivariate test: p = 0.048, between-subject

effects: $p = 9.7 \times 10^{-7}$). Therefore, we concluded that single bursts elicit the amplification via a less common synaptic plasticity mechanism, which results in promoted vesicle priming at MF synapses on FF-INs.
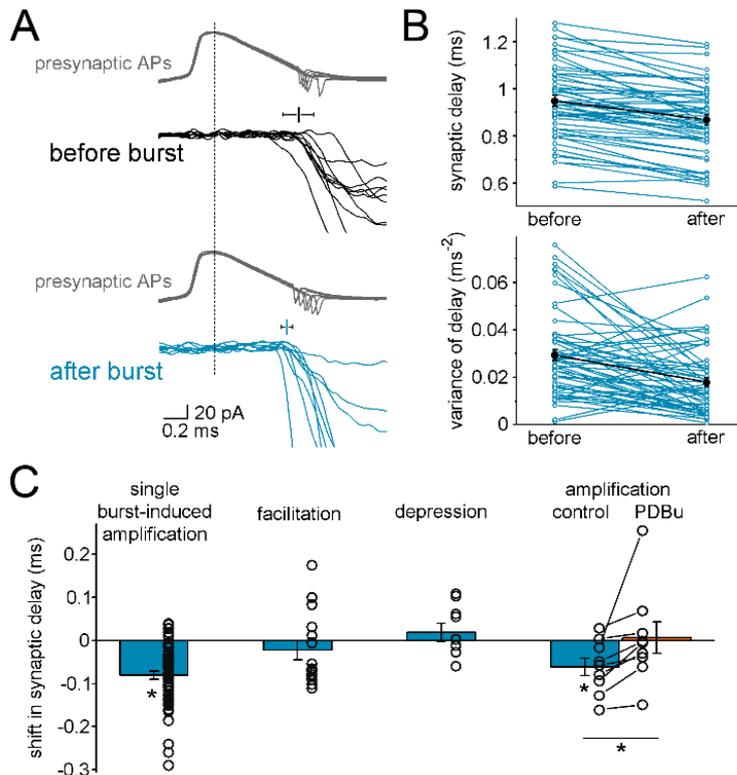
Figure 31. Accelerated release after single burst. A. Individual EPSCs before and after single MF bursts were aligned to the peak of the presynaptic APs. Failures were excluded to highlight the differences between successes. Rods with error bars show the mean and variance of the synaptic onset delay of this pair (measured at each successful event between the AP peak and EPSC onset). **B.** The mean and variance of the synaptic delays in each MF-FF-IN pair before and after single bursts (connected blue symbols) and their average (black). **C.** Changes of the synaptic delays by single bursts are compared with the changes of the delays during facilitation and depression and following PDBu application. The connections were categorized as facilitating or depressing if the control PPRs before the bursts were larger than 1.5 or smaller than 0.67, respectively. Short-term plasticity was not accompanied by shifts in the delays (facilitating, 1st AP delay: 0.911 ± 0.047 ms, 2nd and 3rd APs: 0.889 ± 0.049 ms, p = 0.33, n = 15, paired t test; depressing, 1st AP delay: 0.876 ± 0.051 ms, 2nd and 3rd APs: 0.894 ± 0.05 ms, p = 0.42, n = 9). Symbols indicate the changes in the delay in individual pairs, and columns show the average data. Only those pairs were included in which the changes in the delay were compared before and after the burst (left column); the data were derived from the delays shown in B. Connected symbols on the right-most part indicate the changes in the delay in the same pairs under control conditions and in the presence of PDBu (p = 0.035, n = 9, paired t test).

4.2.9 The amplification does not involve molecular pathways that are known to affect vesicle priming

Currently only a few molecular pathways are known to be able to activity-dependently modify vesicle priming. PKC and Munc13 proteins potentially regulate MF synapses as our PDBu experiments suggested. However, we found that the effect of single bursts on priming was independent of PKC and Munc13, as well as endogenous DAG production by phospholipase C, because the amplification was maintained at a similar level when the

functions of these proteins were selectively blocked with a variety of inhibitors (**Fig. 32**). Furthermore, our experiments with presynaptic loading of the Ca^{2+} chelator EGTA also support the hypothesis that single bursts promote vesicle priming through a PKC- or Munc13-independent pathway because the activation of most isoforms of these proteins require Ca^{2+}-binding (**Fig. 28**).
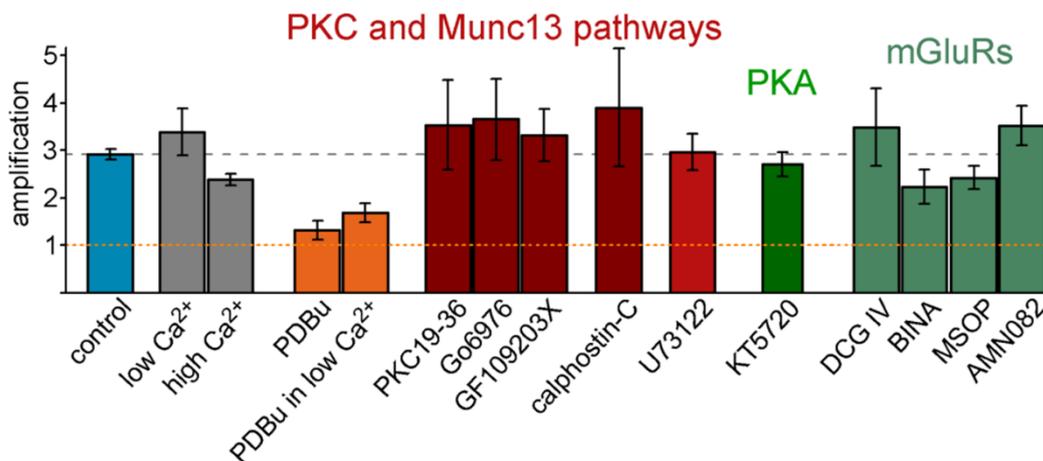
Figure 32. Summary of the pharmacological experiments. The columns show the average amplification at 1.5-6.7 s after single 15-AP bursts (n = 202, 12, 15, 10, 14, 10, 8, 8, 9, 6, 6, 8, 12, 5 and 10 data points). PDBu (1 µM) activates PKCs and Munc13s. PKC19-36 (100 µM, synthetic auto-inhibitory domain, applied intracellularly), Go6976 (0.25 µM) and GF109203X (1 µM, which act on the ATP binding site) are selective PKC inhibitors. Calphostin-C (1 µM) is a PKC and Munc13 inhibitor that acts on their DAG binding domains. U73122 (2.5 µM) is a Phospholipase C inhibitor. KT5720 (200 nM) inhibits PKAs, which are involved in pathways that regulate presynaptic release, including RIM proteins, whose PKA-dependent phosphorylation promotes vesicle priming and PKAs are also involved in post-tetanic potentiation mechanisms at MF synapses onto DG inhibitory cells. DCG IV (0.05-1 µM) is an mGluR2/3 agonist. If DCG IV was applied in high concentration, the extracellular Ca^{2+} concentration was elevated to compensate the inhibition of baseline release. BINA (5 µM) is a selective positive allosteric modulator of mGluR2. MSOP (150 µM) selectively inhibits group III mGluRs including mGluR7. AMN082 (1 µM) is a selective mGluR7 agonist. These ligands were not able to modify the amplification beyond the expected changes, which originate from the effects of these compounds on the basal level of transmission.

An alternative pathway affects vesicle priming involves the RIM/RBP proteins (Südhof, 2012; Acuna et al., 2016). We applied PKA inhibitors, because PKA-dependent phosphorylation of RIM/RBP promotes functions and direct inhibition of this pathway at identified synapses is not possible. However, the single burst-induced amplification also remained intact when PKA function was pharmacologically inhibited (**Fig. 32**). Finally, presynaptic mGluRs have well-known effects on Ca^{2+} dynamics and PKA activity (Shigemoto et al., 1997; Pelkey et al., 2008). However, neither the activation nor

inhibition of mGluR2/3 and mGluR7 changed the single burst induced amplification. Thus, the amplification is mediated by promoted vesicle priming via a yet to be discovered molecular pathway, which is independent of the Ca^{2+}, mGluRs, Munc13, PKA, and PKC-functions.

4.2.10. Single mossy fiber evoked disynaptic IPSCs reflect the strengthening of feedforward inhibition of a non-specific PC population

This robust synaptic phenomenon is expected to have a large impact on the downstream synaptic network. Therefore, to test whether single physiological bursts are indeed capable of selectively enhancing genuine feedforward inhibition within CA3 networks, we next investigated disynaptic GABAergic inhibitory events (diIPSCs) in CA3 pyramidal cells in response to the stimulation of single MFs. The delays and GABAergic properties of these events confirmed that they arose from effective monosynaptic excitation and time-locked spiking of non-recorded FF-IN cells, which directly inhibit the recorded pyramidal cell. We tested the burst protocols in 17 diIPSC pairs (n = 58 data points). The probability of diIPSCs only slightly improved during high-frequency bursts (baseline: $11.8 \pm 2.3\%$, burst: $17.6 \pm 2.2\%$, considering the average probabilities for each AP, p = 0.023, paired t test, **Fig. 33**). However, the probability of diIPSC events almost tripled 1.5-6.7 s after single MF bursts compared with the baseline and was also much higher than that during the bursts ($29.4 \pm 3.5\%$, p = 5×10^{-8} and p = 9×10^{-4}, respectively, n = 33 data points, paired t test). The temporal profile of the increased probability of time-locked diIPSCs matched the strengthened excitation of FF-INs following single bursts. Their higher probability was maintained within 8 s and returned to near-basal levels 9 s after the single MF bursts ($15.7 \pm 0.38\%$, n = 6 data points, p = 0.078). These findings provide evidence for the availability of single-burst-induced amplification in intact FF-INs within the slice and show that single physiological MF bursts functionally rewire the CA3 circuitry by selectively and effectively strengthening the recruitment of feedforward inhibition by subsequent GC activity.
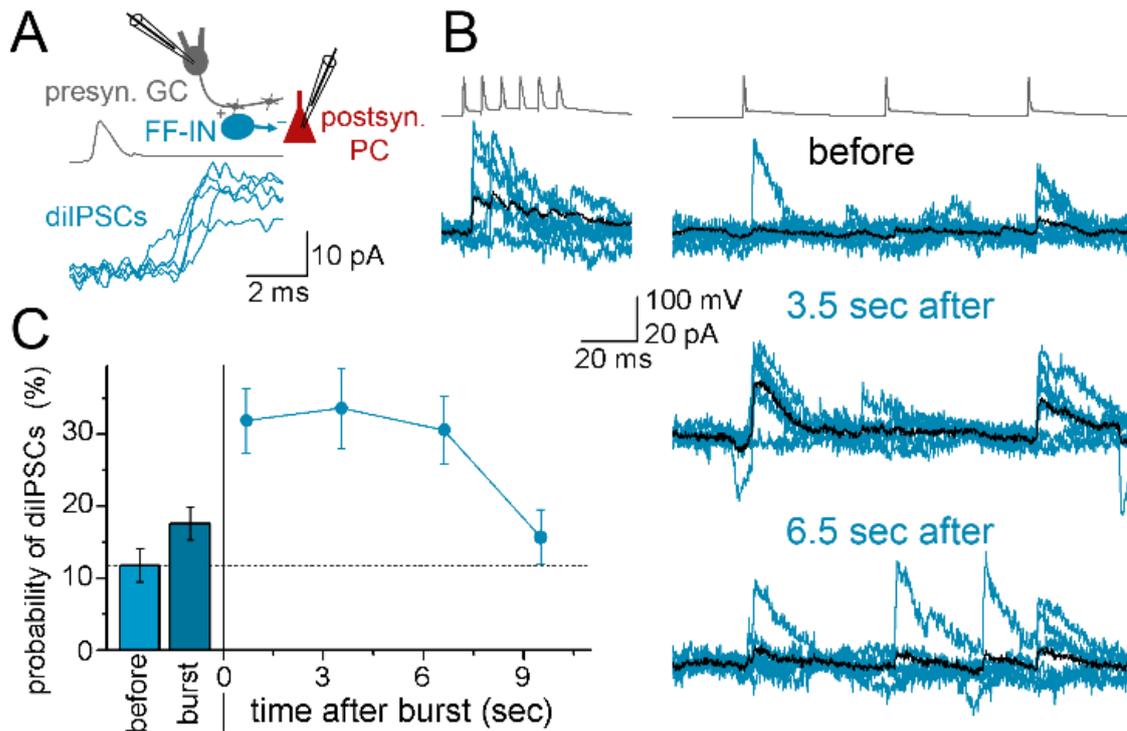
Figure 33. Feedforward inhibitory events in CA3 pyramidal cells are most effectively evoked after the GC bursts. A. Schematics of the recording configuration and sample traces showing the diIPSCs evoked by the presynaptic AP. **B.** Synaptic events in a pyramidal cell during the stimulation of a CA3 GC. The majority of the outward events are disynaptic GABAergic responses, whose probability was increased after single presynaptic bursts. The black average traces also highlight the increased weight of disynaptic inhibition after the bursts. **C.** The summary graph shows the single-burst-effects on the probability of diIPSCs evoked by MF APs before, during and after the bursts in single MFs (n = 17 pairs; n = 6 with 6-AP bursts and n = 11 with 15-AP bursts both at 150 Hz). The probabilities were calculated for each AP.

To understand the consequence of the described phenomenon, it is important to know if a specific PC population is inhibited by the FFI circuit recruited by a single GC. Specifically, we asked whether the network favors lateral inhibition or ensemble specific FFI. Analysis of the disynaptic inhibitory connections onto PCs recruited by single MFs can provide information about the organization of the FFI circuit. We extended our dataset with additional recordings, including monosynaptic MF-PC connections. The presence of both monosynaptic EPSCs and diIPSCs in a single MF-PC pair indicated that the presynaptic GC innervates both the PC and a FF-IN, which innervates the PC as well (ensemble specific FFI). On the other hand, we detected only diIPSCs in many PCs, meaning that these cells received only FFI (lateral inhibition). We analyzed the probability of disynaptic inhibitory connections in both PC groups (either receiving monosynaptic excitation from the recorded MF or not), considering all tested pairs.

70

Altogether, we recorded 42 pairs in which PCs received monosynaptic MF input and found 321 pairs in which PCs were not coupled monosynaptically to the stimulated MFs or CA3 GCs. The probabilities of observing connections with single MF-elicited diIPSCs were not significantly different in the two populations of PCs: **11.9%** (5 out of 42 pairs) vs. **10.6%** (34 out of 321 pairs) for monosynaptically coupled and not coupled pairs, respectively, (Fisher's exact test, p = 0.791). The prevalence of diIPSCs was similar when we considered only those pairs wherein the presynaptic recording was made on giant MF terminals, which presumably originate from DG GCs: 9.4% for mono- and disinaptically innervated (3 out of 32 pairs) vs. 8.9% (10 out of 112 pairs) for only diIPSC receiving PCs. Thus, these results indicate that the FFI is randomly wired between the DG and the CA3. The random wiring scheme indicates that the FFI network recruited by a single GC inhibit a nonspecific population of PCs.

4.2.11. Pyramidal cell firing reflects only ongoing bursts

We then analyzed disynaptic EPSCs (diEPSCs, n = 6 pairs) to provide similar functional insights into the effects of single MF bursts on the firing of intact pyramidal cells (**Fig. 34**). Given the complete lack of connections between GCs, single-MF-evoked diEPSCs in GABAergic cells are most likely mediated by the strong monosynaptic excitation and time-locked spiking of non-recorded pyramidal cells, which directly innervate the recorded neurons. In contrast to diIPSCs, the probability of single-MF-evoked diEPSCs increased significantly during bursts (baseline: $12.6 \pm 5.5\%$, burst: $26 \pm 8.1\%$, n = 6 pairs, p = 0.015, paired t test), functionally reflecting the stronger activation of pyramidal cells due to the facilitation of their MF inputs. Furthermore, the probability of diEPSCs was reduced again after the burst ($10.6 \pm 2.9\%$, 1.5-6.7 s, n = 12 data points, p = 0.017, paired t test vs. burst) and was indistinguishable from baseline levels (p = 0.61, paired t test). These results confirm that MF synapses on pyramidal cells readily detect ongoing bursts and are not sensitized during the forthcoming silent period. The effects may also reflect the efficient suppression of pyramidal cell firing by the strengthened feedforward inhibition. The single MF-evoked disynaptic events confirm the availability of the synaptic mechanisms in undisturbed neurons that enable the CA3 network to reliably distinguish single APs from short GC bursts as distinct neuronal signals, not only during their actual duration but also during the subsequent periods.
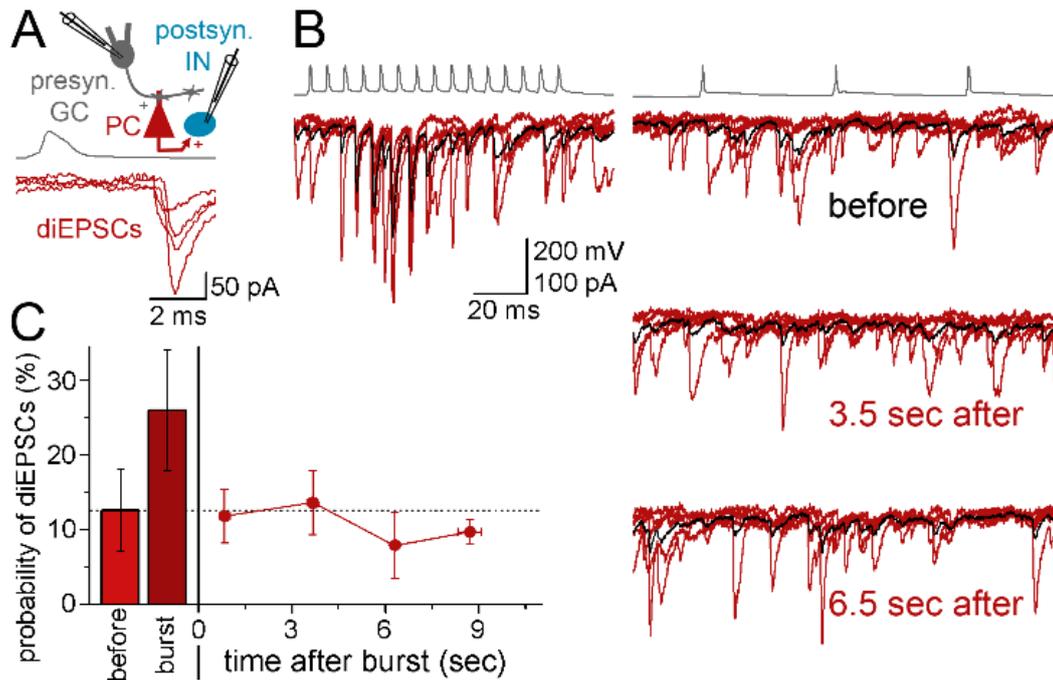
Figure 34. Effects of single MF bursts on disynaptic excitatory events, which reflect the firing of pyramidal cells. A. Schematics of the recording configuration and sample traces showing the disynaptic excitatory events (diEPSCs) evoked by the presynaptic AP. **B.** Representative experiment showing the diEPSCs recorded in a non-identified fast-spiking interneuron during the activation of the presynaptic CA3 GC. Note the frequent diEPSCs during the high-frequency bursts, whereas the occurrence of diEPSCs is negligible during low-frequency GC activity both before and 3.5 or 6.5 s after the bursts. **C.** The summary graph shows the single-burst-effects on the probability of diEPSCs evoked by MF APs before, during and after the bursts in single MFs (average data of 6 pairs all with 15-AP bursts at 150 Hz). The probabilities were calculated for each AP.

5. Discussion

5.1. Adult-born granule cells mature through two functionally distinct states

Two different integrative states of ABGCs

We addressed the maturation process of ABGCs after their integration into the hippocampal circuit. From the third week of their maturation ABGCs are already capable of firing action potentials, they receive synaptic inputs and provide synaptic output to the CA3, thus, they are already functional neurons. Our experiments demonstrated that 3-10 weeks old ABGCs form two functionally distinct subpopulations. These separate populations show highly specific input integration properties that are potentially important for their function in dentate gyrus-dependent computation. There are fundamental differences in how they translate excitatory drive into action potential output, in a manner that is not directly predicted by the cellular age alone. The groups were termed as S- standing for *sensitive*, and L-group referring to their *linear* input-output transformation. Around the third postmitotic week, ABGCs represent a functionally homogeneous population (S-group) characterized by highly variable and sensitive input-output transformation, as indicated by remarkably large increase in the response spike counts for sinusoidal current injections (that mimicked temporally organized input patterns), at certain frequency and input intensity ranges. This variability and sensitivity is characterized by large VAR and ASL value of the individual ABGCs. This characteristic integrative property of young cells potentially underlies the effective disambiguation of input patterns which proposed as a major function of ABGCs (Clelland et al., 2009; Deng et al., 2010; Sahay et al., 2011; Nakashiba et al., 2012). Importantly, most ABGCs retain quantitatively similar integrative capabilities for an extended time period, some of them even until the 9th postnatal week. However, from the fifth week, individual ABGCs start to switch function by losing their sensitivity to a particular input-strength as their output incrementally reports a wide input range (L-group). Thus, the presence of two integrative states of ABGCs facilitate the maturation stage-dependent distinct transformation of DG input to its downstream network (Aimone et al., 2010a; Sahay et al., 2011). Moreover, cells in S-group are tuned to serve similar integrative

function, however being substantially heterogeneous. This heterogeneity might have important functional consequences. For instance, ABGCs could not be divided into two populations based on the offset of the input-output function and these values increased with cellular age among S-group cells. This heterogeneity in the offset values broadens the dynamic range of the input-strengths that the population can process and transform to pattern separated signals.

Due to the sudden transition of individual cells from S- to L-state in an extended maturation period (5-9th postnatal weeks), two overlapping populations with potentially different function are concomitantly maintained. Importantly, our data indicate that "classmate" cells (born during the same period) can contribute to the network with fundamentally different functions; and conversely, similar functions can be served by ABGCs, which were born during different periods of the animal's life. This observation extends previous hypotheses on the plasticity provided by adult neurogenesis, from the maturation of ABGCs being predominantly determined by their post mitotic cellular age. Furthermore, the discovery of functional heterogeneity among ABGCs that are born during the same time challenges previously held concepts that largely relied on predicting similar functions of ABGCs born at the same time. (Aimone et al., 2006, 2010a; Ge et al., 2007; Sahay et al., 2011).

Strikingly, the two functionally distinct populations are maintained in spite of the continuous and gradual changes in their other intrinsic biophysical parameters. Despite their highly variable biophysical properties, the spiking output of the S-group cells is tuned to similar function by being particularly sensitive to certain input ranges. Cluster analysis performed on these multiple parameters was not sufficient to predict the S- and L-functionality probably, because this method considers parameters linearly based on their arithmetical values. It is generally accepted however, that the underlying biophysical parameters contribute nonlinearly to the input-output properties. Therefore, our results suggest, together with the non-concomitant changes in cellular properties along the age of the cells (Mongiat et al., 2009), that precise homeostatic tuning and the complex interactions of the biophysical properties (Marder and Goaillard, 2006) can be underlying factors of the balanced input-output functions of the two functional groups of ABGCs. For instance, decreased spike threshold can be compensated by decrease of the resting membrane potential.

Developmentally generated granule cells

An additional unexpected observation was found when we recorded developmentally generated (not adult born) GCs in young, 17-18 days old animals. We found that their integrative properties were homogenous. Most surprisingly, they performed linear input-output conversion i.e. showed L-group properties. These results raised several questions, however, to unveil them was out of the scope of our study. For example, it raised the possibility that at the level of specific intrinsic cellular properties the developmentally generated and adult-born granule cells may mature differentially or the S-functionality might be a privilege of ABGCs. Nevertheless, these experiments provided a good control for those that addressed the functional properties of ABGCs in adult animals.

Future perspectives

Whether the quick transition between S- and L- integrative states is triggered by intrinsic (e.g. distinct molecular signaling events) or extrinsic signals (e.g. certain activity patterns) remains to be addressed in the future. In addition to the differences in the specific intrinsic cellular properties of ABGCs revealed in our study, their synaptic inputs and outputs also show changes during maturation (Laplagne et al., 2006; Toni et al., 2008; Markwardt et al., 2009, 2011; Marin-Burgin et al., 2012; Vivar et al., 2012). Three to four weeks after cells are born, the amplitudes of unitary glutamatergic synaptic currents are similar in ABGCs (Mongiat et al., 2009). However, later, maturation-state-dependent short-term plasticity (Marin-Burgin et al., 2012), synaptic plasticity (Ge et al., 2007; Gu et al., 2012) and GABAergic inhibition (Markwardt et al., 2009, 2011; Dieni et al., 2013) can potentially either enhance or diminish the separation of the ABGC pool into two functional cell populations. Moreover, environmental conditions that increase or reduce hippocampal neurogenesis may have specific effects on the relative contribution of newly generated granule cells to the S- or L-groups that may explain distinct behavioral consequences of altered neurogenesis (Kempermann et al., 1997; Gould and Tanapat, 1999; van Praag et al., 1999).

5.2. Single bursts of single mossy fibers functionally reorganize feedforward inhibition in the CA3 area

New plasticity phenomenon in MFs

In the second project, we identified a new form of synaptic plasticity of the hippocampal MF pathway that substantially contributes to the determination of the synaptic impact of single GCs during different physiological activity patterns. This unusual form of plasticity is activated by a single physiological burst firing of a single presynaptic GC. *In vivo*, GCs either fire single action potentials or bursts of 2-7 APs with high, 100-200Hz frequency (Buzsáki et al., 1983; Henze et al., 2002). Surprisingly, even 2-3 AP bursts had remarkably large effect on the amplification of the postsynaptic responses measured 3 seconds after the bursts. The amplification of the postsynaptic responses after 10-15 AP bursts even exceeded the 3-fold enhancement. Furthermore, the dynamic range of the amplification evoked by different lengths of bursts matched with the *in vivo* typical burst regime, which also highlights the significance of this plasticity mechanism. The phenomenon has a unique temporal profile, it needs about a second after the burst to develop and then the amplification persists at a similar level for 6-10 seconds. Synaptic plasticity mechanisms acting on this timescale usually referred to as augmentation and post-tetanic potentiation (PTP) in the literature, which involve similar molecular mechanisms (Zucker and Regehr, 2002; de Jong and Fioravante, 2014). There are three reasons arguing that the phenomenon we described is different from the classic forms of the above mechanisms. First, the temporal profile is different, especially PTP is the largest immediately after high-frequency stimulation and continuously decays back to baseline. Second, the presynaptic stimulation protocol required to evoke the well-known short-term plasticity mechanisms is substantially stronger, usually prolonged stimulation involving an order of magnitude more spikes than what we apply during the burst protocols (Alle et al., 2001; Mori et al., 2007). Finally, during PTP and augmentation the accumulation of the calcium in the presynaptic terminals and the subsequent activity of signaling pathways, such as the activity of PKC, PKA, PLC, Munc13 are established molecular mechanisms. PTP specifically in MF-IN synapses was reported to be inhibited by the blockade of both PKA and PKC (Alle et al., 2001). In contrast, in our experiment neither the potentially large calcium influx invading the

presynaptic terminal during the burst was found to be a key component in the burst induced potentiation (experiments with presynaptic EGTA and reduced calcium levels) nor the blockade of multiple signaling pathways (PKA, PKC, PLC, Munc13, mGluR2,3,7) could interfere with the amplification.

Postsynaptic cell type specificity

The single burst induced potentiation was first observed in MF connections to postsynaptic FF-INs. To analyze the potential cell type specificity, we recorded numerous pairs with a variety of postsynaptic partners and tested the connections with the burst protocols. The recorded cells were *post hoc* analyzed and identified based on multiple anatomical and physiological criteria (for further details of the classification see the Materials and methods section). Among the postsynaptic targets of MF connections, we identified IvyCs (n = 55 cells), AACs (n = 10 cells), PV+BCs (n = 5 cells), CCK+INs, (n = 8 cells), SLCs (n = 25 cells) and PC (n = 12 cells).

Interestingly, single MF bursts had remarkably similar effects on all the tested postsynaptic interneurons contributing to the feedforward inhibitory circuit, including IvyCs, AACs, CCK+INs and PV+BCs. This is surprising because the variety of interneurons is evolved to serve specialized roles within the hippocampal network (Klausberger and Somogyi, 2008; Somogyi et al., 2013), on the other hand, the uniformity of described phenomenon in all FF-INs might indicate its significance in hippocampal functions. Furthermore, the effect of the burst was also similar in all the tested cells falling to the not-identified category of postsynaptic cells where the initial release was reliable (i.e. not SLCs). Notably, these cells were probably also FF-INs but the available data was insufficient for their identification.

The MF synapse onto SLCs is apparently different from those targeting other interneurons. These connections have extremely low initial release probability, that increases only after sustained high-frequency presynaptic activity (Szabadics and Soltesz, 2009). Synaptic release onto SLCs was increased shortly after the MF bursts, however, in contrast to postsynaptic FF-INs, the EPSCs after the bursts remained small compared with the compound EPSC amplitudes evoked during the bursts. Moreover, the amplitudes of the single-AP responses quickly returned to the minimal initial release state. To manipulate this synapse, we applied partial presynaptic potassium blockade and increased

extracellular calcium levels that successfully enhanced the otherwise negligible initial transmission, resulting in EPSC amplitudes and short-term plasticity that is comparable with the MF connections onto other GABAergic cells. However, we did not find similar MF burst effects to the other interneuron types, neither in these artificial conditions. SLCs are part of the septal projecting GABAergic cell population and providing negligible local axonal arbor thus, do not contribute substantially to the feedforward inhibition (Gulyás et al., 1992; Spruston et al., 1997; Jinno et al., 2007). Based on the above findings, we concluded that among GABAergic cells, the single MF burst induced potentiation is specific to the FF-INs.

We found moderate level of amplification of the postsynaptic responses for single APs in PCs, however neither its extent, nor its temporal profile was similar to what we measured in the case of FF-INs. The slightly enhanced postsynaptic responses did not decay back to the original level in the tested time window (10-12s), which we assumed to be consistent with previous findings describing the short-term plasticity of this synapse at even lower frequency of activity (Salin et al., 1996; Toth et al., 2000). Comparison of the EPSCs after the burst to the maximal amplitude during the burst highlighted the substantial difference between the two types of MF synapses. Specifically, the excitation of the PCs by MFs is the strongest during ongoing burst activity, as it is already well known, and therefore the MF-PC synapse is considered to be "conditional detonator" (Henze et al., 2002; Lawrence and McBain, 2003; Mori et al., 2004). However, our findings revealed that during the physiological activity of GCs the excitation of FF-INs is the largest several seconds after bursts (typically 1-8s), when further spiking activity of the presynaptic cell occurs. This was further supported by the analysis of disynaptic connections, where effective recruitment of FFI was directly demonstrated in more intact conditions. In contrast, the recruitment of PCs during GC activity unequivocally remained the most effective during the bursts. Importantly, the latter results also validate our experimental conditions.

Mechanisms underlying the burst induced potentiation

We tested whether the amplification of the MF-responses in FF-INs was due to pre- or postsynaptic changes, in order to unveil the underlying synaptic mechanisms of the single-burst-induced amplification. Analysis of both the failure rates and the PPR before

and after the bursts clearly indicated the involvement of presynaptic changes after the bursting activity. On the other hand, no changes were found in the rise times and half-widths of the EPSCs after the burst, precluding the involvement of postsynaptic mechanisms.

The presynaptic origin of the amplification raised the possibility that the burst-evoked large Ca^{2+} influx is a potential mechanism for triggering the amplification. This idea was also consistent with the dependence of the magnitude of the amplification on the numbers of APs within the bursts, however the experiments with presynaptic EGTA and reduced calcium levels excluded this possibility. The first upstream step to Ca^{2+} influx is vesicle priming within the process of synaptic release. To interfere with the vesicle priming process we applied PDBu which is a DAG analog and enhances vesicle priming and release by acting on multiple molecular pathways such as PKC and Munc13 (Rhee et al., 2002; Lou et al., 2008; Fioravante et al., 2014; Taschenberger et al., 2016). In these experiments PDBu effectively enhanced the release from MFs, and during the augmented release state the burst could not evoke the amplification, neither when the robust effect of PDBu on the initial release probability was compensated by decreasing the extracellular calcium concentration. These observations suggest that promotion of vesicle priming occurs during the burst induced plasticity. The decrease of the onset delay changes of the synaptic responses after bursts also lead us to the same conclusion, the promotion of vesicle priming. To identify the molecular pathway responsible for the synaptic mechanism evoked by the burst, in multiple pharmacological experiments we blocked the major signaling pathways that are known to modulate the release probability either acting on vesicle priming or by other mechanisms. However, the blockade of the tested pathways (PKA, PKC, PLC, Munc13, mGluR2,3,7) could not inhibit the amplifying effect of the burst.

In summary, the single MF burst induced plasticity is clearly a presynaptic process, which manifests as a promoted vesicle priming. However, the specific molecular mechanisms responsible for the robust effect evoked by MF burst remain to be answered in the future.

Non-specific feedforward inhibition in the DG-CA3 circuit

Our findings revealed that FF-INs recruited by individual MFs innervate CA3 PCs regardless whether they receive direct excitation from the same presynaptic MFs or not. This means that FFI between the DG and the CA3 is not wired to specifically inhibit a restricted population of PCs determined by their direct excitation from the GCs. In general, our data suggest that the wiring of the FFI at the DG-CA3 interface is random. The random connectivity pattern suggests that primary function of the CA3 FFI network is to adjust the general excitability of the local circuit. It is consistent with the assumed basic function of the DG-CA3 interface, to provide sparse, pattern separated input code for the CA3 region (Acsády and Káli, 2007). Importantly, during sparse GC firing FFI is effective in preventing spiking of CA3 PCs, whereas GC bursts remain capable detonators (Henze et al., 2002; Mori et al., 2004; Acsády and Káli, 2007; Zucca et al., 2016). Thus, sparse excitation of PCs is accompanied by strong and random FFI from the same GC input source, especially with specific history of preceding bursting activity, according to our results.

Future perspectives

Our results showed that the efficacy of the recruitment of FFI inhibition at the DG-CA3 interface is precisely determined by the activity history of the presynaptic GCs. The probability of activating FF-INs, even by sporadic GC spiking, highly increase if the activity is preceded by a short, high frequency burst at the range of 10 seconds. Therefore, our results elucidate that the information carried by short bursts, as distinct neural signal, appears to be more complex than it was known before in the DG-CA3 network (Abbott and Regehr, 2004). Some crucial questions, however, remain unanswered and require further investigation to understand GC bursting. For example, whether the somatically detected bursts of GCs travel faithfully along unmyelinated mossy fibers *in vivo* is not yet determined (Pernia-Andrade and Jonas, 2014; Diamantaki et al., 2016; Kowalski et al., 2016). Nevertheless, the high densities of sodium (Engel and Jonas, 2005) and potassium channels (Geiger and Jonas, 2000; Alle et al., 2011) suggest that GC axons effectively digitize dendritic plateau potentials to axonal bursts, similar to CA1 pyramidal cells (Apostolides et al., 2016).

The identities of the underlying molecular pathways also remain unknown. Several potential mechanisms may mediate the sensitized AP-release coupling that occurs following bursts, including the use-dependent potentiation of Ca^{2+} influx, which would cause larger single-AP-evoked Ca^{2+} influx after bursts (de Jong and Fioravante, 2014), or mechanisms that promote a more reactive mode of one or multiple molecular components of the release machinery (Südhof, 2013). Although some of our observations indirectly support the latter possibility (the shorter delay or the occlusion of the amplification by PDBu in low calcium concentration), future studies must precisely identify the underlying molecular pathway(s) and test their contribution to animal behavior to understand the physiological functions of this unique synaptic phenomenon.

6. Conclusions

My Ph.D. projects focused on the unique physiology of DG GCs. Below I summarize the main conclusions of each project.

Conclusions on the maturation of adult born granule cells:

- The maturation of most of the conventional biophysical properties of ABGCs is continuous, however, their supra-threshold integrative properties mature through two discrete states. ABGCs in S-state are sensitive for certain input intensity ranges, while cells in L-state are characterized by linear input-output conversion.

- During the maturation process of ABGCs, both integrative states are present in a remarkably broad time window (5-9 weeks), during which the proportion of cells belonging to S- or L-group changes. Thus, transition of individual cells from S- to L-function occurs suddenly, but largely independent from their postmitotic age in an extended period.

- Despite the highly variable biophysical properties of the S-group cells (due to their various age), the spiking output of the S-group cells is efficiently tuned to similar integrative function.

Conclusions on the effect of granule cell bursts in the CA3 circuit:

- We identified a new plasticity form of the hippocampal MFs. The single MF spike evoked postsynaptic responses in FF-INs triplicate seconds after a single short high frequency burst. The effect of the burst develops in the first second and remains almost up to 10 seconds.

- The potentiation can be evoked by as short as 2-7 AP-containing single high frequency (150 Hz) bursts, which is exactly the physiologically relevant range for GC bursts.

- The phenomenon is postsynaptic cell type specific, only occurs in FF-INs. Single MF bursts did not have similar effect in postsynaptic PCs or septum-projecting SLCs.

- The MF phenomenon is clearly a presynaptic process, which acts as a promoted vesicle priming. The presynaptic changes probably do not involve the classical

molecular pathways. The specific mechanisms activated by the MF bursts however, remain to be answered in the future.

- The described phenomenon is remarkably robust, the probability whether sporadic GC activity is eliciting APs in FF-INs strongly increases after presynaptic bursts. Thus, single MF bursts effectively rearrange the recruitment of FFI for several seconds.

- FF-INs recruited by individual MFs innervate CA3 PCs regardless whether they receive direct excitation from the same presynaptic MFs or not. This means that the wiring of FFI in the DG- CA3 circuit is random.

7. Summary

The hippocampus is involved in complex cognitive functions such as episodic memory and spatial navigation. During my Ph.D. period, I studied the dentate gyrus granule cells (GCs), one of the principal cell types in hippocampus endowed with many specific features, and I examined their synaptic connections in the CA3 region by electrophysiological recordings in acute slices.

We characterized the functional maturation of adult born granule cells (ABGCs) after their integration into the hippocampal circuit, to unveil their switch from 'young' to 'old' functional phenotype. Currently, it is believed that young ABGCs have distinct physiological role, which is assumed to be the process of 'pattern separation'. However, it was not clear how the continuous maturation of physiological properties enables sustaining two separate functional states instead of a broadly distributed continuum. We recorded birth dated ABGCs with various age (3-10 weeks), and indeed found two distinct populations considering their integrative properties. Strikingly, the two integrative states were present during the entire maturation period, only the proportion of ABGCs with 'old' phenotype increased by time, suggesting quick functional transition in a surprisingly broad time window. Our results revealed that the functional maturation of ABGCs is not continuous, instead, ABGCs form two temporally overlapping but functionally distinct populations.

The second project addressed the physiological effects of the two distinct activity forms of GCs, single action potentials and short high frequency bursts on the postsynaptic CA3 circuit. We revealed remarkable changes in the recruitment of the CA3 feed forward inhibitory circuit, that lasted nearly 10 seconds after single short bursts of GCs. The observed plasticity phenomenon in mossy fibers was found to be a presynaptic process, but did not involve the common molecular pathways known to increase release probability. Our results suggested that the priming of vesicles is transiently promoted during the plasticity. In summary, we described a new synaptic plasticity phenomenon in mossy fiber synapses that is activated during physiologically relevant firing pattern of GCs.

My results provided important contribution to understanding the functions of a unique neuron type, the dentate gyrus granule cells.

8. Összefoglalás

A Ph.D. munkám során a hippokampusz egyik fő sejttípusát, a *gyrus dentatus* szemcsesejtet és szinaptikus kimenetét, a moharost kapcsolatrendszert vizsgáltam túlélő agyszeletekben végzett elektrofiziológiai mérésekkel.

A szemcsesejtek egyik különleges tulajdonsága, hogy nemcsak az embrionális fejlődés során születhetnek. Számos eredmény utalt arra, hogy a felnőtt korban született fiatal szemcsesejteknek megkülönböztetett szerepük van a külvilágból érkező információ feldolgozásában: kulcsfontosságúak a hippokampuszba beérkező hasonló aktivitás mintázatok elkülönítésében. A fiatal szemcsesejtek egy érési folyamaton mennek keresztül a születésüket követő 3-10 hétben, mely során morfológiai és fiziológiai tulajdonságaik megváltoznak. Munkám során először arra kerestük a választ, hogy a sejtek érése során folyamatosan változó fiziológiai tulajdonságok hogyan teszik lehetővé két diszkrét funkcionális állapot (fiatal és idős) fenntartását. Ismert korú szemcsesejteket vizsgálva (születéskor jelölve) azt találtuk, hogy integratív tulajdonságaik szerint valóban két jól elkülöníthető csoportba sorolhatók. Populációs szinten a két integrációs állapot az érés teljes időtartama alatt jelen volt, habár az idősként viselkedő sejtek aránya fokozatosan nőtt. Ez a megfigyelés arra utal, hogy az átmenet a két állapot közt gyors, azonban egy meglepően széles időtartományban történhet meg. Eredményeink rávilágítottak, hogy a felnőtt korban született szemcsesejtek funkcionális érése nem folyamatos; azok két, korban átfedő, de funkcionálisan különböző populációt képeznek.

A második projektben az érett szemcsesejtek két különböző aktivitásának (egyedi akciós potenciál, illetve rövid, nagy frekvenciás tüzelés) hatását vizsgáltuk a CA3 hálózatban. Jelentős növekedést tapasztaltunk nagy frekvenciás tüzelést követően a CA3 régió gátlósejtjeinek aktiválásában közel 10 másodpercig. Kimutattuk, hogy az általunk leírt új plaszticitási forma preszinaptikus folyamat eredménye, és hátterében a vezikula ürülési folyamatának egyik lépése, a "priming" felgyorsulása áll, de a transzmitter ürülés hatékonyságot növelő általánosan ismert molekuláris útvonalak nem játszanak benne szerepet. Összefoglalva, ebben a projektben egy eddig ismeretlen plaszticitási jelenséget írtunk le a moharost kapcsolatrendszertben.

Doktori munkám eredményei hozzájárulnak egy különleges idegsejt típus, a *gyrus dentatus* szemcsesejtek működésének megértéséhez.

9. References

Abbott LF, Regehr WG (2004) Synaptic computation. Nature 431:796–803.

Acuna C, Liu X, Südhof TC (2016) How to Make an Active Zone: Unexpected Universal Functional Redundancy between RIMs and RIM-BPs. Neuron 91:792–807.

Acsády L, Káli S (2007) Models, structure, function: the transformation of cortical signals in the dentate gyrus. Prog Brain Res 163:577–599.

Acsády L, Kamondi A, Sík A, Freund T, Buzsáki G (1998) GABAergic cells are the major postsynaptic targets of mossy fibers in the rat hippocampus. J Neurosci 18:3386–3403.

Acsády L, Katona I, Martínez-Guijarro FJ, Buzsáki G, Freund TF (2000) Unusual target selectivity of perisomatic inhibitory cells in the hilar region of the rat hippocampus. J Neurosci 20:6907–6919.

Agster KL et al. (2014) Individual oligodendrocytes have only a few hours in which to generate new myelin sheaths invivo. Neuron 17:1–10.

Aimone JB, Deng W, Gage FH (2010a) Adult neurogenesis: Integrating theories and separating functions. Trends Cogn Sci 14:325–337.

Aimone JB, Deng W, Gage FH (2010b) Put them out to pasture? What are old granule cells good for, anyway? Hippocampus 20:1124–1125.

Aimone JB, Wiles J, Gage FH (2006) Potential role for adult neurogenesis in the encoding of time in new memories. Nat Neurosci 9:723–727.

Alle H, Jonas P, Geiger JRP (2001) PTP and LTP at a hippocampal mossy fiber-interneuron synapse. Proc Natl Acad Sci 98:14708–14713.

Alle H, Kubota H, Geiger JRP (2011) Sparse But Highly Efficient Kv3 Outpace BKCa Channels in Action Potential Repolarization at Hippocampal Mossy Fiber Boutons. J Neurosci 31:8001–8012.

Alme CB, Buzzetti RA, Marrone DF, Leutgeb JK, Chawla MK, Schaner MJ, Bohanick JD, Khoboko T, Leutgeb S, Moser EI, Moser MB, McNaughton BL, Barnes CA (2010) Hippocampal granule cells opt for early retirement. Hippocampus 20:1109–1123.

Altman J, Das GD (1965) Post-natal origin of microneurones in the rat brain. Nature 207:953–956.

Amaral DG (1978) A Golgi study of cell types in the hilar region of the hippocampus in the rat. J Comp Neurol 182:851–914.

Andersen P, Morris R, Amaral D, Bliss T, O' Keefe J (2007) The Hippocampus Book (Andersen P, Morris R, Amaral D, Bliss T, O'Keefe J, eds). Oxford University Press.

Apostolides PF, Milstein AD, Grienberger C, Bittner KC, Magee JC (2016) Axonal Filtering Allows Reliable Output during Dendritic Plateau-Driven Complex Spiking in CA1 Neurons. Neuron 89:770–783.

Armstrong CM, Hille B (1998) Voltage-gated ion channels and electrical excitability. Neuron 20:371–380.

Aronov D, Nevers R, Tank DW (2017) Mapping of a non-spatial dimension by the hippocampal–entorhinal circuit. Nature 543:719–722.

Augustin I, Rosenmund C, Südhof TC, Brose N (1999) Munc13-1 is essential for fusion competence of glutamatergic synaptic vesicles. Nature 400:457–461.

Basu J, Betz A, Brose N, Rosenmund C (2007) Munc13-1 C1 Domain Activation Lowers the Energy Barrier for Synaptic Vesicle Fusion. J Neurosci 27:1200–1210.

Bayer SA (1980a) Development of the hippocampal region in the rat I. Neurogenesis examined with 3H-thymidine autoradiography. J Comp Neurol 190:87–114.

Bayer SA (1980b) Development of the hippocampal region in the rat II. Morphogenesis during embryonic and early postnatal life. J Comp Neurol 190:115–134.

Bayer SA (1982) Changes in the total number of dentate granule cells in juvenile and adult rats: A correlated volumetric and 3H-thymidine autoradiographic study. Exp Brain Res 46:315–323.

Betz A, Ashery U, Rickmann M, Augustin I, Neher E, Südhof TC, Rettig J, Brose N (1998) Munc13-1 is a presynaptic phorbol ester receptor that enhances neurotransmitter release. Neuron 21:123–136.

Bischofberger J, Engel D, Li L, Geiger JR, Jonas P (2006) Patch-clamp recording from mossy fiber terminals in hippocampal slices. Nat Protoc 1:2075–2081.

Bittner KC, Grienberger C, Vaidya SP, Milstein AD, Macklin JJ, Suh J, Tonegawa S, Magee JC (2015) Conjunctive input processing drives feature selectivity in hippocampal CA1 neurons. Nat Neurosci 18:1133–1142.

Bland BH, Oddie SD, Colom L V (1999) Mechanisms of neural synchrony in the septohippocampal pathways underlying hippocampal theta generation. J Neurosci 19:3223–3237.

Boudkkazi S, Carlier E, Ankri N, Caillard O, Giraud P, Fronzaroli-Molinieres L, Debanne D (2007) Release-Dependent Variations in Synaptic Latency: A Putative Code for Short- and Long-Term Synaptic Dynamics. Neuron 56:1048–1060.

Brunner J, Ster J, Van-Weert S, Andrasi T, Neubrandt M, Corti C, Corsi M, Ferraguti F, Gerber U, Szabadics J (2013) Selective Silencing of Individual Dendritic Branches by an mGlu2-Activated Potassium Conductance in Dentate Gyrus Granule Cells. J Neurosci 33:7285–7298.

Buckmaster PS, Schwartzkroin PA (1995) Interneurons and inhibition in the dentate gyrus of the rat in vivo. J Neurosci 15:774–789.

Buffalo EA (2015) Bridging the gap between spatial and mnemonic views of the hippocampal formation. Hippocampus 25:713–718.

Buzsáki G (1984) Feed-forward inhibition in the hippocampal formation. Prog Neurobiol 22:131–153.

Buzsáki G, Geisler C, Henze DA, Wang XJ (2004) Interneuron Diversity series: Circuit complexity and axon wiring economy of cortical interneurons. Trends Neurosci 27:186–193.

Buzsáki G, Lai-Wo S. L, Vanderwolf CH (1983) Cellular bases of hippocampal EEG in the behaving rat. Brain Res Rev 6:139–171.

Buzsáki G, Moser EI (2013) Memory, navigation and theta rhythm in the hippocampal-entorhinal system. Nat Neurosci 16:130–138.

Cajal SR y (1893) Estructura del asta de Ammon y fascia dentata. An Soc Esp Hist Nat 22:53–114.

Cameron HA, Woolley CS, McEwen BS, Gould E (1993) Differentiation of newly born neurons and glia in the dentate gyrus of the adult rat. Neuroscience 56:337–344.

Carta M, Fièvre S, Gorlewicz A, Mulle C (2014) Kainate receptors in the hippocampus. Eur J Neurosci 39:1835–1844.

Chamberland S, Topolnik L (2012) Inhibitory control of hippocampal inhibitory neurons. Front Neurosci 6:165.

Chu Y, Fioravante D, Leitges M, Regehr WG (2014) Calcium-Dependent PKC Isoforms Have Specialized Roles in Short-Term Synaptic Plasticity. Neuron 82:859–871.

Claiborne BJ, Amaral DG, Cowan WM (1986) A light and electron microscopic analysis of the mossy fibers of the rat dentate gyrus. J Comp Neurol 246:435–458.

Claiborne BJ, Amaral DG, Cowan WM (1990) Quantitative, three-dimensional analysis of granule cell dendrites in the rat dentate gyrus. J Comp Neurol 302:206–219.

Clelland CD, Choi M, Romberg C, Clemenson GD, Fragniere A, Tyers P, Jessberger S, Saksida LM, Barker RA, Gage FH, Bussey TJ (2009) A Functional Role for Adult Hippocampal Neurogenesis in Spatial Pattern Separation. Science (80-) 325:210–213.

Cui Z, Gerfen CR, Young WS (2013) Hypothalamic and other connections with dorsal CA2 area of the mouse hippocampus. J Comp Neurol 521:1844–1866.

Danielson NB, Turi GF, Ladow M, Chavlis S, Petrantonakis PC, Poirazi P, Losonczy A (2017) In Vivo Imaging of Dentate Gyrus Mossy Cells in Behaving Mice. Neuron 93:552–559.e4.

de Jong APH, Fioravante D (2014) Translating neuronal activity at the synapse: presynaptic calcium sensors in short-term plasticity. Front Cell Neurosci 8.

Debanne D, Gähwiler BH, Thompson SM (1998) Long-term synaptic plasticity between pairs of individual CA3 pyramidal cells in rat hippocampal slice cultures. J Physiol 507:237–247.

Del Castillo J, Katz B (1954) Quantal Components of the End-Plate Potential. J Physiol 124:560–573.

Deng W, Aimone JB, Gage FH (2010) New neurons and new memories: how does adult hippocampal neurogenesis affect learning and memory? Nat Rev Neurosci 11:339–350.

Diamantaki M, Frey M, Berens P, Preston-Ferrer P, Burgalossi A (2016) Sparse activity of identified dentate granule cells during spatial exploration. Elife 5.

Dieni C V., Nietz AK, Panichi R, Wadiche JI, Overstreet-Wadiche L (2013) Distinct Determinants of Sparse Activation during Granule Cell Maturation. J Neurosci 33:19131–19142.

Eichenbaum H (2013) Memory on time. Trends Cogn Sci 17:88.

Eichenbaum H (2014) Time cells in the hippocampus: a new dimension for mapping memories. Nat Rev Neurosci 15:732–744.

Engel D, Jonas P (2005) Presynaptic action potential amplification by voltage-gated Na+ channels in hippocampal mossy fiber boutons. Neuron 45:405–417.

Fioravante D, Chu Y, de Jong AP, Leitges M, Kaeser PS, Regehr WG (2014) Protein kinase C is a calcium sensor for presynaptic short-term plasticity. Elife 3:e03011.

Fioravante D, Chu Y, Myoga MH, Leitges M, Regehr WG (2011) Calcium-Dependent Isoforms of Protein Kinase C Mediate Posttetanic Potentiation at the Calyx of Held. Neuron 70:1005–1019.

Fioravante D, Regehr WG (2011) Short-term forms of presynaptic plasticity. Curr Opin Neurobiol 21:269–274.

Freund TF, Antal M (1988) GABA-containing neurons in the septum control inhibitory interneurons in the hippocampus. Nature 336:170–173.

Freund TF, Buzsáki G (1998) Interneurons of the hippocampus. Hippocampus 6:347–470.

Ge S, Yang C hao, Hsu K sen, Ming G li, Song H (2007) A Critical Period for Enhanced Synaptic Plasticity in Newly Generated Neurons of the Adult Brain. Neuron 54:559–566.

Geiger JRP, Jonas P (2000) Dynamic control of presynaptic Ca2+ inflow by fast-inactivating K+ channels in hippocampal mossy fiber boutons. Neuron 28:927–939.

Glickfeld LL, Scanziani M (2006) Distinct timing in the activity of cannabinoid-sensitive and cannabinoid-insensitive basket cells. Nat Neurosci 9:807–815.

GoodSmith D, Chen X, Wang C, Kim SH, Song H, Burgalossi A, Christian KM, Knierim JJ (2017) Spatial Representations of Granule Cells and Mossy Cells of the Dentate Gyrus. Neuron 93:677–690.e5.

Gould E, Tanapat P (1999) Stress and hippocampal neurogenesis. In: Biological Psychiatry, pp 1472–1479.

Gu Y, Arruda-Carvalho M, Wang J, Janoschka SR, Josselyn SA, Frankland PW, Ge S (2012) Optical controlling reveals time-dependent roles for adult-born dentate granule cells. Nat Neurosci 15:1700–1706.

Gulyás AI, Miettinen R, Jacobowitz DM, Freund TF (1992) Calretinin is present in non-pyramidal cells of the rat hippocampus-I. A new type of neuron specifically associated with the mossy fibre system. Neuroscience 48:1–27.

Gulyás AI, Miles R, Sik A, Tóth K, Tamamaki N, Freund TF (1993) Hippocampal pyramidal cells excite inhibitory neurons through a single release site. Nature 366:683–687.

Gundlfinger A, Breustedt J, Sullivan D, Schmitz D (2010) Natural spike trains trigger short- and long lasting dynamics at hippocampal mossy fiber synapses in rodents Tsien JZ, ed. PLoS One 5:e9961.

Guzman SJ, Schlogl A, Frotscher M, Jonas P (2016) Synaptic mechanisms of pattern completion in the hippocampal CA3 network. Science (80-) 353:1117–1123.

Hafting T, Fyhn M, Molden S, Moser M-B, Moser EI (2005) Microstructure of a spatial map in the entorhinal cortex. Nature 436:801–806.

Hainmuller T, Krieglstein K, Kulik A, Bartos M (2014) Joint CP-AMPA and group I mGlu receptor activation is required for synaptic plasticity in dentate gyrus fast-spiking interneurons. Proc Natl Acad Sci 111:13211–13216.

Hájos N, Acsády L, Freund TF (1996) Target selectivity and neurochemical characteristics of VIP-immunoreactive interneurons in the rat dentate gyrus. Eur J Neurosci 8:1415–1431.

Hartley T, Lever C, Burgess N, O'Keefe J (2013) Space in the brain: how the hippocampal formation supports spatial cognition. Philos Trans R Soc B Biol Sci 369:20120510–20120510.

Henze DA, Wittner L, Buzsáki G (2002) Single granule cells reliably discharge targets in the hippocampal CA3 network in vivo. Nat Neurosci 5:790–795.

Holmes MM, Galea LAM, Mistlberger RE, Kempermann G (2004) Adult Hippocampal Neurogenesis and Voluntary Running Activity: Circadian and Dose-Dependent Effects. In: Journal of Neuroscience Research, pp 216–222.

Holtmaat A, Caroni P (2016) Functional and structural underpinnings of neuronal assembly formation in learning. Nat Neurosci 19:1553–1562.

Holtmaat A, Svoboda K (2009) 1. Holtmaat A, Svoboda K. Experience-dependent structural synaptic plasticity in the mammalian brain. Nat Rev Neurosci. 2009;10(9):647–658. doi:10.1038/nrn2721.Experience-dependent structural synaptic plasticity in the mammalian brain. Nat Rev Neurosci 10:647–658.

Jackman SL, Regehr WG (2017) The Mechanisms and Functions of Synaptic Facilitation. Neuron 94:447–464.

Jacobs J, Weidemann CT, Miller JF, Solway A, Burke JF, Wei X-X, Suthana N, Sperling MR, Sharan AD, Fried I, Kahana MJ (2013) Direct recordings of grid-like neuronal activity in human spatial navigation. Nat Neurosci 16:1188–1190.

Jessberger S, Zhao C, Toni N, Jr GDC, Li Y, Gage FH (2007) Seizure-Associated , Aberrant Neurogenesis in Adult Rats Characterized with Retrovirus-Mediated Cell Labeling. J Neurosci 27:9400–9407.

Jinno S (2009) Structural organization of long-range GABAergic projection system of the hippocampus. Front Neuroanat 3:13.

Jinno S, Klausberger T, Marton LF, Dalezios Y, Roberts JDB, Fuentealba P, Bushong EA, Henze D, Buzsaki G, Somogyi P (2007) Neuronal Diversity in GABAergic Long-Range Projections from the Hippocampus. J Neurosci 27:8790–8804.

Jung MW, McNaughton BL (1993) Spatial selectivity of unit activity in the hippocampal granular layer. Hippocampus 3:165–182.

Kempermann G, Kuhn HG, Gage FH (1997) More hippocampal neurons in adult mice living in an enriched environment. Nature 386:493–495.

Kepecs A, Fishell G (2014) Interneuron Cell Types: Fit to form and formed to fit. Nature 505:318–326.

Kesner RP (2007) Behavioral functions of the CA3 subregion of the hippocampus. Learn Mem 14:771–781.

Killian NJ, Jutras MJ, Buffalo EA (2012) A map of visual space in the primate entorhinal cortex. Nature 491:761–764.

Klausberger T (2009) GABAergic interneurons targeting dendrites of pyramidal cells in the CA1 area of the hippocampus. Eur J Neurosci 30:947–957.

Klausberger T, Somogyi P (2008) Neuronal Diversity and Temporal Dynamics: The Unity of Hippocampal Circuit Operations. Science (80-) 321:53–57.

Knierim JJ, Neunuebel JP (2016) Tracking the flow of hippocampal computation: Pattern separation, pattern completion, and attractor dynamics. Neurobiol Learn Mem 129:38–49.

Kohara K, Pignatelli M, Rivest AJ, Jung H-Y, Kitamura T, Suh J, Frank D, Kajikawa K, Mise N, Obata Y, Wickersham IR, Tonegawa S (2013) Cell type–specific genetic and optogenetic tools reveal hippocampal CA2 circuits. Nat Neurosci 17:269–279.

Korogod N, Lou X, Schneggenburger R (2007) Posttetanic potentiation critically depends on an enhanced Ca(2+) sensitivity of vesicle fusion mediated by presynaptic PKC. Proc Natl Acad Sci U S A 104:15923–15928.

Kowalski J, Gan J, Jonas P, Pern??a-Andrade AJ (2016) Intrinsic membrane properties determine hippocampal differential firing pattern in vivo in anesthetized rats. Hippocampus 26:668–682.

Körber C, Kuner T (2016) Molecular machines regulating the release probability of synaptic vesicles at the active zone. Front Synaptic Neurosci 8.

Kriegstein A, Alvarez-Buylla A (2009) The Glial Nature of Embryonic and Adult Neural Stem Cells. Annu Rev Neurosci 32:149–184.

Krueppel R, Remy S, Beck H (2011) Dendritic integration in hippocampal dentate granule cells. Neuron 71:512–528.

Laplagne DA, Espósito MS, Piatti VC, Morgenstern NA, Zhao C, Van Praag H, Gage FH, Schinder AF (2006) Functional convergence of neurons generated in the developing and adult hippocampus Macklis J, ed. PLoS Biol 4:2349–2360.

Lawrence JJ, McBain CJ (2003) Interneuron Diversity series: Containing the detonation - Feedforward inhibition in the CA3 hippocampus. Trends Neurosci 26:631–640.

Leutgeb JK, Leutgeb S, Moser M, Moser EI, Moser I (2007) Pattern Gyms in the Dentate Separation and CA3 of the Hippocampus. Science (80-) 315:961–966.

Lisman JE (1997) Bursts as a unit of neural information: Making unreliable synapses reliable. Trends Neurosci 20:38–43.

Lorente de Nó R (1934) Studies on the Structure of the Cerebral Cortex: Continuation of the study of the ammonic system. II.

Lou X, Korogod N, Brose N, Schneggenburger R (2008) Phorbol Esters Modulate Spontaneous and Ca2+-Evoked Transmitter Release via Acting on Both Munc13 and Protein Kinase C. J Neurosci 28:8257–8267.

Lovett-Barron M, Turi GF, Kaifosh P, Lee PH, Bolze F, Sun X-H, Nicoud J-F, Zemelman B V, Sternson SM, Losonczy A (2012) Regulation of neuronal input transformations by tunable dendritic inhibition. Nat Neurosci 15:423–430.

Maccaferri G (1998) Target-Specific Expression of Presynaptic Mossy Fiber Plasticity. Science (80-) 279:1368–1371.

Marder E, Goaillard J-M (2006) Variability, compensation and homeostasis in neuron and network function. Nat Rev Neurosci 7:563–574.

Marin-Burgin A, Mongiat LA, Pardi MB, Schinder AF (2012) Unique Processing During a Period of High Excitation/Inhibition Balance in Adult-Born Neurons. Science (80-) 335:1238–1242.

Markwardt SJ, Dieni C V, Wadiche JI, Overstreet-Wadiche L (2011) Ivy/neurogliaform interneurons coordinate activity in the neurogenic niche. Nat Neurosci 14:1407–1409.

Markwardt SJ, Wadiche JI, Overstreet-Wadiche LS (2009) Input-Specific GABAergic Signaling to Newborn Neurons in Adult Dentate Gyrus. J Neurosci 29:15063–15072.

Marr D (1971) Simple memory: a theory for archicortex. Philos Trans R Soc Lond B Biol Sci 262:23–81.

McNaughton BL, Barnes CA, Gerrard JL, Gothard K, Jung MW, Knierim JJ, Kudrimoti H, Qin Y, Skaggs WE, Suster M, Weaver KL (1996) Deciphering the hippocampal polyglot: the hippocampus as a path integration system. J Exp Biol 199:173–185.

McNaughton BL, Morris RGM (1987) Hippocampal synaptic enhancement and information storage within a distributed memory system. Trends Neurosci 10:408–415.

Miller JF, Neufang M, Solway A, Brandt A, Trippel M, Mader I, Hefft S, Merkow M, Polyn SM, Jacobs J, Kahana MJ, Schulze-Bonhage A (2013) Neural Activity in Human Hippocampal Formation Reveals the Spatial Context of Retrieved Memories. Science (80-) 342:1111–1114.

Mishra RK, Kim S, Guzman SJ, Jonas P (2016) Symmetric spike timing-dependent plasticity at CA3–CA3 synapses optimizes storage and recall in autoassociative networks. Nat Commun 7:11552.

Mongiat LA, Espósito MS, Lombardi G, Schinder AF (2009) Reliable activation of immature neurons in the adult hippocampus Reh TA, ed. PLoS One 4:e5320.

Mori M, Abegg MH, Gähwiler BH, Gerber U (2004) A frequency-dependent switch from inhibition to excitation in a hippocampal unitary circuit. Nature 431:453–456.

Mori M, Gahwiler BH, Gerber U (2007) Recruitment of an inhibitory hippocampal network after bursting in a single granule cell. Proc Natl Acad Sci 104:7640–7645.

Moser EI, Roudi Y, Witter MP, Kentros C, Bonhoeffer T, Moser M-B (2014) Grid cells and cortical representation. Nat Rev Neurosci 15:466–481.

Munoz MD, Nunez A, Garcia-Austt E (1990) In vivo intracellular analysis of rat dentate granule cells. Brain Res 509:91–98.

Nakashiba T, Cushman JD, Pelkey KA, Renaudineau S, Buhl DL, McHugh TJ, Barrera VR, Chittajallu R, Iwamoto KS, McBain CJ, Fanselow MS, Tonegawa S (2012) Young dentate granule cells mediate pattern separation, whereas old granule cells facilitate pattern completion. Cell 149:188–201.

Neunuebel JP, Knierim JJ (2012) Spatial Firing Correlates of Physiologically Distinct Cell Types of the Rat Dentate Gyrus. J Neurosci 32:3848–3858.

Nusser Z (2009) Variability in the subcellular distribution of ion channels increases neuronal diversity. Trends Neurosci 32:267–274.

O'Keefe J, Dostrovsky J (1971) The hippocampus as a spatial map. Preliminary evidence from unit activity in the freely-moving rat. Brain Res 34:171–175.

O'Keefe J, Nadel L (1978) The Hippocampus as a Cognitive Map. New York: Oxford Univ. Press.

Papp OI, Karlócai MR, Tóth IE, Freund TF, Hájos N (2013) Different input and output properties characterize parvalbumin-positive basket and Axo-axonic cells in the hippocampal CA3 subfield. Hippocampus 23:903–918.

Pelkey KA, Lavezzari G, Racca C, Roche KW, McBain CJ (2005) MGluR7 is a metaplastic switch controlling bidirectional plasticity of feedforward inhibition. Neuron 46:89–102.

Pelkey KA, Topolnik L, Yuan XQ, Lacaille JC, McBain CJ (2008) State-Dependent cAMP Sensitivity of Presynaptic Function Underlies Metaplasticity in a Hippocampal Feedforward Inhibitory Circuit. Neuron 60:980–987.

Penttonen M, Kamondi A, Sik A, Acsády L, Buzsáki G (1997) Feed-forward and feed-back activation of the dentate gyrus in vivo during dentate spikes and sharp wave bursts. Hippocampus 7:437–450.

Pernia-Andrade AJ, Jonas P (2014) Theta-Gamma-Modulated Synaptic Currents in Hippocampal Granule Cells InVivo Define a Mechanism for Network Oscillations. Neuron 81:140–152.

Pouille F, Marin-Burgin A, Adesnik H, Atallah B V, Scanziani M (2009) Input normalization by global feedforward inhibition expands cortical dynamic range. Nat Neurosci 12:1577–1585.

Pouille F, Scanziani M (2001) Enforcement of temporal fidelity in pyramidal cells by feed-forward somatic inhibition. Science (80-) 293:325–331.

Rhee JS, Betz A, Pyott S, Reim K, Varoqueaux F, Augustin I, Hesse D, Südhof TC, Takahashi M, Rosenmund C, Brose N (2002) β phorbol ester- and diacylglycerol-induced augmentation of transmitter release is mediated by Munc13s and not by PKCs. Cell 108:121–133.

Rich PD, Liaw H-P, Lee AK (2014) Large environments reveal the statistical structure governing hippocampal representations. Science (80-) 345:814–817.

Rollenhagen A, Satzler K, Rodriguez EP, Jonas P, Frotscher M, Lubke JHR (2007) Structural Determinants of Transmission at Large Hippocampal Mossy Fiber Synapses. J Neurosci 27:10434–10444.

Rolls ET (2007) An attractor network in the hippocampus: Theory and neurophysiology. Learn Mem 14:714–731.

Rolls ET, Treves A (2011) The neuronal encoding of information in the brain. Prog Neurobiol 95:448–490.

Rosenmund C, Sigler A, Augustin I, Reim K, Brose N, Rhee JS (2002) Differential control of vesicle priming and short-term plasticity by Munc13 isoforms. Neuron 33:411–424.

Ruediger S, Vittori C, Bednarek E, Genoud C, Strata P, Sacchetti B, Caroni P (2011) Learning-related feedforward inhibitory connectivity growth required for memory precision. Nature 473:514–518.

Sahay A, Scobie KN, Hill AS, O'Carroll CM, Kheirbek MA, Burghardt NS, Fenton AA, Dranovsky A, Hen R (2011) Increasing adult hippocampal neurogenesis is sufficient to improve pattern separation. Nature 472:466–470.

Salin PA, Scanziani M, Malenka RC, Nicoll RA (1996) Distinct short-term plasticity at two excitatory synapses in the hippocampus. Proc Natl Acad Sci U S A 93:13304–13309.

Sargolini F (2006) Conjunctive Representation of Position, Direction, and Velocity in Entorhinal Cortex. Science (80-) 312:758–762.

Schmidt-Hieber C, Jonas P, Bischofberger J (2004) Enhanced synaptic plasticity in newly generated granule cells of the adult hippocampus. Nature 429:184–187.

Schmidt-Hieber C, Jonas P, Bischofberger J (2007) Subthreshold dendritic signal processing and coincidence detection in dentate gyrus granule cells. J Neurosci 27:8430–8441.

Schneggenburger R, Rosenmund C (2015) Molecular mechanisms governing Ca(2+) regulation of evoked and spontaneous release. Nat Neurosci 18:935–941.

Schneider CJ, Bezaire M, Soltesz I (2012) Toward a full-scale computational model of the rat dentate gyrus. Front Neural Circuits 6:83.

Scoville WB, Milner B (1957) Loss of recent memory after bilateral hippocampal lesions. J Neurol Neurosurg Psychiatry 20:11–21.

Senzai Y, Buzsáki G (2017) Physiological Properties and Behavioral Correlates of Hippocampal Granule Cells and Mossy Cells. Neuron 93:691–704.e5.

Shigemoto R, Kinoshita a, Wada E, Nomura S, Ohishi H, Takada M, Flor PJ, Neki a, Abe T, Nakanishi S, Mizuno N (1997) Differential presynaptic localization of metabotropic glutamate receptor subtypes in the rat hippocampus. J Neurosci 17:7503–7522.

Sik A (1997) Interneurons in the hippocampal dentate gyrus: An in vivo intracellular study. Eur J Neurosci 9:573–588.

Sik A, Tamamaki N, Freund TF (1993) Complete Axon Arborization of a Single CA3 Pyramidal Cell in the Rat Hippocampus, and its Relationship With Postsynaptic Parvalbumin-containing Interneurons. Eur J Neurosci 5:1719–1728.

Somogyi P, Freund TF, Cowey A (1982) The axo-axonic interneuron in the cerebral cortex of the rat, cat and monkey. Neuroscience 7:2577–2607.

Somogyi P, Katona L, Klausberger T, Lasztoczi B, Viney TJ (2013) Temporal redistribution of inhibition over neuronal subcellular domains underlies state-dependent rhythmic change of excitability in the hippocampus. Philos Trans R Soc B Biol Sci 369:20120518–20120518.

Spruston N, Lübke J, Frotscher M (1997) Interneurons in the stratum lucidum of the rat hippocampus: An anatomical and electrophysiological characterization. J Comp Neurol 385:427–440.

Squire LR (1992) "Memory and the hippocampus: A synthesis from findings with rats, monkeys, and humans": Correction. Psychol Rev 99:582–582.

Squire LR (2009) The Legacy of Patient H.M. for Neuroscience. Neuron 61:6–9.

Staley KJ, Otis TS, Mody I (1992) Membrane properties of dentate gyrus granule cells: comparison of sharp microelectrode and whole-cell recordings. J Neurophysiol 67:1346–1358.

Südhof TC (2012) The presynaptic active zone. Neuron 75:11–25.

Südhof TC (2013) Neurotransmitter release: The last millisecond in the life of a synaptic vesicle. Neuron 80:675–690.

Szabadics J, Soltesz I (2009) Functional Specificity of Mossy Fiber Innervation of GABAergic Cells in the Hippocampus. J Neurosci 29:4239–4251.

Szabadics J, Varga C, Brunner J, Chen K, Soltesz I (2010) Granule Cells in the CA3 Area. J Neurosci 30:8296–8307.

Szabó GG, Papp OI, Máté Z, Szabó G, Hájos N (2014) Anatomically heterogeneous populations of CB1 cannabinoid receptor-expressing interneurons in the CA3 region of the hippocampus show homogeneous input-output characteristics. Hippocampus 24:1506–1523.

Takács VT, Freund TF, Gulyás AI (2008) Types and synaptic connections of hippocampal inhibitory neurons reciprocally connected with the medial septum. Eur J Neurosci 28:148–164.

Taschenberger H, Woehler A, Neher E (2016) Superpriming of synaptic vesicles as a common basis for intersynapse variability and modulation of synaptic strength. Proc Natl Acad Sci 113:E4548–E4557.

Tashiro A, Dunaevsky A, Blazeski R, Mason CA, Yuste R (2003) Bidirectional regulation of hippocampal mossy fiber filopodial motility by kainate receptors: A two-step model of synaptogenesis. Neuron 38:773–784.

Toni N, Laplagne DA, Zhao C, Lombardi G, Ribak CE, Gage FH, Schinder AF (2008) Neurons born in the adult dentate gyrus form functional synapses with target cells. Nat Neurosci 11:901–907.

Torborg CL, Nakashiba T, Tonegawa S, McBain CJ (2010) Control of CA3 Output by Feedforward Inhibition Despite Developmental Changes in the Excitation-Inhibition Balance. J Neurosci 30:15628–15637.

Tóth K, Freund TF, Miles R (1997) Disinhibition of rat hippocampal pyramidal cells by GABAergic afferents from the septum. J Physiol 500:463–474.

Tóth K, McBain CJ (1998) Afferent-specific innervation of two distinct AMPA receptor subtypes on single hippocampal interneurons. Nat Neurosci 1:572–578.

Toth K, Suares G, Lawrence JJ, Philips-Tansey E, McBain CJ (2000) Differential mechanisms of transmission at three types of mossy fiber synapse. J Neurosci 20:8279–8289.

Treves A, Rolls ET (1992) Computational constraints suggest the need for two distinct input systems to the hippocampal CA3 network. Hippocampus 2:189–199.

Treves A, Rolls ET (1994) Computational analysis of the role of the hippocampus in memory. Hippocampus 4:374–391.

van Praag H, Kempermann G, Gage FH (1999) Running increases cell proliferation and neurogenesis in the adult mouse dentate gyrus. Nat Neurosci 2:266–270.

Vida I, Frotscher M (2000) A hippocampal interneuron associated with the mossy fiber system. Proc Natl Acad Sci U S A 97:1275–1280.

Viney TJ, Lasztoczi B, Katona L, Crump MG, Tukker JJ, Klausberger T, Somogyi P (2013) Network state-dependent inhibition of identified hippocampal CA3 axo-axonic cells in vivo. Nat Neurosci 16:1802–1811.

Vivar C, Potter MC, Choi J, Lee J-Y, Stringer TP, Callaway EM, Gage FH, Suh H, van Praag H (2012) Monosynaptic inputs to new neurons in the dentate gyrus. Nat Commun 3:1107.

Vyleta NP, Jonas P (2014) Loose coupling between Ca2+ channels and release sensors at a plastic hippocampal synapse. Science 343:665–670.

Wang S, Scott BW, Wojtowicz JM (2000) Heterogenous properties of dentate granule neurons in the adult rat. J Neurobiol 42:248–257.

Wilke SA, Antonios JK, Bushong EA, Badkoobehi A, Malek E, Hwang M, Terada M, Ellisman MH, Ghosh A (2013) Deconstructing Complexity: Serial Block-Face Electron Microscopic Analysis of the Hippocampal Mossy Fiber Synapse. J Neurosci 33:507–522.

Williams PA, Larimer P, Gao Y, Strowbridge BW (2007) Semilunar granule cells: glutamatergic neurons in the rat dentate gyrus with axon collaterals in the inner molecular layer. J Neurosci 27:13756–13761.

Wittner L, Henze DA, Záborszky L, Buzsáki G (2006) Hippocampal CA3 pyramidal cells selectively innervate aspiny interneurons. Eur J Neurosci 24:1286–1298.

Wixted JT, Squire LR, Jang Y, Papesh MH, Goldinger SD, Kuhn JR, Smith KA, Treiman DM, Steinmetz PN (2014) Sparse and distributed coding of episodic memory in neurons of the human hippocampus. Proc Natl Acad Sci 111:9621–9626.

Yuste R, Bonhoeffer T (2001) Morphological changes in dendritic spines associated with long-term synaptic plasticity. Annu Rev Neurosci 24:1071–1089.

Zhao C, Teng EM, Summers RG, Ming G-L, Gage FH (2006) Distinct morphological stages of dentate granule neuron maturation in the adult mouse hippocampus. J Neurosci 26:3–11.

Zucca S, Griguoli M, Malézieux M, Grosjean N, Carta M, Mulle C (2016) Control of spike transfer at hippocampal mossy fiber synapses in vivo by GABAA and GABAB receptor mediated inhibition. J Neurosci 37:587–598.

Zucker RS, Regehr WG (2002) Short-Term Synaptic Plasticity. Annu Rev Physiol 64:355–405.

10. List of publications

Publications related to this thesis:

Neubrandt M[1], Olah VJ[1], Brunner J, Szabadics J
Feedforward inhibition is randomly wired from individual granule cells onto CA3 pyramidal cells.
HIPPOCAMPUS. 2017 Jul 11.
[1] equal contribution

Brunner J[2], **Neubrandt M**[2], Van-Weert S, Andrasi T, Kleine Borgmann FB, Jessberger S, Szabadics J
Adult-born granule cells mature through two functionally distinct states.
ELIFE. 2014 Jul 24;3:e03104.

[2] equal contribution

Neubrandt M, Oláh VJ, Brunner J, Soltesz I, Szabadics J.
Single bursts of individual granule cells rearrange feed-forward inhibition.
Under revision.

Other publications:

Róna G, Borsos M, Ellis JJ, Mehdi AM, Christie M, Környei Z, **Neubrandt M**, Tóth J, Bozóky Z, Buday L, Madarász E, Bodén M, Kobe B, Vértessy BG
Dynamics of re-constitution of the human nuclear proteome after cell division is regulated by NLS-adjacent phosphorylation
CELL CYCLE. 2014;13(22):3551-64.

Brunner J, Ster J, Van-Weert S, Andrási T, **Neubrandt M**, Corti C, Corsi M, Ferraguti F, Gerber U, Szabadics J
Selective Silencing of Individual Dendritic Branches by an mGlu2-Activated Potassium Conductance in Dentate Gyrus Granule Cells
J NEUROSCI. 2013 Apr 24;33(17):7285-98.

11. Acknowledgements